TIMING AND REGULATION OF COHESIN DEPLETION DURING MAMMALIAN OOGENESIS

Randy Ballesteros Mejia

Supervisors: Professor Mary Herbert & Professor Doug Turnbull

**Institute of Genetic Medicine, Newcastle Fertility Centre,
International Centre for Life**

**A thesis submitted for the degree of Doctor of Philosophy
February 2017**

Abstract

Sexual reproduction depends on the transmission of exactly one copy of each chromosome by the maternal and paternal gametes. This is accomplished during meiosis when diploid progenitors undergo two consecutive rounds of chromosome segregation following a single round of DNA replication. In most organisms, this relies on the establishment of bivalent chromosomes consisting of replicated parental homologues physically linked at sites of meiotic recombination. In female mammals, bivalents are formed during fetal development when the lifetime stock of primordial-stage oocytes is established. However, they are not resolved until shortly before ovulation. Extending this period beyond ~35 years results in a dramatic increase in embryo aneuploidy. Depletion of the lifetime stock of oocytes during ageing culminates in menopause. Our previous studies indicate that Rec8-containing cohesin complexes also become depleted from oocyte chromosomes during female ageing. Consistent with cohesin's role in maintaining chromosome structure, depletion of Rec8 is associated with destabilisation of bivalents chromosomes. Nevertheless, the mechanisms and timing of cohesin depletion remain unknown.

Here, I investigated the possibility that age-related cohesin depletion is a consequence of leaky inhibition of the protease separase, which cleaves Rec8 during anaphase. I found that oocyte-specific deletion of *separase* did not prevent depletion of oocyte cohesin during female ageing. I, therefore, conclude that age-related depletion occurs by a separase-independent mechanism. I next investigated the timing, during oogenesis, at which cohesin loss occurs. I found that cohesin is predominantly lost at the primordial stage before oocytes are recruited for growth. In addition, using an oocyte-specific deletion of *Pten*, I determined that this occurs independently of the decline in the ovarian stock of primordial-stage oocytes. Together, these results indicate that age-related cohesin depletion occurs at the primordial stage by a separase-independent mechanism. Other possible of mechanisms of cohesin depletion include protein damage and/or age-related deterioration of chromatin structure. From a clinical perspective, my work suggests that "rejuvenation' of fertility by activating the residual pool of primordial oocytes is unlikely to be successful in older women.

Acknowledgments

I would like to thank my supervisor Professor Mary Herbert for her support, guidance and trust on me even from before I arrived at the United Kingdom. To Dame Margaret Barbour and Barbour foundation for they generous contribution to my career and life. To the Graduate School team of the Faculty of Medical Science for their patience, understanding and support with all my problems.

I also want thank to all my friends for their love, good company, laughs, guidance and support. Many thanks to Lisa, Dimitri, Daniel, Raveen, Amy, Jess, Hannah, Toni, Kassia, Beth, Naomi, Ella, Pete, Rob, Thais… essentially the whole team of Newcastle Fertility Centre and the Institute of Genetic Medicine. You all were part of the most challenging time of my life.

Principalmente quiero agradecer a mi Maestro sin su luz y ayuda no hubiera podido lograr nada. A mis padres y a mis hermanos que, desde sitios lejanos, separados por océanos y montañas me brindaron amor, compañía, apoyo y energía positiva como si estuviesen a mi lado. A Ivone por su compañía y cariño.

Table of Contents

List of figures

List of tables

Chapter 1. Introduction

1.1. Why is maternal ageing important?

Sexual reproduction requires that maternal and paternal gametes transmit to the embryo exactly one copy of each chromosome. Lethality during preimplantation development, miscarriage and birth defects are the possible outcomes for mammalian embryos carrying the wrong number of chromosomes, which is termed “aneuploidy” (Hassold and Jacobs, 1984; Munne *et al.*, 2007). Down syndrome was the first birth defect associated with advanced maternal age and this was first reported in the early 1930’s (Penrose, 1933). It is now well established that the risk of transmitting too few or too many chromosomes increases with advanced maternal age and is the principal cause of pregnancy loss and birth defects (Hunt and Hassold, 2010). Current socio-economic circumstances such as education and participation in the labour force drive women to postpone childbearing (Mills *et al.*, 2011). In developed countries where a larger proportion of women enter third level education and participate in the workforce, the trend to delay childbearing has resulted in a dramatic increase of trisomic pregnancies and involuntary childlessness in older women.

Since 1989 the National Down Syndrome Cytogenic Register (NDSCR) has been recording all antenatal and postnatal diagnoses of Down syndrome in England and Wales. Since the beginning of the surveillance in 1989 to 2013, the number of diagnoses per year for this particular syndrome has progressively increased from 1066 to 1806 diagnoses (Morris and Springett, 2014). The highest number of reported diagnosis come from an antenatal screening of Down Syndrome established in 1986 for women older than 35 years. This has resulted in only a modest increase (~1%) in trisomy 21 births as ~ 90% of women carrying a baby diagnosed with Down Syndrome decide to terminate the pregnancy.

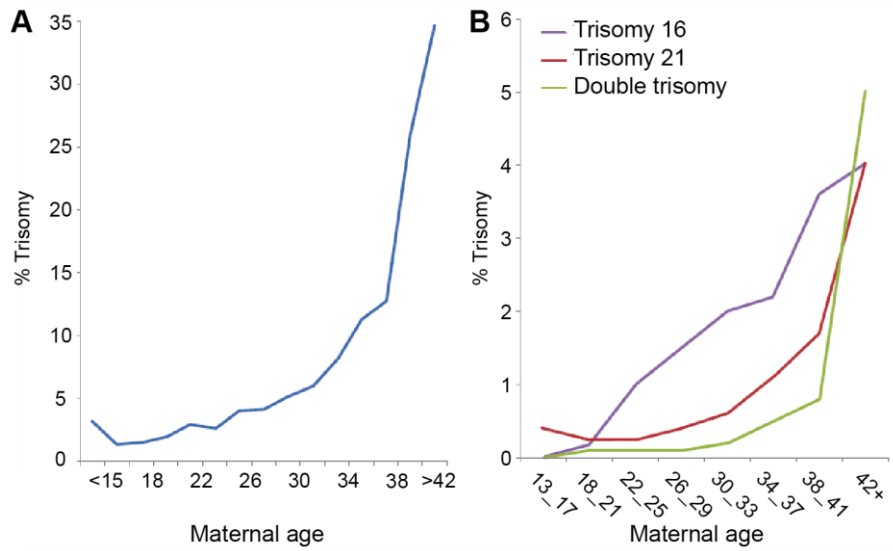

Figure 1.1 Incidence of trisomic pregnancies

Graphs have been taken from (Hunt and Hassold, 2010). They show that the risk of having trisomic pregnancy increases as women get older. **A** The incidence of trisomic pregnancies increases exponentially from mid-thirties onwards. **B** Graph shows separate incidences for the most common trisomies

The vast majority of meiotic aneuploidies appear to result in early embryonic lethality resulting in failed implantation. Thus infertility is by far the most common manifestation of age-related errors in female meiosis. Because of the even increasing trend to postpone childbearing, female-age related infertility is likely to make a considerable contribution to the overall decline in birthrate, the undesirable demographic consequences of which were outlined in a report the Institute and Faculty of Actuaries (More Babies, who needs them?, 2004). For example, the number of babies born during the first two decades of the XXI century can have an adverse impact on the economy, especially in the pension system (Lewis *et al.*, 2004). The progressive decrease in the birth rate and an increase in life expectancy will reduce the number of working people who support every person aged over 65 in 2050. The reported ratio in 2004 was 3.9 people supporting every per person over 65 years old while the projected ratio in 2050 will reduce to 2.2 (Lewis *et al.*, 2004). Despite the profound reproductive and demographic consequences, little was

understood about the molecular basis of why the risk of embryo aneuploidy increases as women get older.

1.2. How to make haploid gametes – The mechanics of meiosis

Production of haploid gametes from diploid progenitors requires a specialised form of cell division known as meiosis. This process involves two rounds of chromosome segregation following a single round of DNA replication (Petronczki *et al.*, 2003). As in most organisms, mammal meiosis requires that replicated parental homologues establish physical linkages to form bivalent (tetrads) chromosomes. These linkages are formed when maternal and paternal homologues undergo reciprocal DNA exchange to create crossovers (chiasmata) (Neale and Keeney, 2006). Mouse oocytes lacking the DNA mismatch repair protein (MLH1) fail to form crossovers resulting in aberrant chromosomes orientation in prometaphase, which makes oocytes unable to complete the first round of chromosome segregation (Woods *et al.*, 1999). This shows that formation of crossovers is required for correct orientation of bivalents in the meiotic spindle (Woods *et al.*, 1999) and also necessary to generate genetic diversity (Baudat *et al.*, 2013). Stability of the chiasma, which is maintained by cohesion between chromosome arms, is essential for preserving the integrity of the bivalent chromosome structure (Moore and Orr-Weaver, 1998; Petronczki *et al.*, 2003)

The four constituent chromatids of the bivalent are resolved during two successive meiotic divisions, first reductional (MI) and second equational (MII). Resolution of the chiasmata during the first meiotic division (MI) converts bivalent into dyad chromosomes. For correct bi-orientation bivalent chromosomes at prometaphase I kinetochores need to bind with microtubules emanating from the same spindle pole. This is achieved only if sister centromeres adopt a side-by-side configuration to create monopolar kinetochore-microtubule attachments (Hauf and Watanabe, 2004). Once bivalent chromosomes are appropriately bi-oriented, cohesion along the arms is dissolved and the pulling forces of the meiotic spindle segregate the recombined maternal and paternal homologues (dyads) to opposite poles during anaphase I (Kudo *et al.*, 2006).

Mammalian oocytes arrest at metaphase II and anaphase II is not triggered until after sperm entry. To ensure that the haploid gamete contains exactly one copy of each chromosome after the second meiotic division (MII), cohesion between sister centromeres must be retained to maintain an intact dyad chromosome following anaphase I (Petronczki *et al.*, 2003; Watanabe, 2005). During metaphase of MII, sister centromeres of dyad chromosome establish bipolar kinetochore-microtubule attachments and become bi-oriented (Petronczki *et al.*, 2003; Hauf and Watanabe, 2004). When anaphase II is triggered, cohesion between sister centromeres is dissolved and the pulling forces of the MII spindle segregate chromatids to opposite poles (Nasmyth, 1999; Petronczki *et al.*, 2003).

While male meiosis produces four spermatozoa, female meiosis ejects two non-viable structure know as polar bodies and produces only a single viable oocyte which retains most of the cytoplasm to support subsequent embryo development (Herbert *et al.*, 2015). Although the mechanics of meiosis are similar between female and male, female mammals possess unique features associated with its coordination with a long process of oogenesis.

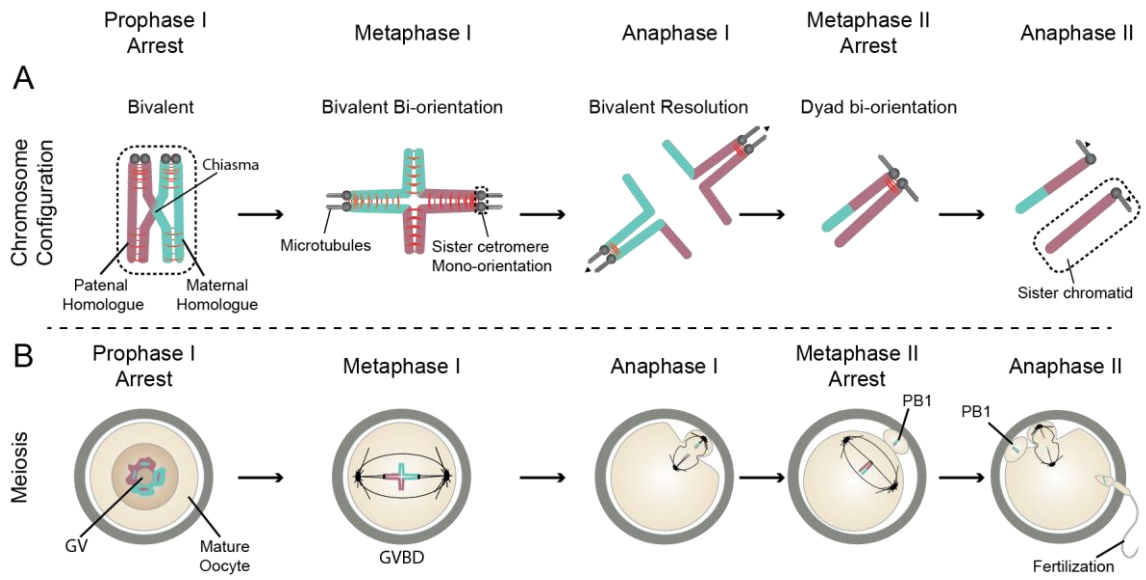

Figure 1.2 Meiotic division in female mammals

The schematic illustrates the process for haploidization in the context of female meiosis; the process begins on the right and arrows indicate the flow. **A** Bivalent chromosomes formed by recombined parental homologues are maintained during prophase arrest. Bi-orientation of bivalent during metaphase I occur when sister centromeres become mono-oriented. During anaphase I, bivalents are resolved to dyad chromosomes. At metaphase II sister centromeres become bi-oriented and sister chromatids are separated during anaphase II. **B** Cytological changes during female meiosis. During prophase arrest oocyte remains at germinal vesicle (GV) stage. Bivalent chromosomes align in the metaphase plate after germinal vesicle breakdown (GVBD). Half of the chromosomes segregate to the 1st polar body during anaphase I. The oocyte then arrests at metaphase II awaiting for fertilisation, which triggers anaphase II and extrusion of the second polar body. The figure has been modified from (Herbert *et al.*, 2015).

1.3. The unique features of female meiosis

During early embryonic development, primordial germ cells (PGCs) migrate from the vitelline sac to the primitive gonad where they undergo several rounds of mitotic divisions with incomplete cytokinesis. The resulting interconnected cells (oogonia) then form cysts (de Cuevas *et al.*, 1997; Pepling and Spradling, 1998). While still part of the cyst mitotically dividing cells, finally enter meiosis following a last pre-meiotic round of DNA replication. Maternal and paternal homologues undergo reciprocal exchange of DNA to form crossovers to form bivalent chromosomes. This occurs during prophase of meiosis I, which, based on cytological observations, is divided into four phases of meiotic prophase (Leptotene, Zygotene, Pachytene and Diplotene) (Pepling and Spradling, 1998; Pepling and Spradling, 2001).

During the first stage of meiotic prophase, called Leptotene, chromatin condenses in thin strands. Subsequently, sister chromatids organise along the Axial Element (AE), which align matching sequences of Spo11-mediated DNA double strand breaks (DSB's) of homologue chromosomes (Kleckner, 2006). In Zygotene, the axial elements become linked by transverse filaments to form the Synaptonemal Complex (SC), which is the scaffold that assists the reciprocal exchange of DNA between parental homologues. At the end of Zygotene and beginning of Pachytene, synapsis between homologue chromosomes is complete and the four chromatids are aligned and held by the SC (Page and Hawley, 2004; Kleckner, 2006). After Dmc1-mediated repair, the DSB's mature into double-Holliday junctions (dHjs) which will resolve to form crossovers (Kleckner, 1996). The process of DNA DSB's repair can also result in the formation of non-crossover (Neale and Keeney, 2006). Chromosome decondensation and SC disassemble occur during Diplotene (Svetlanov and Cohen, 2004). Oocytes then remain arrested in meiotic prophase in a state also referred as dictyate.

Somatic cells from the cortex of the ovary invade the prophase-arrested oocyte cyst enclosing each oocyte within a single layer of flattened cells (pre-granulosa cells) to form the pool of primordial follicles (Borum, 1961; Borum, 1967; Pepling and Spradling, 2001). In mice, the cyst can be appreciated after 13.5 days post coitum (dpc). However, cyst-breakdown does not occur until the second day postpartum (dpp) (Borum, 1967; Pepling and Spradling, 2001). By contrast, in humans,

primordial follicles are already seen between 18 to 20 weeks of gestation (Maheshwari and Fowler, 2008). This process is accompanied by a widespread oocyte death, which reduces their number in the ovary. In humans, the oocyte number is estimated in about 7 million at the moment cyst-breakdown and reduces to 1 million at birth (te Velde *et al.*, 1998). Similarly, in mice, around 20,000 oocytes are present in the cyst at 13.5 dpc (days post coitum) but reduces to 7000 at two dpp (McClellan *et al.*, 2003).

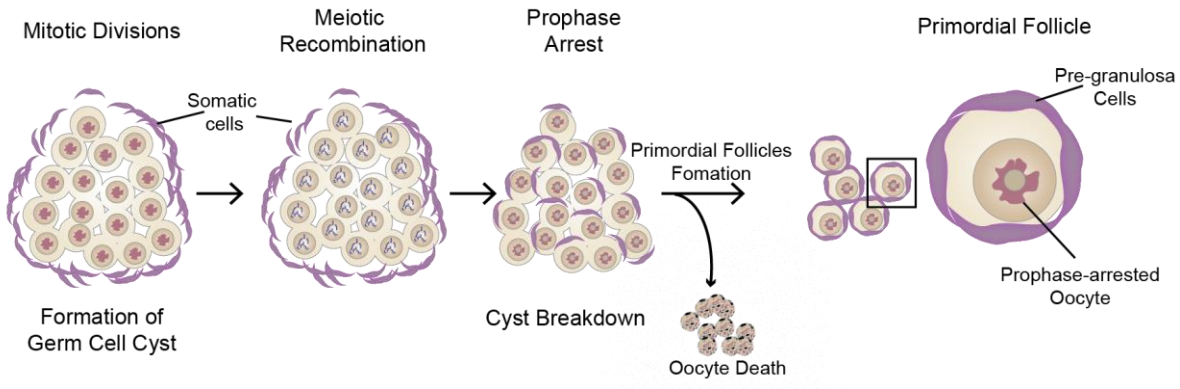

Figure 1.3 Formation of primordial follicles

Schematic shows the process during which primordial follicles are formed. Several rounds of mitotic divisions of the migrating germ cells form cysts in which they begin the first steps meiosis. The process of recombination occurs while oocytes are still in the cyst. Programmed cyst breakdown, which occurs after oocyte arrest at prophase just after diplotene, enclose individual oocytes within a single layer of flattened cells (pre-granulosa cells) to form primordial follicles. Cyst breakdown is accompanied by a widespread oocyte death. Primordial follicles consist of a prophase-arrested oocyte in a relatively quiescent state surrounded by a single layer of pre-granulosa cells.

The long-established view that the pool of oocytes is formed during fetal life (Borum, 1967) was challenged during the last decade when evidence indicating that neo-oogenesis occur during postnatal life from germ stem cells (Johnson *et al.*, 2004). However, this new view remains controversial due to several technical concerns on

the presented experimental approach (Zhang *et al.*, 2013; Handel *et al.*, 2014; Zhang *et al.*, 2015)

During female reproductive lifespan the number of primordial follicles becomes depleted from the ovary throughout the combined effect of the following three fates: i) remain in the quiescent state ii) succumb to death through atresia either in the primordial follicle stage or after being selected for growth iii) be recruited for growth, develop and ovulate after puberty (Adhikari and Liu, 2009). The progressive decline in the dormant population of primordial follicles throughout life leads to ovarian ageing and culminates in menopause (Faddy and Gosden, 1996).

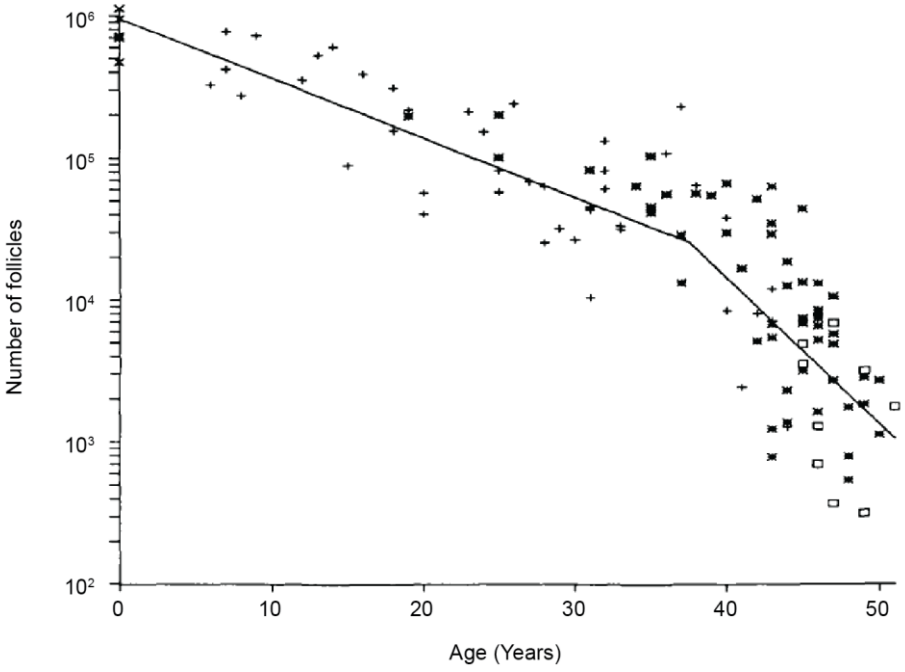

Figure 1.4 Biphasic decline in follicle number during female reproductive lifespan

Graph shows the biphasic model for decline of follicle number proposed by (Faddy *et al.*, 1992) in human ovaries from neonatal life to 51 years

Oocytes spend most of their life cycle at the primordial follicle stage, and most of them die at this stage by a process known as atresia (Gosden and Spears, 1997).

Throughout life, primordial follicles are recruited for growth on an ongoing basis by a Pten-AKT-mTOR –mediated mechanism (Reddy *et al.*, 2008). After mTOR is released from its inhibitor TSC1/TSC2 by AKT (Yang and Guan, 2007; Adhikari and Liu, 2009), the oocyte enters a period of high metabolic activity, increasing in diameter from ~10µm to approximately 80µm in mice before reaching the pre-ovulatory stage (Adhikari and Liu, 2014). Recruitment of primordial follicles for growth is accompanied by differentiation of the pre-granulosa cells from a flattened to a cuboidal shape (granulosa cells). Subsequent proliferation of granulosa cells adds several layers of cells around the oocyte, and theca cells from outside of the basal lamina become vascularized to provide nutritional support to developing follicles (Campbell *et al.*, 2013).

In my literature review, I found that all developmental stages of the ovarian follicles are well classified according to their size, shape and number of cells (Pedersen and Peters, 1968; Picton, 2001). However, the oocytes contained within them have no classification despite the marked differences in metabolism between an oocyte within a primordial follicle and a fully grown oocyte capable of supporting a new life within an antral follicle. For the purpose of this manuscript, we will refer to the oocyte enclosed within the primordial follicles as “primordial-stage oocyte” due to their relatively quiescent state. Oocytes within the growing follicles will be called “growing oocytes”.

While the mechanism by which primordial follicles are recruited for growth has been elucidated, how they are selectively activated remains elusive (Adhikari and Liu, 2009). After puberty, oocytes can reach the pre-ovulatory stage only if the growing follicle become dominant among the whole cohort of growing follicles (Baker and Spears, 1999). Those oocytes contained within growing follicles that cannot reach dominance succumb to atresia (Gosden and Spears, 1997). Follicular dominance is a mechanism by which mammalian can regulate the number of oocytes to ovulate and therefore control the size of the litter (Spears *et al.*, 1996). In women, a tiny fraction of the oocytes formed during fetal life will be ovulated during the 30 to 40 years interval between puberty and menopause.

Growing follicles pass through two selection phases before reaching ovulation (Baker and Spears, 1999). Most of the recently recruited primary follicles progress through

the early stages in a process independent of gonadotropins (Figure 1.5). Under cyclical basis from puberty to menopause, only a fraction of preantral follicles from the cohort are selected to develop the later antral stages in the presence of optimal levels of circulating follicle-stimulating hormone (FSH) (Kumar *et al.*, 1997; Baker and Spears, 1999).

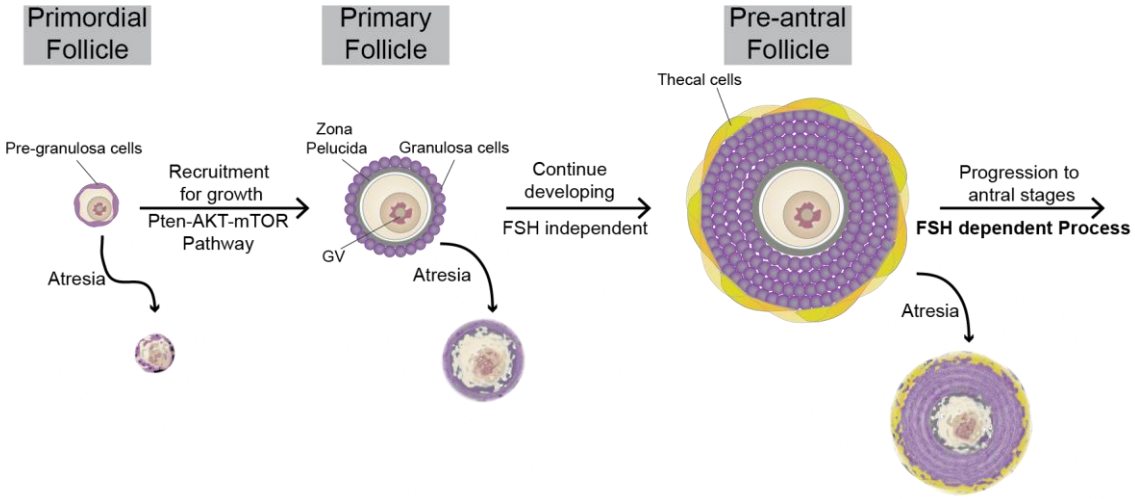

Figure 1.5 Recruitment for growth of primordial follicles and initial stages of follicular development.

The diagram illustrates the gonadotrophin-independent stages of follicular development. Primordial follicles are recruited for growth by the Pten-AKT-mTOR pathway. The pre-granulosa cells surrounding the primordial-stage oocyte differentiate into granulosa cells concomitant with the initiation of oocyte growth. In a process independent of FSH primary follicles form additional layers of granulosa cells and ovarian somatic cells give rise to the theca cells, which form an outer layer of cells. This process continues until the follicle reaches the pre-antral stage. The transition from pre-antral to antral follicles is dependent upon increased levels of circulating FSH. Follicles can succumb to atresia at any of these stages of follicular development. The figure has been modified from (Herbert *et al.*, 2015).

Dominant follicles emerge after the second phase of selection. To achieve dominance, the largest follicles have to firstly increase levels of oestradiol and inhibin in the circulatory system to initiate the decline of FSH levels produced by the pituitary gland. Secondly, they have to exert inter-follicular control to reduce the responsiveness of subordinated follicles (less developed) to FSH (Baker and Spears, 1999) by increasing the production of anti-müllerian hormone (AHM) and other signaling such as inhibin (Durlinger *et al.*, 1999; Durlinger *et al.*, 2002; Gruijters *et al.*, 2003). Dominant follicles develop an antrum and reach a preovulatory stage in which granulosa cells are divided into two types, those who remain associated with the oocyte (cumulus cells), others that will continue to be associated with the basal lamina (mural cells) (Adhikari and Liu, 2014) (Figure 1.6).

The preovulatory surge of luteinizing hormone (LH) dissociates the oocyte-cumulus complex closing their gap junctions (Granot and Dekel, 1994), this stops the flow of cGMP, which prevent hydrolysis of cAMP, from the cumulus cells to the oocyte (Mehlmann, 2005; Norris *et al.*, 2009). The oocyte restarts meiosis when the decreasing levels of cAMP activate Cdk1. Activation of Cdk1 promotes association of APC/C with Cdc20 (Fujimitsu *et al.*, 2016) which triggers the entry of the oocyte in anaphase I. During anaphase I, which occurs shortly before ovulation, bivalents are converted to dyad chromosomes upon dissolution of arm cohesion. Dyad chromosomes align on the MII spindle and oocytes remain arrested at this stage until after sperm entry.

In summary, accurate segregation during MI requires that bivalent chromosomes, formed during foetal life, must remain intact until shortly before ovulation, which can correspond to more than four decades in women. By contrast, spermatozoa are produced continuously throughout the male reproductive lifespan and only ~8 days in mice (Griswold, 2016) and ~24 days in human (Heller and Clermont, 1963; Amann, 2008) elapse between formation and resolution of bivalent chromosomes. The co-ordination of oogenesis with meiosis necessitates an extraordinarily long period of arrest in prophase of meiosis I, which may render the bivalent chromosome

architecture susceptible to structural defects that may subsequently increase the risk of missegregation.

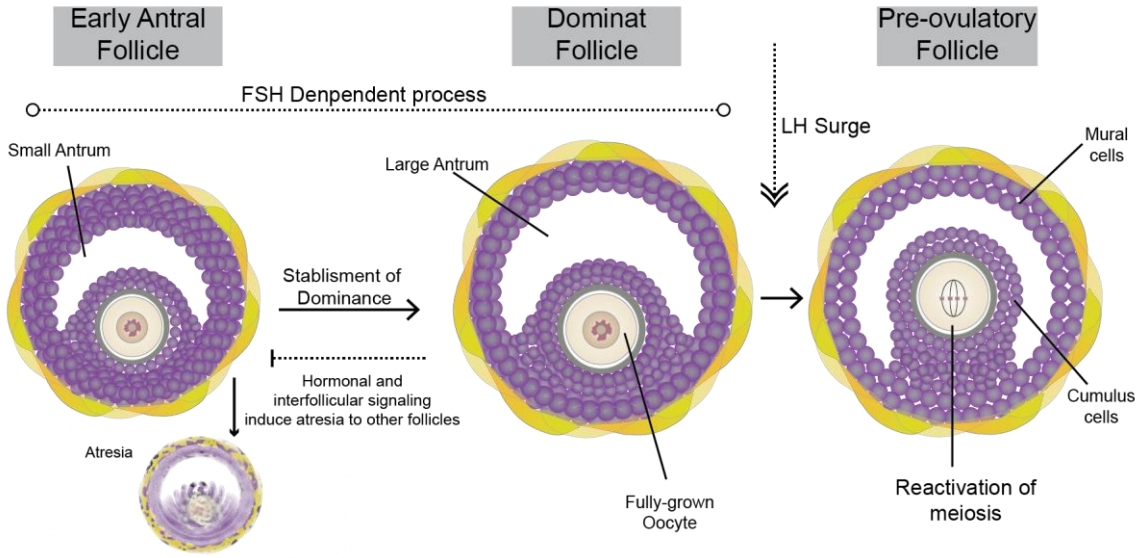

Figure 1.6 Antral stages of folliculogenesis

Schematic illustrating ovarian follicle development during the gonadotrophin-dependent stages. The development of the early antral follicles is dependent on the levels of FSH. Through the establishment of dominance, the largest antral follicles are selected to ovulate. To appropriate most of the available FSH, large antral follicles limit the consumption of FSH by smaller follicles slowing their growth. Ovulation of the dominant follicles is triggered by the LH surge, which is released by the pituitary in response to increasing levels of estradiol. The gap junctions between the oocyte and the cumulus cells close and the fully-grown oocyte makes the transition from prophase arrest to M-phase of meiosis I. The figure has been modified from (Herbert *et al.*, 2015).

1.4. Molecular regulation of chromosome segregation during meiosis

In most organisms, accurate segregation of homologous chromosomes requires that they become physically linked at the sites of meiotic recombination to form a bivalent

chromosome structure. Bivalents are stabilised by arm cohesion distal to the site of crossovers. As in mitosis cohesion between chromosome arms (and centromeres) is mediated by the Cohesin complex (Nasmyth and Haering, 2009).

1.4.1. *Cohesin – structure, function and establishment of cohesion*

Cohesin is a multi-subunit protein complex consisting of two core subunits members of the structural maintenance chromosomes (SMC) family and one α-kleisin subunit. The two core subunits Smc1 and Smc3 fold themselves in a hinge domain and extend in an antiparallel coiled-coil structure ending in an ATPase head formed by the N- and C- terminals (Hirano and Hirano, 2002; Nasmyth and Haering, 2009; Peters and Nishiyama, 2012). Smc1 and Smc3 bind together by their hinge domain and the ATPase heads are interconnected by the α-kleisin subunit (Scc1) which acts as a bridge between the two heads (Haering *et al.*, 2004; Nasmyth and Haering, 2009; Peters and Nishiyama, 2012). These subunits form a ring-like structure (Figure 1.7), which is thought to entrap and hold sister chromatids together.

Two versions have been proposed to explain how cohesin rings hold sister chromatids together (Nasmyth and Haering, 2009). The ring entrapment model proposes that a single ring embraces sister chromatids (Haering *et al.*, 2008). This model was supported when sucrose gradient sedimentation and purification through electrophoresis showed that sister chromatids of circular minichromosomes from yeast were concatenated by a monomeric cohesin ring, whose subunits are covalently cross-linked (Haering *et al.*, 2008). However, arguments against the ring entrapment model suggest that it is not flexible enough to allow cohesin to carry out its other functions during DNA replication (Zhang *et al.*, 2008b). The handcuff model proposed that cohesion is established by two different rings interacting by an SA1/SA2 (SA3 in meiosis) subunit; each one of them embracing separate sister chromatids (Zhang *et al.*, 2008b). In support of this handcuff model, coimmunoprecipitation of α-kleisin cohesin subunits (Flag-Rad21 and Myc-Rad21) was blocked by silencing SA2 using siRNA (Zhang *et al.*, 2008b). Nevertheless, it is considered that physiological formation of multimeric cohesin rings to establish chromatid cohesion lack of firm evidence (Nasmyth and Haering, 2009). Currently,

the ring entrapment model is the most accepted and also referred as the “strong” version, while dimeric ring models of cohesion such as the handcuff or the interconnected cohesin rings are referred as the “weak” version (Nasmyth and Haering, 2009).

Cohesin has been found to be involved in a wide variety of functions such as repair of DNA double-strand breaks, assembly of replication factories during S-Phase and regulation of transcription among others (Nasmyth, 2011). However, the fundamental function of cohesin is to ensure accurate chromosome segregation by clamping sister chromatids together from the time they are formed in S-phase until they disjoin in anaphase. In meiosis, cohesin entraps replicated DNA molecules and hold sister chromatids together to stabilise the bivalents and assist kinetochores to co-orient correctly in the spindle during both meiotic divisions (Petronczki *et al.*, 2003; Peters and Nishiyama, 2012). Meiotic-specific subunits of the subunit of cohesin in mammalian gametes include Smc1β (Figure 1.7), which is the homologue of the mitotic Smc1, and Rad21L which is a recently discovered α-kleisin subunit (Lee and Hirano, 2011). The cohesin’s α-kleisin subunit Rec8 (Figure 1.7), which is the meiotic paralog of mitotic α-kleisin Scc1, plays an important role in the ability of meiotic cells to undergo two consecutive rounds of chromosome segregation without an intervening phase of DNA replication.

Inducing metaphase I arrest by injecting fag-Mad2 in mouse oocytes whose endogenous Rec8 contains TEV recognitions sites (*Rec8*$^{TEV/TEV}$), Tachibana-Konwalski *et al.* (2010) observed that oocyte microinjection of TEV mRNA protease triggers the conversion of bivalent chromosomes into dyads and subsequently into individual chromatids. In similar experiments using *Scc1*$^{TEVMyc/TEVMyc}$ mouse oocytes, it was observed that Scc1-Myc is abundant in the chromatin of GV stage oocytes but none was detected after the injection of TEV protease in metaphase I arrested *Scc1*$^{TEVMyc/TEVMyc}$ oocytes. Interestingly, bivalent chromosomes remain intact after the injection of TEV protease in metaphase I arrested *Scc1*$^{TEVMyc/TEVMyc}$ oocytes. These experiments evidence that only Rec8-containing cohesin complexes are essential for establishing chromosome cohesion in postnatal mouse oocytes (Tachibana-Konwalski *et al.*, 2010).

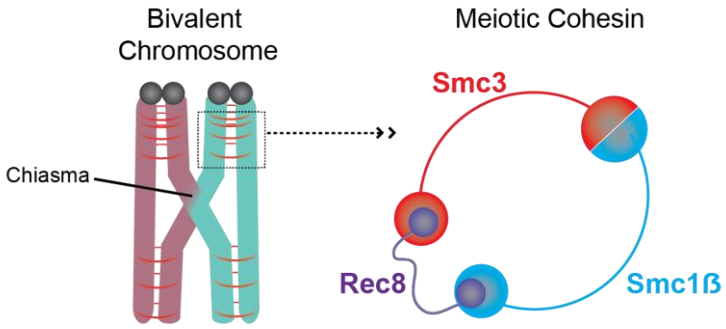

Figure 1.7 Structure of meiotic cohesin

The drawing illustrates cohesin rings (shown in red) on a bivalent chromosome. Cohesin is embracing sister chromatids together to stabilise the chiasma. Arrow points to a magnified meiotic cohesin complex, constituted by three subunits: Smc3, Smc1β and Rec8. The figure has been modified from (Herbert *et al.*, 2015).

In vertebrate cells, cohesin begins loading onto the chromosomes from the telophase stage (Gerlich *et al.*, 2006), which occurs after anaphase. However, the tethering of emerging DNA from the replication fork occurs during S-Phase (Uhlmann and Nasmyth, 1998). Entry of sister DNAs into the ring occurs at the Smc1-Smc3 interface (Nasmyth, 2011). To hold sister chromatids together, cohesin entraps replicated DNA molecules when Smc3 subunit is acetylated at lysine residues K105 and K106 by ESCO1 and ESCO2 during S-Phase (Zhang *et al.*, 2008a). How stable is the cohesin-DNA association is determined by the interaction of Pds5, WAPL and Sororin with cohesin (Figure 1.8). The cohesin's α-kleisin subunit recruits Pds5 which forms a heterodimer with WAPL (Panizza *et al.*, 2000; Kueng *et al.*, 2006). Cohesin association with the WAPL-Pds5 heterodimer leads to a dynamic DNA-cohesin interaction as WAPL dissociates the α-kleisin-Smc3 interface of cohesin which results in cohesin unloading from the DNA (Peters and Nishiyama, 2012). Sororin antagonises WAPL and promotes stable DNA-cohesin interaction by interacting with Pds5 and displacing WAPL (Nishiyama *et al.*, 2010). It has been recently discovered that sororin actively maintains sister chromatid cohesion during S-Phase, G2 and prometaphase in mitotic cells (Ladurner *et al.*, 2016).

Burkhardt *et al.* (2016) designed a cohesion rescue assay adding a conditional silent BAC containing a STOP cassette flanked by *loxP* sites (*TG STOP-Rec8-Myc*) to activate Rec8-Myc expression in *Rec8*$^{TEV/TEV}$ mouse oocytes. They induced the Cre-mediated deletion of the STOP cassette by injecting tamoxifen in adult mice to test whether the cohesin lost during ageing is restored by new cohesin rings containing Rec8-Myc. Two and four months after the tamoxifen injection, they harvested GV-stage oocytes and injected then with TEV protease. (Burkhardt *et al.*, 2016) observed that 100% of the oocytes with activated Rec8-Myc exhibit single chromatids in meiosis I (Burkhardt *et al.*, 2016)

These experiments suggest that in meiosis only Rec8-containing cohesin complexes loaded during fetal life can confer cohesion to oocyte chromosomes without a detectable turnover during the adult life (Burkhardt *et al.*, 2016).

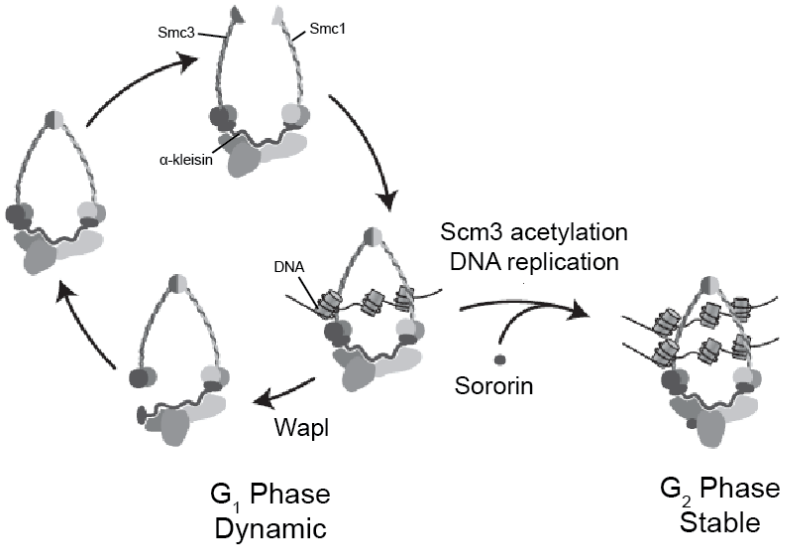

Figure 1.8 Establishment of cohesion

The schematic shows how cohesin establishes cohesion between sister chromatids. The drawing at the top shows a cohesin ring opened at the Smc3-Smc1 hinge to facilitate entry of sister DNA molecules. During G_1 phase, WAPL antagonises cohesion establishment by opening the α-kleisin-Smc3 interface of the cohesin ring. WAPL activity induces dynamic binding of cohesin rings and DNA, creating a cycle of DNA loading and unloading. During S-phase, Smc3 acetylation and the antagonising action of sororin against WAPL create stable DNA-cohesin associations that can hold sister chromatids together. Figure modified from (Peters and Nishiyama, 2012)

1.4.2. *Removal of cohesin – chromosome segregation in mitosis*

Chromosome segregation during anaphase is a highly regulated event, which ensures transmission of the genome to daughter cells. Synchronisation between the pulling forces exerted by the spindle and the dissociation of cohesin from sister chromatids is essential to guarantee accurate chromosome segregation. To understand the molecular mechanisms that regulate chromosome segregation in

meiosis, it is important to first understand how the process is regulated in mitotic cell division.

In contrast to meiosis, mitotic cells undergo only one round of chromosome segregation following a single round of DNA replication. Two distinct mechanisms remove cohesin from the chromosome (Waizenegger *et al.*, 2000). Dissolution of cohesion during mitotic anaphase depends on cleavage of Cohesin's α-kleisin subunit, Scc1 (Rad21) by separase (Uhlmann *et al.*, 1999).The proteolytic activity of separase is controlled prior anaphase by its inhibitory chaperone securin and by phosphorylation mediated by Cdk1-CyclinB1 (Stemmann *et al.*, 2001; Herbert *et al.*, 2003). Hence activation of separase requires degradation of securin and cyclin B1. Once kinetochores are attached and chromosomes correctly aligned on the metaphase plate, the spindle assembly checkpoint (SAC) allows Cdc20 to activate the E3 ubiquitin ligase anaphase-promoting complex/cyclosome (APC/C) (Lara-Gonzalez *et al.*, 2012). As a result, separase is released when APC/C^{Cdc20} target for destruction securin and CyclinB1 (Peters, 2002). Consequently, separase cleaves Scc1 and dissociates residual cohesin from the chromosome arms and the centromeres (Figure 1.9, B). The pulling forces of the spindle segregate disjoined sister chromatids to opposite poles (Ciosk *et al.*, 1998; Peters, 2002). Mitosis concludes with two diploid daughter cells after cytokinesis.

A second separase-independent pathway for removing the bulk of cohesin from the chromosome arms was discovered and named "the prophase pathway" (Waizenegger *et al.*, 2000). During mitotic prophase, Scc1 and SA2 subunits are phosphorylated. Experiments in mitotic *Xenopus* eggs extracts showed that Polo-like kinase (Plk1) mediates phosphorylation of Scc1 and SA2 decreasing the binding of cohesin to the chromosomes (Sumara *et al.*, 2002). However, this is not sufficient to remove cohesin. WAPL overexpression during prophase results in premature loss of sister cohesin while depletion of WAPL reduces cohesin dissociation in prophase (Gandhi *et al.*, 2006; Kueng *et al.*, 2006). These experiments showed that WAPL has a key role dissociating cohesin from the chromosomes during mitotic prophase (Figure 1.9, A)(Gandhi *et al.*, 2006; Kueng *et al.*, 2006). Cohesin is removed from the chromosome arms through the prophase pathway by applying the synergic forces of Plk1 and WAPL.

The prophase pathway is able to distinguish arm cohesin from centromeric cohesin thanks to the protective action of Shugoshin 1 (Sgo1). This was evident as depletion of Sgo1 caused premature dissociation of sister centromeres (McGuinness *et al.*, 2005). To protect centromeric cohesin from removal by the prophase pathway, Sgo1 binds to the phosphatase PP2A to prevents phosphorylation of SA2 (Riedel *et al.*, 2006) and counteract WAPL by maintaining a hypophosphorylated state of sororin bound to cohesin (Liu *et al.*, 2013). Centromeric localisation of Sgo1 requires the presence of PP2A at the centromeres (Tang *et al.*, 2006) and its localisation is regulated via phosphorylation of histone H2A at threonine 120 by Bub1 (Kawashima *et al.*, 2010). Immunofluorescence microscopy experiments showed that some Scc1 and Sgo1 was also localised at the chromosome arms at the onset of anaphase, suggesting that not all cohesin can be dissociated from the chromosome arms by the prophase pathway (Nakajima *et al.*, 2007). The residual cohesin along chromosome arms and at centromeres is then removed during anaphase by a separase-mediated cleavage of cohesin's α-kleisin subunit Scc1 (Uhlmann *et al.*, 2000).

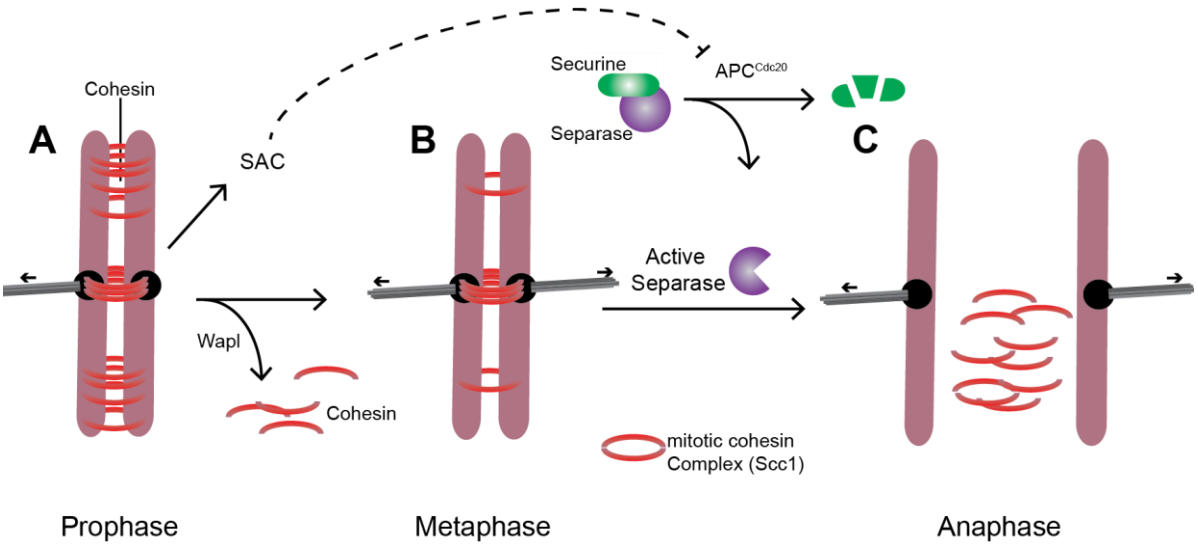

Figure 1.9 Cohesin dissolution and chromosome segregation during mitosis
The diagram shows a representation of the two mechanisms to remove cohesin from the chromosomes during mitosis. **A** shows two sister chromatids held together by cohesin. During prophase part of cohesin is removed from the arms by WAPL; SAC prevents the activation of APC/C until the chromosomes are correctly bi-oriented. **B** in metaphase chromosomes are correctly bi-oriented the APC/C is activated to ubiquitinate securin. Separase is released to remove cohesin from the centromeres and the remnants of cohesin in the chromosome arms. **C** The pulling forces of the spindle segregate the sister chromatids to opposite poles of the spindle. Figure modified from (Herbert *et al.*, 2015) and (Petronczki *et al.*, 2003)

1.4.3. *Removal of cohesin – chromosome segregation in meiosis*

Similar yet different, in meiosis, two consecutive rounds of chromosome segregation are possible thanks to the meiotic-specific α-kleisin Rec8, the paralog of mitotic Scc1. Disjunction of homologue chromosomes during the first meiotic division requires separase-mediated cleavage of Rec8 along the chromosome arms (Kudo *et al.*, 2006; Kudo *et al.*, 2009). Adequate function of separase requires the phosphorylation of cohesin's α-kleisin subunit. While in yeast Cdc5 phosphorylates Rec8 (Brar *et al.*,

2006), SDS-PAGE assay showed that, in mouse oocytes, Rec8 is reduced in a dose-dependent manner by Plk1. In addition, two cleavage sites of Rec8 appear in the presence of active separase suggesting that Plk1 phosphorylates cohesin's α-kleisin subunit in mouse oocytes (Kudo *et al.*, 2009).

As in mitosis, activation of separase is regulated by the APC/C (Herbert et al, 2013, Kudo et al, 2006). The goal of the first meiotic division is to resolve the chiasma and segregate recombined maternal and paternal homologues to opposite poles. Bi-orientation of the bivalent chromosome at metaphase I needs that sister centromeres adopt a side-by-side configuration to create monopolar kinetochore-microtubule attachments (Hauf and Watanabe, 2004). Upon correct bi-orientation of all bivalent chromosomes on the metaphase plate, SAC releases the APC/C cofactor cdc20 which will ubiquitinate the separase inhibitory chaperone known as securin (Wassmann *et al.*, 2003; Homer *et al.*, 2005) (Figure 1.10)

Separase-mediated cleavage of Rec8 removes cohesin from the chromosome arms in anaphase I (Kudo *et al.*, 2006). Crucially, cohesin at the centromeres persists. Loss of arm cohesin resolves the chiasmata and converts bivalents to dyad chromosomes. Protection of centromeric cohesin is essential for accurate segregation during anaphase of MII.

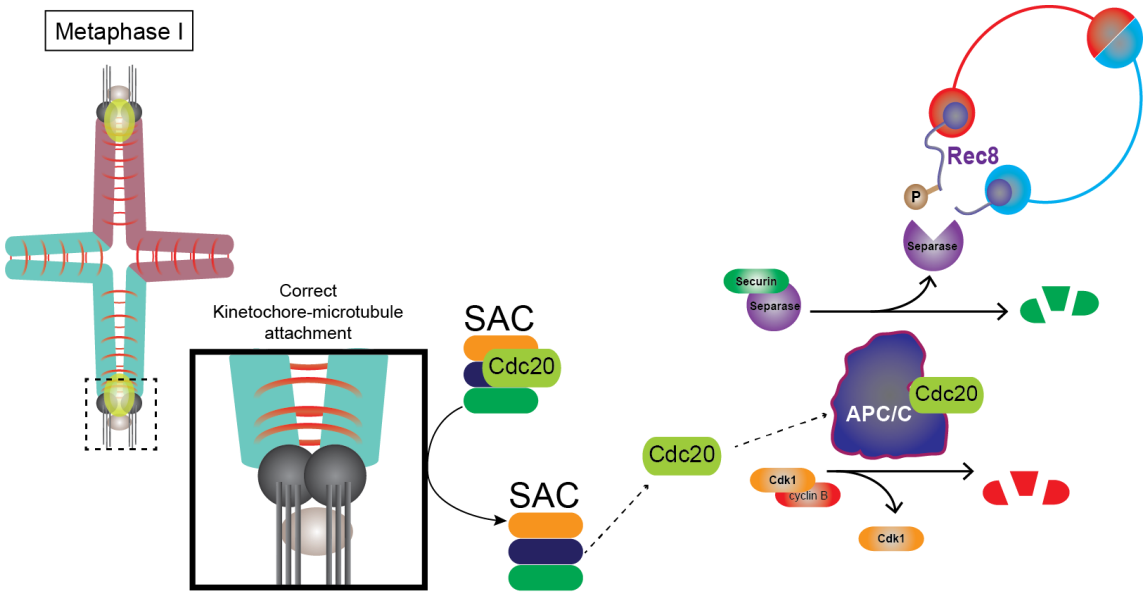

Figure 1.10 Activation of Separase

The diagram explains the chain of events occurring during metaphase I that leads to the activation of separase in anaphase I. In metaphase I bivalent chromosomes bi-orient in the MI spindle. The inset is showing a magnification of sister centromeres adopting a side-by-side configuration essential for monopolar kinetochore-microtubule attachments. Under the control of the SAC, Cdc20 targets cyclin B and securin to the APC/C. Ubiquitination of cyclinB1 and securin by the APC/C will release separase. The cleavage of phosphorylated Rec8 by separase will remove cohesin from the chromosome arms during anaphase I. The figure has been modified from (Herbert *et al.*, 2015).

How is centromeric cohesin protected from the proteolytic activity of separase during anaphase I? In yeast, separase cleavage of Rec8 requires its phosphorylation by Hrr25 and Cdc7 (Katis et al, 2010). This property enables Rec8 to be protected from separase by a counteracting phosphatase. The discovery of Shugoshin (Sgo) proteins ("guardian spirit" in Japanese) (Kitajima *et al.*, 2004; Watanabe, 2005) solved one of the major mysteries of meiosis. Shugoshin, which is a homologue of Drosophila MeiS332 (Kitajima *et al.*, 2004), protects centromeric cohesin by recruiting the phosphatase PP2A.

The aim of the second meiotic division is to segregate sister chromatids and produce a single copy of each chromosome. To achieve this, sister kinetochores adopt a back-to-back configuration to establish bipolar kinetochore-microtubule and become bi-oriented on the MII spindle (Hauf and Watanabe, 2004). In yeast, accumulation and disappearance of securin (Cut2) occur during metaphase I and subsequently during metaphase II (Kitajima *et al.*, 2003). This suggests that separase (Cut1) is activated momentarily twice during meiosis, the first one in anaphase I, and the second one in anaphase II (Kitajima *et al.*, 2003).

In mammals, anaphase II is triggered by the sperm entry. The mechanism by which centromeric Rec8 protection is alleviated to enable centromeric cohesin to be cleaved during anaphase II is controversial. One group has proposed that "deprotection" occurs upon establishment of tension following bi-orientation of sister centromeres in MII (Lee *et al.*, 2008). According to this model, oocytes may be rendered vulnerable to premature loss of centromeric cohesin during the period when they are arrested at MII in preparation of fertilisation. An alternative proposal is that a histone chaperone I2PP2A inhibits PP2A (Chambon *et al.*, 2013). However, how such a mechanism might be regulated has not been elucidated.

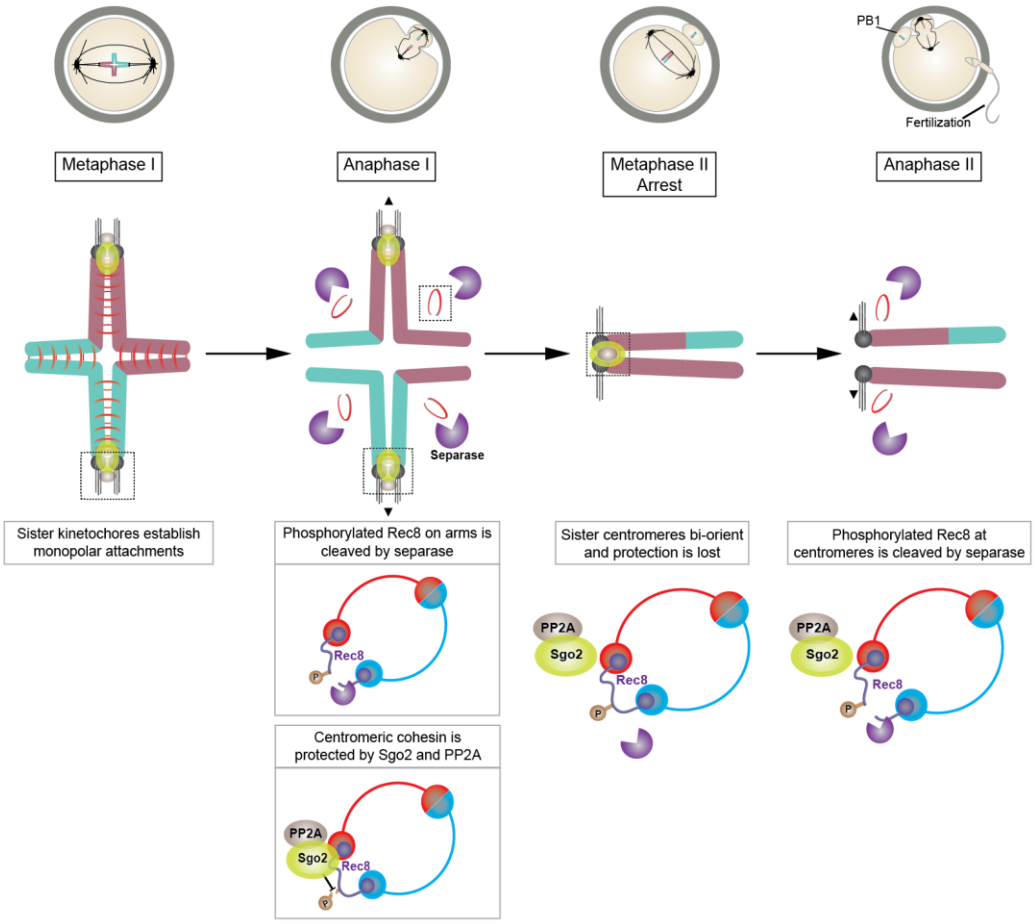

Figure 1.11 Cohesin removal from the chromosomes in the context of female meiosis

Diagram illustrates the architecture of the chromosomes depending on where is cohesin located in each one of the stages of meiosis. In metaphase bivalent chromosomes are aligned in the metaphase plate and bi-oriented in the MI spindle with sister kinetochores establishing monopolar attachments; cohesin is located along the chromosome arms and at the centromeres. During anaphase I, cohesin along the chromosome arms is removed by separase, while centromeric cohesin is protected by Sgo2-PP2A. Loss of arm cohesin converts bivalents to dyads. Oocyte arrest at metaphase II, sister centromeres establish bipolar kinetochore attachments and bi-orient in the MII spindle; only centromeric cohesin hold sister chromatids together and its protection by Sgo2-PP2A must be disabled before the onset of anaphase II. Upon fertilisation, separase is reactivated and centromeric cohesin is removed during anaphase II; dyad chromosomes are resolved to single chromatids. The figure has been modified from (Herbert *et al.*, 2015)

1.5. What do we know about the maternal age-effect at the molecular level?

Although, for a very long time birth defects have been associated with increasing maternal age (Penrose, 1933), plausible molecular candidates have only recently begun to emerge. While population studies indicated that the risk of trisomy 21 was linked to the position and number of crossovers formed during fetal life, this was later found not to be the case for older women (Lamb *et al.*, 2005; Oliver *et al.*, 2008). These findings indicated that trisomy in older women is due to events occurring subsequent to crossover formation.

More recently work in our lab (Lister *et al.*, 2010) and others (Chiang *et al.*, 2010) has provided support to the "cohesin deterioration" hypothesis. According to this hypothesis, cohesin becomes gradually depleted from oocyte chromosomes during female ageing. In support of this, mice carrying a functional deletion of the meiosis-specific SMC1β subunit show an age-related deterioration in bivalent chromosome structure (Hodges *et al.*, 2005). Furthermore, Immunofluorescence experiments of chromosome spread from MI and GV-stage oocytes obtained from naturally aged wild-type mice showed that chromosomal Rec8 is reduced in oocytes from older mice. (Chiang *et al.*, 2010; Lister *et al.*, 2010). This indicates that chromosome-associated cohesin declines during female ageing. Crucially, work in mice indicates that there is no reloading of cohesin during prophase arrest (Tachibana-Konwalski *et al.*, 2010; Burkhardt *et al.*, 2016).

In addition, to cohesin depletion, we found that recruitment of Sgo2 to centromeres is reduced in oocytes from aged females. Moreover, the finding indicated that cohesin is either directly or indirectly required for recruitment of Sgo2 to oocyte chromosomes at the transition from prophase to M phase of MI (Lister et al, 2010). Thus, age-related loss of cohesin is likely to be amplified by reduced recruitment of Sgo2.

We (Lister *et al.*, 2010) and others (Chiang *et al.*, 2010) also perform immunofluorescence staining of centromeres using CREST and reported that there is an increased distance between sister centromeres in oocytes from older females during MI (Chiang *et al.*, 2010; Lister *et al.*, 2010). In addition, oocytes from older mice have increased proportion of distally associated homologues compared to

oocytes from younger females. This suggests that age-related depletion of cohesin is associated with destabilisation of bivalents chromosomes (Lister *et al.*, 2010).

Findings in humans showed that loss of bivalent integrity together with the loss of the unified configuration of sister centromeres increase the risk of merotelic kinetochore-microtubule attachments, which prompt chromosome missegregation in advance maternal age (Zielinska *et al.*, 2015).This is compatible with the types of segregation errors observed in mouse oocytes (Sakakibara *et al.*, 2015). Immunofluorescence experiments showed that the three meiotic-specific cohesin subunits (Rec8, Smc1β and Smc3) participate in chromosomal cohesion in human oocytes from prophase to metaphase II (Garcia-Cruz *et al.*, 2010). However, results of direct cohesin measurements with functional assays in human oocytes during female ageing has not been reported yet.

While cohesin's functions together with loss provide a plausible explanation for age-related oocyte aneuploidy, it has also been proposed that defects in oocyte SAC function may underlie age-related segregation errors (Sebestova *et al.*, 2012). However, while the SAC prevents activation of the APC/C in the existence of unattached kinetochores, it has been observed in yeast and mice that it cannot detect the presence of bi-oriented sister centromeres in MI (Kouznetsova *et al.*, 2007; Sakuno *et al.*, 2011). This suggests that meiotic SAC is not sensitive to detection of premature separation of sister centromeres, which is the most prevalent age-related defect in mouse and human oocytes. We, therefore, consider that cohesin depletion is the current "front-runner" in terms of identifying a molecular culprit for the maternal-age effect.

Chiang *et al.,* (2011) injected naturally aged wild-type mouse oocytes with mutated separase that was resistant to inhibition by securin. With this experiments, they showed that oocytes from old mice were more susceptible to cohesion loss (Chiang *et al.*, 2011). However, this experiments did not show whether the depletion of cohesin was due to premature activation of separase in oocytes from older mice. These results point that separase could be the prime culprit of cohesin depletion during female ageing.

To date, most of the experimental models that have been used for determining the mechanisms of oocyte aneuploidy during ageing have been performed from the stage fully-grown GV oocyte onwards. Tsutsumi *et al.,* (2014) reported that there was not reduction in levels of cohesin in ovarian oocytes from older women. However, the caveat of this study lies in the fact that the stages of oocyte development were not specified (Tsutsumi *et al.*, 2014). Therefore, a complete study of cohesin depletion during the protracted period of oocytes development has not been addressed until now.

The “line production” hypothesis stipulates that the first oocytes to enter meiosis are the first in ovulating and that these oocytes contain more crossovers (Henderson and Edwards, 1968). Therefore, the increase in oocyte aneuploidy is related to the decreasing number of oocytes in the ovary. This hypothesis has been used to explain the maternal age effect for several decades. Rowsey *et al.,* (2014) challenged this hypothesis using immunofluorescence experiments to study the foci number of crossover-associated proteins (MLH1) of prophase-stage oocytes in relation with gestational age. They found that there was no association between the number and placement of MLH1 foci with gestational age (Rowsey *et al.*, 2014), giving conclusive evidence that the “line production” hypothesis cannot explain the maternal age effect. Recently, a case-study report showed that the risk of trisomic pregnancies increases in cases of ovarian insufficiency (Haadsma *et al.*, 2010). However, whether cohesin depletion is linked to the depletion of the oocyte pool has never been shown.

Using the mouse model, the primary aims of my project were to investigate the mechanism and timing during oogenesis of age-related cohesin depletion. I also aimed to investigate the relationship between the age-related cohesin depletion and the decline in the ovarian reserve of oocytes. These questions are fundamental to gaining further insight into the possibility of developing strategies to reduce reproductive risk in older women.

Chapter 2. Objectives

2.1. Overall Objective

To understand the mechanisms and timing of cohesin depletion, to investigate whether cohesin depletion is linked to the exhaustion of the ovarian reserve of primordial-stage oocyte during ageing

2.2. Specific Objectives

1) Increased susceptibility of aged wild-type mouse oocytes to separase that is resistant to inhibition by securin (Chiang *et al.*, 2011) points to “separase” as the prime culprit for cohesin depletion during female ageing. Therefore, I aimed to determine whether age-related cohesin depletion is a consequence of leaky inhibition of separase activity leading to the gradual removal of cohesin during prophase of meiosis I in mouse oocytes. Here, I used a conditional *separase* knockout mouse to prevent age-related depletion of cohesin.

2) Meiosis has to coordinate with the prolonged period of oogenesis and it is still unclear whether cohesin depletion occurs at any particular stage of oogenesis (Tsutsumi *et al.,* 2014). Therefore, I aimed to determine whether all stages of oogenesis are equally susceptible to cohesin depletion. Here, I measured chromosome-associated cohesin at all stages of oocyte development during female ageing in mouse oocytes.

3) As the number of trisomic pregnancies increases in cases of ovarian insufficiency (Haadsma *et al.,* 2010), it appears that the depletion of the ovarian reserve of oocytes could be mechanistically linked to the depletion of cohesin. I aimed to determine whether age-related depletion of cohesin occurs by a parallel but independent mechanism to the exhaustion of the ovarian reserve. Here, I used a conditional *Pten* knockout mouse to accelerate the recruitment of primordial follicles into the growing pool to induce ovarian ageing in young mice.

Chapter 3. Material and methods

3.1. Mouse strains

For this project, I worked with three different mouse lines. Our collaborators, Kim Nasmyth and Nobuaki Kudo, kindly provided the *Separase* conditional knockout mouse which was generated using C57BL6 strain (Kudo et al., 2006). In this mouse, iCre recombinase activity was driven from the Gdf9 promoter. Also, our collaborators provided the *TG Rec8-Myc* which was generated on the B6CBAF2 background using a BAC transgene containing 9 copies of the human Myc-tag at the Rec8 C-terminus (Kudo et al., 2009). The *PTEN* knockout mouse was imported from Jackson Laboratories. This mouse was generated in C57BL/6J strain; crossed in our laboratory with *FVB-Ddx4-CreERT2* and backcrossed for six generations to C57BL/6J-*PTEN*. CreERT2 recombinase activity for this mouse model was induced in mice aged two weeks injecting 75mg/kg body weight of Tamoxifen (Sigma-Aldrich T5648) via intraperitoneal every 24 hours for five consecutive days according to Jackson Laboratories protocols and others (Madisen *et al.*, 2010).

The mice were housed and bred at the Institute of Human Genetics, Newcastle University. All procedures were conducted in accordance with the regulation of the Home Office.

3.2. Genotyping

Ear clips were taken from mice aged 2 weeks (youngest) following a code to assign the ID. For DNA extraction from the ear biopsy, 1ml lysis buffer (see section 3.15) supplemented with 10µl proteinase K (Roche Diagnostics Ltd – 3115887001) was prepare before the digestion. From this lysis solution, 100µl was added to the Eppendorf tube containing the biopsy and incubated at 55ºC overnight.

After the overnight incubation, 100µl of phenol:chloroform (Sigma-Aldrich - P3803) were incorporated to the digestion and mixed for 10 minutes in the rotatory platform (it is important to check that the digestion becomes white). Afterwards, the

Eppendorfs were centrifuged at 14000rpm for 10min, the supernatant was carefully retrieved ~80µl (is best to leave some DNA than collect contaminants) and place in a different Eppendorf pre-labelled with the same mouse-ID. To precipitate the DNA, 400µl of 100% ethanol precooled at 4ºC and 1µl of glycogen (Affymetrix UK Ltd - 77534 1 ML) were added and then centrifuged at 4ºC at 14000rpm for 30min.

Being careful not disturb the pellet, the whole solution (ethanol + extraction) was pipetted out from the tube. The pellet was washed adding to the tube 400µl of 70% ethanol (RNase and DNase free) and centrifuged again at 14000rpm for 10min (room temperature). The whole supernatant was pipetted out again and the Eppendorf opened was placed in the oven to allow the pellet to dry out in the oven at 37ºC for 15min (until the ethanol has evaporated). After the incubation 20µl of 1x TE (see section 3.15) were pipetted to allow the pellet to dissolve, the tube was closed and incubated at 50ºC for 30min in the oven. The final concentration of DNA was approximately 50ng/µl.

PCR-primers for all genetically modified mice lines are described in the following tables:

Table 1: Separase primers

Primer Type	**Sequence**
Forward	ACT GAC CGT GAC ATT GAC CGT TAC
Reverse	TTC ATC ACC CAA GCT CCA AGC AG

Table 2: Gdf9-iCre primers

Primer Type	**Sequence**
Forward	TCT GAT GAA GTC AGG AAG AAC C
Reverse	GAG ATG TCC TTC ACT CTG ATT C

Table 3: PTEN primers

Primer Type	**Sequence**
Forward	CAA GCA CTC TGC GAA CTG AG
Reverse	AAG TTT TTG AAG GCA AGA TGC

Table 4: Ddx4-CreERT2 Primers

Primer Type	**Sequence**
Transgene Reverse	GGC CAG GCT GTT CTT CTT AG
Internal Positive Control Forward	CTA GGC CAC AGA ATT GAA AGA TCT
Internal Positive Control Reverse	GTA GGT GGA AAT TCT AGC ATC ATC C
Transgene Forward	ATA CCG GAG ATC ATG CAA GC

Reactant for Polymerase Chain Reaction are: Nuclease-free water (Thermo Fisher Scientific Ltd - AM9930), 10xBuffer and Taq polymerase (New England Biolabs (UK) Ltd - M0267S) dNTP's (Roche Diagnostics Ltd – 11581295001)

The volume of the reactants for one PCR reaction and cycling are described in the following table according to the gene:

Table 5: PCR reactant volumes for Separase, PTEN and Gdf9-iCre

Reactant	***Separase* / *PTEN* / *Gdf9-iCre***
dH_2O	19.88 µl
10x Buffer	2.5 µl
10mM dNTP's	0.5 µl
Forward Primer	0.5 µl
Reverse Primer	0.5 µl
Taq polymerase	0.13 µl

Table 6: PCR reactant volumes for Ddx4-CreERT2

Reactant	*Ddx4-CreERT2*
dH_2O	18.88 µl
10x Buffer	2.5 µl
10mM dNTP's	0.5 µl
Forward Primer / 1	0.5 µl
Internal (+) control FWD / 2	0.5 µl
Internal (-) Control RVS / 3	0.5 µl
Reverse Primer / 4	0.5 µl
Taq polymerase	0.13 µl

Table 7: PCR Cycling for Separase, Gdf9-iCre and PTEN

Step	Temp ºC	Time	Note
1	94	2 min	
2	94	1 min	
3	58	2 min	
4	72	2 min	Repeat steps 2 to 4 for 30 cycles
5	72	5 min	
6	4	α	

Table 8: PCR Cycling for Ddx4-CreERT2

Step	Temp ºC	Time	Note
1	94	2 min	
2	94	20 sec	
3	65	15 sec	
4	68	10 sec	Repeat steps 2 to 4 for 10 cycles
5	94	15 sec	
6	60	15 sec	
7	72	10 sec	Repeat steps 5 to 7 for 28 cycles
8	72	2 min	
9	4	α	

3.3. Oocyte harvest

Only *Separase* and *TG Rec8-Myc* mice aged 2 and 15 months were super-ovulated by intraperitoneal injection of 7.5 IU of pregnant mare serum gonadotropin (PMSG) (Sigma- Aldrich, G4527) 48 hours prior oocyte retrieval.

After postmortem dissection, ovaries we transported in 15ml tubes containing pre-warm M2 medium (Sigma-Aldrich, M7167). In a heated laminar hood equipped with a stereoscope, ovaries were transferred to 60x15mm diameter culture dish (BD Biosciences, 351016) containing M2 medium supplemented with 100µM isobutylmethylxanthine (IBMX) (Sigma-Aldrich, I7018). This is to maintain high the levels of cAMP in the oocytes and prevent the onset of anaphase when released from the granulosa cells, a procedure that was carefully done by puncturing antral and large secondary follicles using insulin needles. Oocytes were handled using denudation pipettes (BioTipp, 14306) and stored at 37ºC in 35x10mm diameter culture dish (BD Biosciences, 353001) within 40µl M2+IBMX drops covered with filtered mineral oil (Sigma-Aldrich, M8410) until ready to culture.

3.4. Oocyte culture

At least 4 hours prior the culture, 35x10mm diameter culture dishes were set up with 5x 40µl drops of G-IVF Plus media (Vitrolife, 10134) covered with filtered mineral oil and equilibrated in a 5% CO_2 incubator at 37 ºC. For a synchronous resumption of meiosis, oocytes were meticulously washed through 9 G-IVF drops before placing them in the drop where they would mature. Within the first 2 hours of culture, oocytes were scored for GVBD and also for Polar Body extrusion after overnight maturation.

3.5. Oocyte Chromosome Spreads

On the day we aimed to fix the chromosomes on the slide, we dissolve 0.25g of Paraformaldehyde (PFA, Merck, 104005) in a 50ml falcon tube (Starlab, E1450-0) by adding 22.5ml of MilliQ water and 8µl of 5M Sodium Hydroxide (VWR, 102524X). The solution was incubated at 60ºC and vortexed regularly until the PFA was completely dissolved. Afterwards, the solution was cooled to room temperature and pH adjusted to 9.5 with 50mM boric acid (Sigma-Aldrich, B6768). Before the procedure for chromosome spreads, the solution of PFA is supplemented with 175µl of 20% Triton X-100 (Sigma-Aldrich, T8787) and 150µl of 0.5M DTT (Sigma-Aldrich, D9163) then it is filter sterilised.

The procedure for chromosome spread was carried out using a stereoscope on the bench at room temperature (20ºC) and oocytes were manipulated using glass denudation pipettes. A 60x15mm diameter culture dish was set up of 2x 40µl drops of acid tyrodes, 4x 40µl drops of warmed M2 media, 2x 40µl drops of 0.5% sodium citrate (VWR, 102425M). Before each round of chromosome spread, a polysine slide (Fisher Scientific, MNJ- 800-010F) is labelled, drawn a guideline on the back and placed on the PFA solution for coating. For general oocyte handling a maximum of 8 oocytes were transferred at the same time. From the maturation dish, oocytes are moved to acid tyrodes and washed in the two drops until the zona pellucida is completely removed. Afterwards, oocytes are washed throughout the four drops of M2 media to remove the acid tyrodes. Subsequently, oocytes are left in one of the drops of sodium citrate for two minutes. When the oocytes have 50 seconds left in the sodium citrate the slide is removed from the PFA, the excess tapped off on a

paper towel and place in an humidified chamber. Oocytes are picked up from the sodium citrate 20 seconds before the end of their 2 minutes incubation. The humidified chamber is positioned under the microscope, focus on the guide line on the back of the slide. Oocytes are expelled onto the slide in as little sodium citrate as possible and observed when they burst. Marking where the first and last oocytes were dropped. Slides are left to dry overnight in the humidified chamber.

Next day, a box is drawn with Immedge Hydrophobic Barrier Pap pen (Vector Laboratories, H-4000) around the spread using the marks as a guide; the pap pen is left to dry for about 30 minutes. Afterwards, using a Coplin jar slides are washed 2x 2 minutes in H_2O+Photoflo (Silverprint, 90662) and 2x 2 minutes in 1x PBS (PBS) (Melford Laboratories, P3206). Slides are then stored in the final PBS at 4ºC until required for staining; Slides can be stored for several months, but I always stained them in within a month.

3.6. Ovarian embedding: wax

After postmortem dissection, ovaries were rinsed in PBS and incubated at 4ºC for 16 hours in 4% PFA pH 7.4 dissolved in 1X PBS. Afterwards, The ovaries were then rinsed again in fresh PBS. A 12 well plate (Helena Biosciences, 92012t) was pre-set with different concentration of ethanol (50%, 70%, 95%, 100%). On a shaking platform ovaries were washed as follow: 30min in 50% ethanol, 2x 30min 70% ethanol, 30min 95% ethanol, and 2x 30min in 100% ethanol. Glass bijou (SLS, TUB1236) containing 50/50 Histoclear and Paraffin Wax (VWR, 361336E) was placed on a hot block at 70ºC.

The ovaries were then transferred into a glass bijou containing 100% Histoclear and washed 2x 10minutes. After that, ovaries placed in the 50/50 Histoclear and Paraffin Wax vial located in the hot block for 15 minutes. The histoclear:paraffin solution was poured out in the disposal container making sure the ovaries were still in the vial. Ovaries were then washed 3x20min with wax in the hot block at 70ºC.

One bed at the time of the plastic 7x7x5 dispomoulds (CellPath, GAD-0702-02A) was filled with melted wax, and one ovary was placed on each bed using pre-warm

tweezers. An embedding ring (CellPath, GAB-0102-10A) has been put on top of each mould and then filled to the top with wax. Blocks were left at room temperature to solidify the wax.

3.7. Ovarian embedding: OCT

After postmortem dissection, ovaries were rinsed PBS and then equilibrated within a mixture of 50/50 PBS/OCT embedding matrix (Cellpath KMA 0100-00A) for 10 minutes. A polystyrene box (40cm^3) was carefully filled with liquid nitrogen to 1 inch from the bottom of the box. A 2 inches high rack was placed in the centre of the box, and the lid was placed back to allow the box to cool down for about 10 minutes. The beds of the plastic 7x7x5 dispomoulds were filled with OCT and one ovary at the time was placed on each bed. The dispomoulds containing the ovaries were placed on top of the 2 inches high rack inside the polystyrene box and closed allowing the OCT to freeze. After the OCT has become completely white the blocks of OCT:ovaries are removed from the bed and stored in at -80ºC until the need for sectioning.

3.8. Cryo-sectioning

Thirty minutes before the start, the blade was carefully placed in the blade clamp of the cryostat (Leica CM1860) and the angle adjusted to 10º, the temperature of the machine in the cryostat should be -20ºC. For security reasons, the knife safe was placed to cover the blade while the rest of the equipment is prepared for the proceeding. A brush and tweezers were also placed inside the machine. Frozen blocks of OCT containing the ovaries were attached to the chunk by applying some OCT at room temperature. The chunk with the specimen on top was placed in the cooling plate, this solidifies the OCT making the specimen to stick on the chunk.

The chunk was placed and clamped in the chunk holder. Afterwards, the knife safe removed. The sample was brought to close to the blade using the electronic controls and few sections were cut by unlocking and rotating the handle wheel on the right-hand side. Once the tissue was reached, a smooth and constant rotation pattern of

the handle wheel resulted important in preserving the morphology of the tissue. Each section was loaded on a room temperature pre-labeled polysine slide (this step was carefully performed as it can severely modify the morphology of the tissue). The thickness of the section varied according to the nature of the study; sections were cut at 30µm for imaging the whole nucleus of oocytes at primordial follicle stage, and 12µm for standard staining. After all sections were loaded, slides were left at room temperature for 30min then stored at -20ºC.

3.9. Chromosome spread immunofluorescence

Slides carrying chromosome spreads were placed in a dark humidified after the excess of PBS was tapped off on tissue paper. Slides were then incubated for 1 hour in blocking solution prepared as follow. PBTT (0.25% Triton X-20 & Tween 20 in PBS) was supplemented with 10% (v/v) goat serum (Stratech Scientific Ltd - 005-000-121) or donkey serum (Sigma-Aldrich - D9663) depending on the which animal secondary antibody were raised in (i.e. if secondary antibodies were raised in goat, then the goat serum was used). Afterwards, the block was tapped off on a tissue paper and primary antibody diluted in blocking solution was pipetted in and incubated overnight at 4ºC.

After overnight incubation of primary antibodies slides were washed at room temperature on a shaking platform as follow: 1x 10min 0.4% (v/v) Photo-flo in PBS; 2x 10min 0.01% (v/v) Triton X-20 in PBS; 1x 10min 0.4% (v/v) Photo-flo in PBS; and 1x 2min PBS. Following the washes, spreads were incubated on the dark humidified chamber with the corresponding secondary antibody (Table 9) diluted in blocking solution for one hour at room temperature. After the incubation, the washes above are repeated. Chromosome spreads were the covered using Vectashield with DAPI (Vector Laboratories Ltd - H-1200) using coverslips No.1.5 (Scientific Laboratory Supplies Ltd - MIC3248) and sealed with rubber solution (Amazon - B004VQOUE6).

3.10. Immunohistochemistry proceedings

3.10.1. *Wax sections immunohistochemistry*

Slides carrying the sections were washed in 2x 10min 100% histoclear. Then, the tissue was rehydrated throughout decreasing concentrations of ethanol as follow: 2x 5min 100%, 1x 3min 95%, 1x 3min 70%, 1x 3min 50% and 1x 5min PBS. Antigen retrieval was performed in a pressure cooker ensuring all of the slides are immersed in citrate buffer (see section 3.15). With the hob in max, I waited around 22 min for hissing to start, then once hissing from the steam reaches maximum (24-26min), then, timed max steam for a further 8 minutes. Carefully, removed the pressure cooker from the hot plate and turn the valve to steam setting to release the pressure, once pressure is released the metal rack with the slides is removed into a plastic container and with some sodium citrate to cool down.

The slides were washed 3x 5min TBS-T (0.025% triton X-20 in TBS), borders of the slide around the section were wiped with a piece paper tissue to draw a pap pen box. Sections were incubated with blocking buffer for 1 hour in 10% (v/v) serum in TBS-T following the same principles as in section 3.9. Primary antibody, diluted in blocking solution was incubated overnight. After overnight incubation slides were washed 3x 10min TBS then 1x 5min 0.3%H_2O_2, 2x 5 min TBS-T. Conjugated HRP antibody was incubated for 1h following the same principles as in section 3.9. Afterwards, slides were washed 3x 10min TBS, and then DAB (Vector Laboratories Ltd - SK-4100) was applied according to the instructions of the manufacturer. Sections were counterstained with hematoxylin (Vector Laboratories Ltd - H-3404) following manufacturer instruction and mounted with mounting media (Vector Laboratories Ltd - H-5000) using coverslips No.1.5.

3.10.2. *Cryo-sections immunohistochemistry*

Slides were defrosted in a dark humidified chamber at room temperature for1 hour, then OCT was dissolved in 1x 10min PBS wash. Sections were permeabilized in 1x 10min PBS-T (1% v/v Triton X-100 in PBS) then 1x 5m PBS. Sections were then fixed in 4% PFA pH 7.4 for 15 minutes. Slides were washed again 2x 5min in PBS.

From here the steps follow the same principles of chromosome spreads staining (section 3.9) with just a few variations in the buffers as follow: blocking buffer (0.2%v/v Triton X-100, 1%v/v DMSO in PBS). Washes were done in PBS only. After primary antibody incubation slides are washed 1x 5min 1% (v/v) lipsol in PBS (Lipsol-Fisher Scientific UK – 12549965).

3.11. Microscopy methods

3.11.1. *Confocal microscope*

Images for fluorescence quantification of chromosome spreads and ovarian sections were acquired on a Nikon A1R confocal microscope, using a Plan Apo VC 60x and 40x /1.40 Oil DIC N2 objective. Sequential (Channel series ON)/Simultaneous (Channel series OFF) excitation at 405nm, 488nm, 561nm and 642nm was provided by the 405nm Cube Laser (Coherent), 488nm Argon Laser (Melles Griot), Sapphire 561nm Laser (Coherent) and Red Diode 642nm Laser (Melles Griot), respectively. Emission filters BP 425-475nm, BP 525-555nm, 570-620nm and 662-737nm were used to collect DAPI, Alexa 488, Cy3 and Cy5 signal respectively. Images, with a frame size of (512 pixels) and a (4x) line average, were captured using the Nikon Elements AR software package

3.11.2. *Apotome microscope*

Images of ovarian sections for primordial follicle identification training were acquired using a Zeiss Axio Imager Z1 microscope fitted with a Zeiss ApoTome 2. Using plan-apochromat 40x and 63X Oil objective. Images were captured using a Zeiss AxioCam HRm Rev3 camera in combination with the Axiovision 4.8 software package. Excitation source is a Mercury short arc lamp (HBO 100 W/2)

3.11.3. *Colour camera microscope*

Ovarian section stained with DAB (wax sections immunohistochemistry) for follicular counts were imaged in a Zeiss Axioplan 2 Imaging – Upright Widefield microscope for slides. AxioCam HRc camera (up to 13MP): RGB (colour images) or BW (monochrome images). Used for Brightfield, Phase, DIC. Lenses: Plan Neofluar 2.5x/0.075, Plan Neofluar 5x/0.15 Ph1, Plan Neofluar 10x/0.3 Ph1, Plan Neofluar 20x/0.5 Ph2, Plan Neofluar 40x/0.75 Ph2 (no immersion).

3.12. Image analysis

3.12.1. *Volocity*

Images were loaded onto the software. Under the measurement tab of the software, I selected the following options from the bottom-left menu to establish the protocol for segmentation of the primordial-stage oocyte nucleus:

- Find objects (Rec8-myc):
  - Thresholding: all oocytes within the slide were treated equally, the threshold was set including all Rec8-myc signal in primordial-stage oocytes from old females (Lower: ~202 it might variate between slides).
  - Clip to ROI'
  - Separate touching objects (0.03µm^3)
- Find Objects (TO-PRO3):
  - Thresholding: was applied following the same rule as for Rec8-myc (lower: ~269)
  - Clip to ROI's
- Exclude non-touching objects:
    - Exclude: Rec8-myc
    - Non-touching: TO-PRO3

I selected the freehand tool to select the region of interest (ROI) which is the nucleus of the primordial-stage oocyte. The result of measurements, which appear at the bottom of the screen, were transferred to a Microsoft Excel spreadsheet

3.12.2. *Imaris*

Chromosome spreads were acquired on a confocal microscope, background subtraction on Nikon elements software is automatically applied. Centromeres analysed using surface segmentation tool. Manual thresholds could variate according to with the intensity of the signal. However, all chromosomes from the same slide were treated equally entering the following values in the surface segmentation wizard.

Source Channel:

- Source Channel Index = CREST
- Enable Smooth = true
- Surface Grain Size = 0.0820 µm
- Enable Eliminate Background = true
- Diameter Of Largest Sphere = 0.388 µm

Threshold:

- Enable Automatic Threshold = false
- Manual Threshold Value = 243
- Active Threshold = true
- Enable Automatic Threshold B = true
- Manual Threshold Value B = 1588.07
- Active Threshold B = false

At the end of the wizard, Imaris gives the option to double check that the segmentation is correct and the results are exported to a Microsoft Excel spreadsheet.

3.12.3. *Primordial follicle counts*

Primordial follicles were counted from every 5th section the following a formula (McClellan *et al.*, 2003) to calculate the total number of follicles in the ovary was applied:

$$\bar{Y} = \frac{\bar{y}/\bar{a}}{A/F} \quad (1)$$

Where

$$\bar{y} = \frac{\sum y_\iota}{n} \quad (2)$$

$$\bar{a} = \frac{\sum a_\iota}{n} \quad (3)$$

Equation (1) refers to the calculated number of primordial follicles ($\bar{Y}$) where "$\bar{y}$" is the mean number of primordial follicles and $\bar{a}$ is the mean area of all counted sections. "*A"* is the estimated total area of the ovary. The correlation factor "*F"* is found by the measurement of the nucleus diameter of 20 primordial follicles in two different directions and the mean nuclear diameter is the divided by the thickness of the section. In equation (2) "y_ι" refers to the total number of primordial follicles in the "ι^{th}" section, n refers to the number of counted sections. In the equation (3) "a_ι" refers to the area in microns of the "ι^{th}" section.

3.13. Statistical analysis

All statistical analysis for this project were perform using Minitab (Minitab Inc., USA) or GraphPad Prism (GraphPad Software, Inc., USA) software. Normal distribution of the data was assessed using the either the Kolmogorov-Smirnov test or the Ryan-Joiner (similar to Shapiro-Wilk) Test. If the data was normally distributed, the appropriate parametric test was carried out. On the contrary, if normality was rejected, the appropriate non-parametric tests were executed. The common parametric tests used in this project were the two sample t-test and one-way ANOVA, followed by a post hoc Tukey's multiple comparison test. The most common non-parametric tests were the Mann-Whitney U test and the Kruskal-Wallis test, followed by a post hoc Dunn's multiple comparison test. In case a different test was used it will be specified alongside the relevant group of data throughout this manuscript.

3.14. Antibodies and Dyes

Table 9: Antibodies and dilutions

Primary	Source	Dilution	Secondary	Source	Dilution
rabbit-anti-Rec8	Maureen Eijpe	1:100	goat-anti-rabbit AlexaFluor 488	Life Technologies Limited - A11008	1:800
human-anti-CREST	Europa Bioproducts FZ90C-CS1058	1:50	goat-anti-human Cy5	Jackson Immuno 109-175-003	1:400
mouse-anti-Myc Tag, clone 4A6	Millipore UK Ltd - 05-724	1:100	goat-anti-mouse AlexaFluor 488	Life Technologies Limited - A11001	1:800
Mouse-anti-Myc Tag, clone 4A6 Alexa Fluor 488 conjugated	Millipore UK Ltd - 16-224	1:50	N/A	N/A	N/A
rabbit-anti-Foxo3A	Proteintech Europe Ltd - 10849-1-AP	1:50	goat-anti-mouse AlexaFluor 488	Life Technologies Limited - A11001	1:800
rabbit-anti-active Caspase3	ABCAM Plc - ab13847	1:100	goat-anti-mouse AlexaFluor 488 Or Goat Anti-Rabbit IgG H&L (HRP)	Life Technologies Limited - A11001 Or ABCAM Plc - ab6721	1:800 Or 1:400
rabbit-anti-Gdf9	ABCAM Plc - ab93892	1:50	goat-anti-mouse AlexaFluor 488	Life Technologies Limited - A11001	1:800
mouse-anti-TOMM20	ABCAM Plc - ab56783	1:100	goat-anti-mouse AlexaFluor 488	Life Technologies Limited - A11001	1:800
rabbit-anti-DRP1	ABCAM Plc - ab184247	1:100	goat-anti-rabbit AlexaFluor 647	Life Technologies Limited – A21244	1:800
rabbit-anti-Cre	ABCAM Plc - ab190177	1:50	goat-anti-mouse AlexaFluor 488	Life Technologies Limited - A11001	1:800
rabbit-anti-PTEN	Novus Biologicals Ltd - MAB847-SP	1:50	goat-anti-mouse AlexaFluor 488	Life Technologies Limited - A11001	1:800

Table 10: Dyes and assays

Dye / Assay	Source	Dilution
TOPRO-3-iodide (642/661)	Life Technologies Limited - T3605	1:1000
In situ cell death Detection Kit, TMR red	Roche Diagnostics Ltd - 12156792910	Instructions kit

3.15. Reagents

All reagents in this section were purchased from Sigma-Aldrich UK

Lysis Buffer: Stock solution: 1M Tris-HCl Ph8, 0.5M EDTA, 20% (w/v) SDS
Working solution: 10mM Tris-HCl, 10mM EDTA, 0.5% (w/v) SDS

0.01M Citrate Buffer pH6: 1.92g citric acid in 1 litre H20. pH with NaOH.

Acid Tyrode solution: 0.8g NaCl, 0.02g KCl, 0.024g $CaCl_2.2H_2O$, 0.01g $MgCl_2.6H_2O$, 0.1g Glucose, 0.4g Polyvinylpyrrolidone. Added to 100ml Milli-Q water and pH adjusted to 2.5 with 5M HCl. Aliquoted and stored at -20°C.

0.5M DTT: 77.1g/ml DTT in Milli-Q water. Aliquoted and stored at -20°C

50mM Boric Acid: 0.15g in 50ml of Milli-Q water

0.5% tri-Sodium Citrate: 0.25g $Na_3C_6H_5O_7$ in 50ml Milli-Q water

PBS: Diluted from 10x to 1x with Milli-Q water

TBS: To prepare 1L; 100ml 1M Tris-HCl pH 7.5, 30ml 5M NaCl, 870ml Milli-Q water

Chapter 4. Results: Mechanisms of cohesin depletion

4.1. Separase: The prime suspect of cohesin depletion

In female mammals, bivalent chromosomes form during fetal life when maternal and paternal homologues undergo reciprocal exchange of DNA and are not resolved until adult life, shortly just before ovulation. This process takes decades in the case of human and months in the case of mice. During this time bivalent chromosomes are stabilised by cohesion between arms of sister chromatids. According to our current understanding, this depends on cohesin complexes loaded early during oogenesis, which in the case of female mammals, occurs during fetal life (Tachibana-Konwalski *et al.*, 2010; Burkhardt *et al.*, 2016).

Chromosome separation is considered one of the most dramatic and highly regulated events during the cell cycle (Nasmyth, 1999). Accurate chromosome segregation during anaphase requires the pulling forces exerted from the spindle and simultaneous removal of chromosomal cohesion (Uhlmann *et al.*, 1999; Buonomo *et al.*, 2000; Wirth *et al.*, 2006; Nasmyth and Haering, 2009). In prophase of mitotic cells, WAPL removes most of the arm cohesion during the process known as the prophase pathway (Waizenegger *et al.*, 2000) by opening cohesin at the kleisin-Smc3 interface (Nasmyth, 2011). Removal of the residual arm and centromeric cohesin during anaphase requires the cleavage of its kleisin subunit by the proteolytic activity of separase (Uhlmann *et al.*, 2000).

Prior to anaphase, Securin and inhibitory phosphorylation by CDK1-cyclin B1 (Stemmann *et al.*, 2001; Herbert *et al.*, 2003) control the proteolytic activity of separase (Ciosk *et al.*, 1998). Anaphase is triggered when the anaphase-promoting complex (APC/C) binds to its cofactor Cdc20 destroying securin, which in consequence unleashes separase. Production of haploid gametes from diploid progenitors requires two consecutive rounds of chromosome segregation following a single round of DNA replication. To achieve this, the removal of cohesin from the chromosomes occurs in two stages: Firstly, during the first meiotic division, the physical linkages (chiasmata) formed at the sites of crossover formation, are resolved when cohesin is removed only from chromosome arms. Secondly, during

the second meiotic division, which in mammalian oocytes, occurs upon fertilisation, the remaining cohesin at the centromeres is removed. (Kudo *et al.*, 2006) showed in mouse oocytes that to resolve the chiasmata cohesin is removed from chromosome arms by separase-mediated cleavage of the meiotic-specific cohesin α-kleisin (Rec8). During meiosis I Shugoshin (Sgo2) “guardian spirit” in Japanese prevents cohesin removal at the centromeres by protecting Rec8 from separase-mediated cleavage (Watanabe, 2005; Watanabe and Kitajima, 2005).

Here, we tested the hypothesis that the depletion of chromosomal cohesin observed in oocytes of older females and associated with destabilisation of bivalent chromosomes, is due to leaky inhibition of separase. If so, then the deletion of the *Separase* gene would prevent the age-related depletion of cohesin in older oocytes.

4.2. A mouse model to test the role of separase in age-related cohesin depletion: Specific deletion of *Separase* gene in primordial follicle stage mouse oocytes

Since (Sauer and Henderson, 1989) discovered that the bacterial protease *Cre* could induce DNA recombination at *loxP* sites in mammalian cells, it has been possible to silence genes in a tissue-specific manner at defined developmental stages or during the lifetime of an organism.

Using C57BL6 mouse strain, (Wirth *et al.*, 2006) generated a mouse model to delete the separase peptidase domain by flanking the COOH terminal with *loxP* sites from exon 24 to exon 31. This model was first used to demonstrate that separase is essential for triggering chromosome disjunction in eukaryotic cells during mitotic anaphase (Wirth *et al.*, 2006). Subsequent studies with this model in mouse oocytes showed that separase proteolytic activity is required to remove cohesin from chromosome arms during meiosis I resulting in the conversion of bivalents to dyad chromosomes (Kudo *et al.*, 2006). We used the *Separase* knockout mouse model to test whether leaky inhibition of separase results in age-related depletion of cohesin from oocyte chromosomes. As a strategy to test this hypothesis, We aimed to delete separase from non-growing oocytes as soon as the pool of primordial follicles is

established, which occurs during the first three days after birth in the mouse (Pepling and Spradling, 2001).

While separase has previously been deleted in mouse oocytes (Kudo et al, 2006) using the ZP3 promoter, this promoter is not activated until oocytes are recruited for growth (Lewandoski *et al.*, 1997). However, oocytes from older females are distinguished from their younger counterparts by remaining in the non-growing phase for an extended period. To gain insight into the age-effect, it is, therefore, essential to delete separase from the non-growing pool of oocytes as soon as the primordial follicles are formed.

The Growth Differentiation Factor-9 (GDF-9) is a member of the transforming growth factor-β (TGF-β) superfamily, expressed specifically in the oocytes (McGrath *et al.*, 1995). The promoter GDF-9 is key in the formation of primordial follicles (Bayne *et al.*, 2015; Zhao *et al.*, 2016) and is expressed in the non-growing pool of oocytes where it can drive the *Cre recombinase* activity (Lan *et al.*, 2004). By crossing females whose *Separase* peptidase domain has been flanked by *loxP* sites ($Sep^{f/f}$) with males carrying *iCre* recombinase ($Sep^{f/f}$*;Gdf9-iCre*) will produce females with oocyte-specific deletion of separase ($Sep^{f/f}$*;Gdf9-iCre*.) (Figure 4.1), and also $Sep^{f/f}$ females (controls). Female expressing *iCre* are infertile while males are still fertile (Kudo *et al.*, 2006). This is advantageous for the breeding scheme as $Sep^{f/f}$*;Gdf9-iCre* males obtained from the crossing can become future sires and $Sep^{f/f}$ females future dams (Figure 4.2).

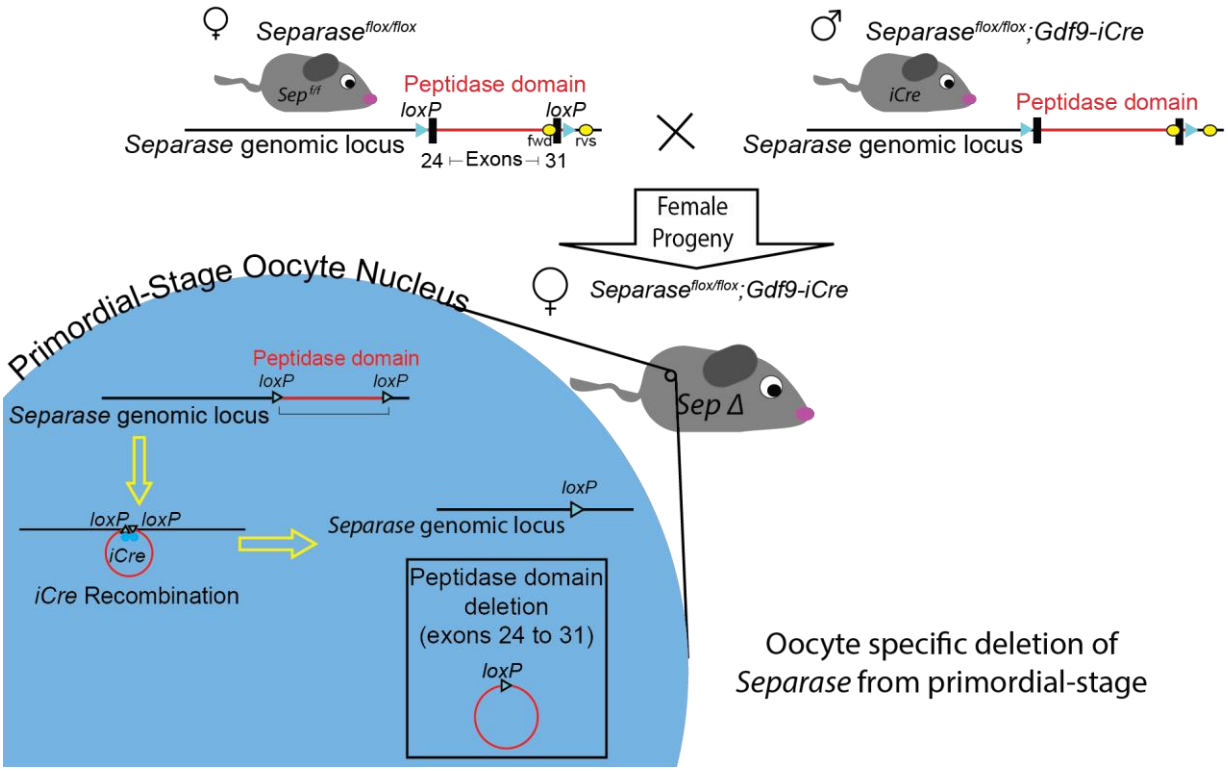

Figure 4.1 Oocyte-specific deletion of *Separase* gene

Schematics illustrate the breeding process to generate female mice carrying separase deleted oocytes. At the top of the figure, cartoons represent the cross between a *Sep*$^{f/f}$ female and a male *Sep*$^{f/f}$*;Gdf9-iCre*, the line beneath the mice, is a representation of the location of the *loxP* (small triangles) at exons 24 and 31 of the separase genomic locus, and PCR primer (yellow ovals). The resulting progeny of this cross will produce *Sep*$^{f/f}$*;Gdf9-iCre* females, which will have separase deleted oocytes. Similar to a magnifying glass, the big half circle (Blue) on the bottom left of the diagram represents the magnification of the nucleus of a primordial stage oocyte from a *Sep*$^{f/f}$*;Gdf9-iCre* female. Within the oocyte nucleus, it is shown how iCre recombinase the *loxP* and excises from exon 24 to 31 from the separase genomic locus. This knockout mouse was generated by (Wirth *et al.*, 2006).

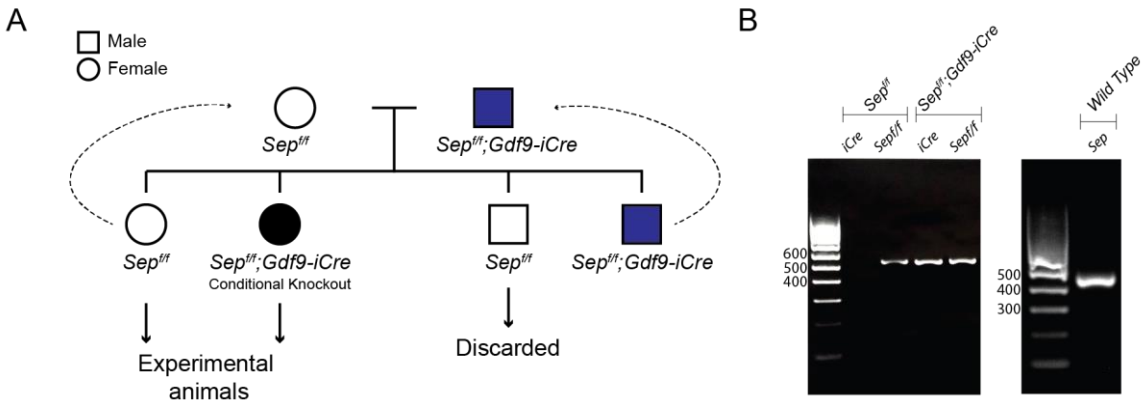

Figure 4.2 Breeding strategy and genotyping

A Diagram shows the possible progeny genotype from the cross between *Sep$^{f/f}$* females with *Sep$^{f/f}$;Gdf9-iCre* males. Females are represented with circles and males with squares. White filling denotes that the genotype is *Sep$^{f/f}$*, for both male and female. Females from this genotype are used as a control and can also be used for breeding. Black filling represents *Sep$^{f/f}$;Gdf9-iCre* females carry separase deleted oocyte and are infertile, females with this genotype are experimental animals. Dark blue filling represents *Sep$^{f/f}$;Gdf9-iCre* males, which are fertile therefore can pass on the iCre recombinase to the female progeny. **B** Pictures of genotyping gels showing the band size for *separase* with inserted *loxP* sites and *iCre* in *Sep$^{f/f}$* and *Sep$^{f/f}$;Gdf9-iCre* females, also *separase* in a wild-type female. *Separase* is 100 base pairs bigger when flanked by *loxP* sites (*Sep$^{f/f}$)* than *Separase* wild-type.

4.2.1. *Mouse husbandry*

Because these experiments involved keeping mice for up to 15 months, I adapted the standard cage conditions in the interest of the welfare of the animals and to reduce obesity, which could have a confounding effect. The performance of the species-specific behavioural repertoire is essential for the normal physiological function of the animal (Van Loo *et al.*, 2004; Baumans, 2005). Prolonged confinement and boredom in laboratory animals are associated with abnormal repetitive movements, and an

increase in food intake as a consequence of boredom, resulting in obesity (Reinhardt, 2004). Environmental enrichment has been found to produce a positive effect for preventing behavioural diseases and minimise obesity (Schroeder *et al.*, 2011) in laboratory animals during long-term confinement periods. Therefore, in addition to the standard environmental enrichment provided by the Compared Biology Centre (CBC), I implemented the use of igloos, which provide an additional hiding place, walking surface and promotes nesting (Figure 4.3, A). This had a positive effect on the corporal condition of the mice during ageing as mice did not show signs of obesity at the time of harvest (Ullman-Cullere and Foltz, 1999).

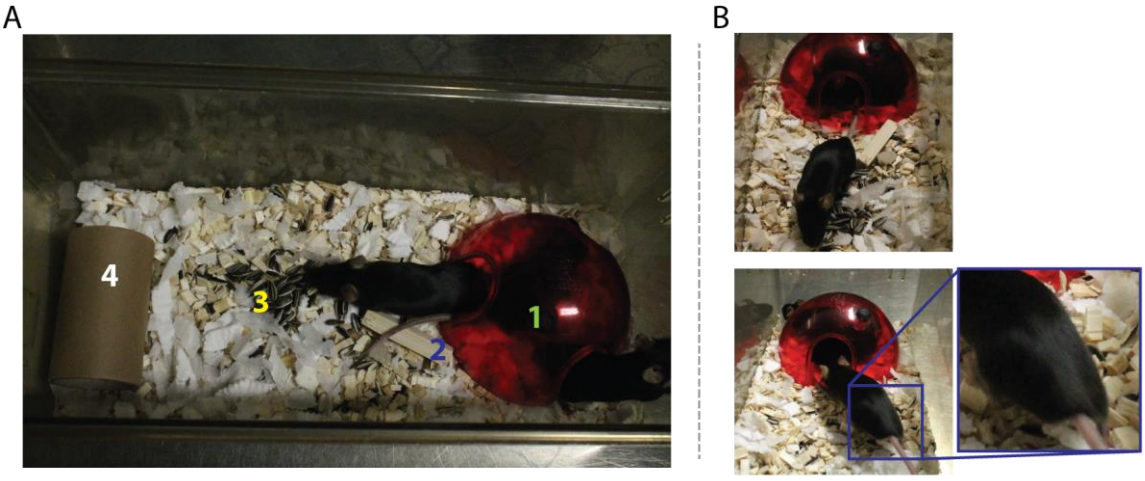

Figure 4.3 Mouse housing

Images show the general setting for mouse housing. **A** Picture shows the typical location of the component used to prevent abnormal repetitive movement. 1) igloo, 2) chewing stick, 3) sunflower seeds, 4) cardboard tube. **B** Representative image of a mouse aged 12 months housed under these conditions, the inset shows rear legs of the mouse in which the dorsal pelvis is not prominent but can be palpable.

4.3. Anaphase I is inhibited in *Sep$^{f/f}$;Gdf9-iCre* mouse oocytes

Deletion of separase using the ZP3 promoter results in failure to convert bivalent into dyad chromosomes during anaphase I (Kudo *et al.*, 2006). To test that excision of the *Separase* peptidase domain from the genome using the Gdf-9 promoter inhibits anaphase of the first meiotic division, I cultured 2-month-old oocytes from *Sep$^{f/f}$* and *Sep$^{f/f}$;Gdf9-iCre* mice to metaphase II.

Consistent with the deletion of separase previously reported (Kudo *et al.*, 2006) anaphase is inhibited in 100% of *Sep$^{f/f}$;Gdf9-iCre* oocytes (n=31 from 3 mice) and bivalent chromosomes remain intact after overnight (16 hours) culture. In contrast, 94% of *Sep$^{f/f}$* oocytes (n=58 from 3 mice) can convert bivalent into dyad chromosomes after overnight culture (Figure 4.4). This indicates that separase-mediated cleavage of Rec8 is inhibited by deleting *Separase* exons 24 to 31 using the promoter GDF-9 to induce expression of *iCre recombinase* activity.

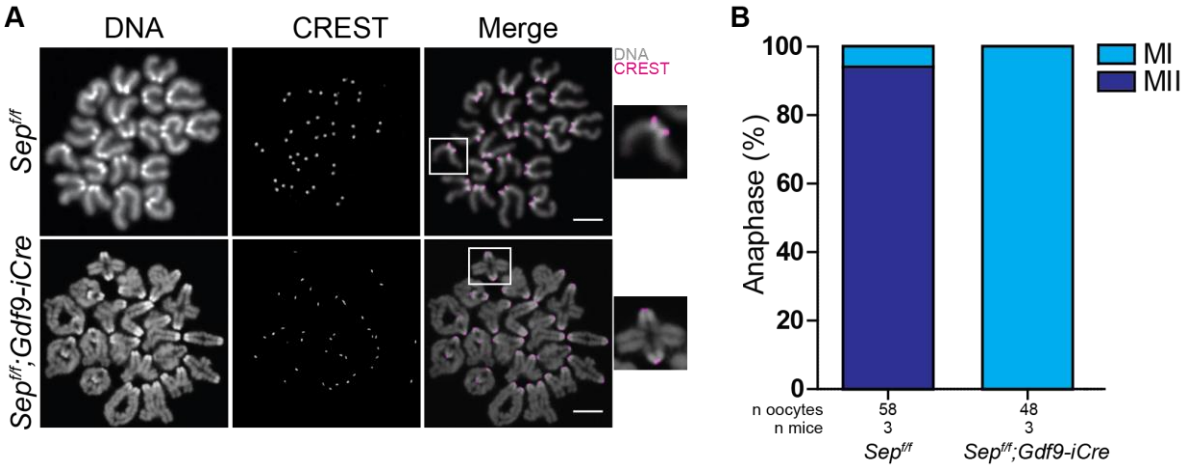

Figure 4.4 Anaphase is inhibited in *Sep$^{f/f}$;Gdf9-iCre* mouse oocytes

A Images show representative oocyte chromosomes, spread after overnight culture, stained for DNA (DAPI) and CREST, images show that oocytes from 2-month-old *Sep$^{f/f}$* females can convert bivalent into dyads chromosomes and arrest at in metaphase II. Oocytes from 2-month-old *Sep$^{f/f}$;Gdf9-iCre* females are unable to undergo anaphase I, and bivalent chromosomes cannot convert to dyads. Insets show a dyad chromosome from *Sep$^{f/f}$* and a bivalent chromosome from *Sep$^{f/f}$;Gdf9-iCre* (scale bar 10µm). **B** The bar chart shows the percentage of anaphase comparing oocytes from 2-month-old *Sep$^{f/f}$* vs. *Sep$^{f/f}$;Gdf9-iCre* after overnight culture; the percentage of oocytes that can undergo anaphase I and arrested at metaphase II (MII) are represented in dark blue. Oocytes unable to undergo anaphase I and metaphase I (MI) are represented in blue. Oocytes from *Sep$^{f/f}$;Gdf9-iCre* do not undergo anaphase I. The numbers of mice and oocytes are shown in the graph.

4.4. Key structural features of bivalent chromosomes are lost during ageing after *Separase* deletion in oocytes.

Previous findings in our laboratory (Lister *et al.*, 2010) and others (Chiang *et al.*, 2010) indicated that the physical linkages between homologues and sister centromeres become disrupted during ageing. This instability of the bivalent chromosomes was associated with the age-related depletion of chromosomal cohesin. Both, the proportion of distally associated homologues and the distance between sister centromeres increase with age in wild-type C57BL/Icrfa^{t} mice (Lister *et al.*, 2010). The mouse strain C57BL6 was used to generate the *Separase* knockout model. We, therefore, asked first whether these previously observed structural defects on the bivalent chromosomes were also present in aged *Sep$^{f/f}$* oocytes.

For these experiments, I compared oocytes from young (2-month-old) and old (15-month-old) *Sep$^{f/f}$* and *Sep$^{f/f}$;Gdf9-iCre* mice. Oocytes from the two age groups were spread on the same slide during prometaphase of meiosis I (GBVD+5hr). To assess bivalent chromosomes, I performed immunolabeling using CREST antiserum, which binds to the centromeric proteins CENP-A, CENP-B and CENP-C, as a centromere marker (Earnshaw and Cooke, 1989) and DAPI to visualise the DNA (Figure 4.5, A). Consistent with previous observations in wild-type mice (Lister *et al.*, 2010), the proportion of distally associated homologues in aged *Sep$^{f/f}$* oocytes (14.5%) is significantly larger than in young *Sep$^{f/f}$* oocytes (7.2%) ($p<0.001$, χ^2 test, Figure 4.5, B).

If leaky inhibition of separase is the cause of cohesin depletion during ageing, the disruption of bivalent chromosomes associated with cohesin depletion observed in aged wild-type oocytes should not occur in aged *Sep$^{f/f}$;Gdf9-iCre*. However, I found that this was not the case, oocytes from 15-month-old *Sep$^{f/f}$;Gdf9-iCre* exhibit a significantly larger proportion of distally associated homologues (11.5%) compared with 2-month-old *Sep$^{f/f}$;Gdf9-iCre* (3.2%, $p<0.001$, χ^2 test, Figure 4.5, B). Also, I found an increase in the proportion of distally associated homologues in aged *Sep$^{f/f}$;Gdf9-iCre* oocytes compared with young and was similar to observations in aged *Sep$^{f/f}$* oocytes ($p=0.265$ χ^2 test. Figure 4.5, B).

It is interesting to notice that oocytes from both, young and old, *Sep$^{f/f}$;Gdf9-iCre* females have a lower proportion of distally associated homologues compared to their *Sep$^{f/f}$* counterpart. This observation could point that separase has an age-independent effect on the chromosomes which possibly occurs during the oocyte growth phase or during prometaphase. Although the sudden destruction of YFP-securin in oocytes occurs at GVBD+7hrs (Kudo *et al.*, 2006), and separase biosensor in mitotic cells showed activity for one minute (Yaakov *et al.*, 2012), I speculate that perhaps separase in mammalian oocytes could somehow be gradually activated.

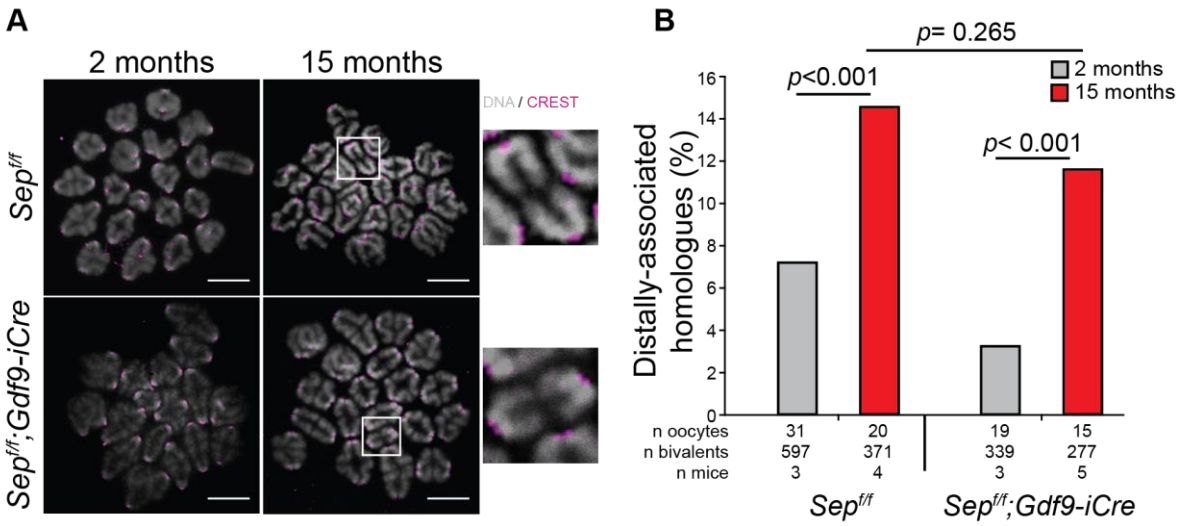

Figure 4.5 Distally associated homologues increase during ageing in *Sep$^{f/f}$;Gdf9-iCre* oocytes

A The panel shows representative images of oocyte chromosome spread at prometaphase (GVBD+5hrs) stained for DNA (DAPI) and CREST. Comparing the proportion of distally associated homologues between young and aged oocytes from *Sep$^{f/f}$* and *Sep$^{f/f}$;Gdf9-iCre* females. The insets show examples of distally associated homologues in oocytes from old *Sep$^{f/f}$* and *Sep$^{f/f}$;Gdf9-iCre* females (scale bars 10µm). **B** The bar chart shows a parallel comparison between *Sep$^{f/f}$* and *Sep$^{f/f}$;Gdf9-iCre* analysing the proportion of distally associated homologues in oocytes from young vs. old females. Oocytes from old *Sep$^{f/f}$;Gdf9-iCre* have increased proportion of distal association compared to young ($p<0.001$, χ^2 test), and that increment is similar to oocytes from old *Sep$^{f/f}$* ($p=0.265$ χ^2 test). The number of oocyte and mice are shown in the graph.

To determine whether female ageing and oocyte cohesin depletion were also accompanied by splitting of sister centromeres in *Sep$^{f/f}$;Gdf9-iCre* oocytes I used the Plot Profile tool incorporated in FIJI (Fiji is Just ImageJ) open source software (Schindelin *et al.*, 2012). This tool allowed me to detect the core of saturated pixels

on each centromere and measure the distance between them (Figure 4.6, A). The frequency distribution for the distance between sister centromeres in young *Sep$^{f/f}$* oocytes shows that ~80% of sister centromere pairs were 0.1-0.3 µm apart (Figure 4.6, B). By contrast, aged *Sep$^{f/f}$* oocytes display a broad range (0.1 -1.1µm) of distances between sister centromeres (Figure 4.6, B). As expected, aged *Sep$^{f/f}$* oocyte chromosomes exhibit a significantly larger distance between centromeres than young *Sep$^{f/f}$* chromosomes. (p<0.001 Mann-Whitney U Test, Young: n= 431 Cent. Pairs from 12 oocytes, three mice, Aged: n=324 Cent. Pairs from 9 eggs, four mice, Figure 4.6, C).

The frequency distribution for sister centromeric distances in *Sep$^{f/f}$;Gdf9-iCre* are remarkably similar to their counterpart young and aged *Sep$^{f/f}$* oocytes. The vast majority of sister centromere pairs in 2-months-old *Sep$^{f/f}$;Gdf9-iCre* fall within the 0.1-0.3 µm range, whereas in 15-month-old *Sep$^{f/f}$;Gdf9-iCre* show a widespread (0.1-1.1µm) in the range of values and the mean was significantly reduced compared with oocytes from young mice. (p<0.001 Mann-Whitney U Test, Young: n= 264 Cent. Pairs from 7 oocytes, three mice, Aged: n=254 Cent. Pairs from 7 eggs, five mice, Figure 4.6, E). It could be argued that there is an age-independent effect of separase function as in the frequency distribution of young *Sep$^{f/f}$;Gdf9-iCre* the 20% of centromeres are at a distance 0.1µm vs a 40% in *Sep$^{f/f}$*. However, this is contradictory to the separase function as in the absence of separase sister centromeres should maintain a closer unified structure. Perhaps, increasing the number of samples and the use of a separase biosensor could reveal the new insights of any age-independent effect of separase in mouse oocytes, which is not the focus of my current research.

In summary, these results show that although the protease responsible for the opening of cohesin ring was deleted from the non-growing oocyte stage chromosome deterioration during ageing is still occurring. Additionally, the extent of the deterioration of the bivalent structure during ageing appears to be the same even in the absence of separase.

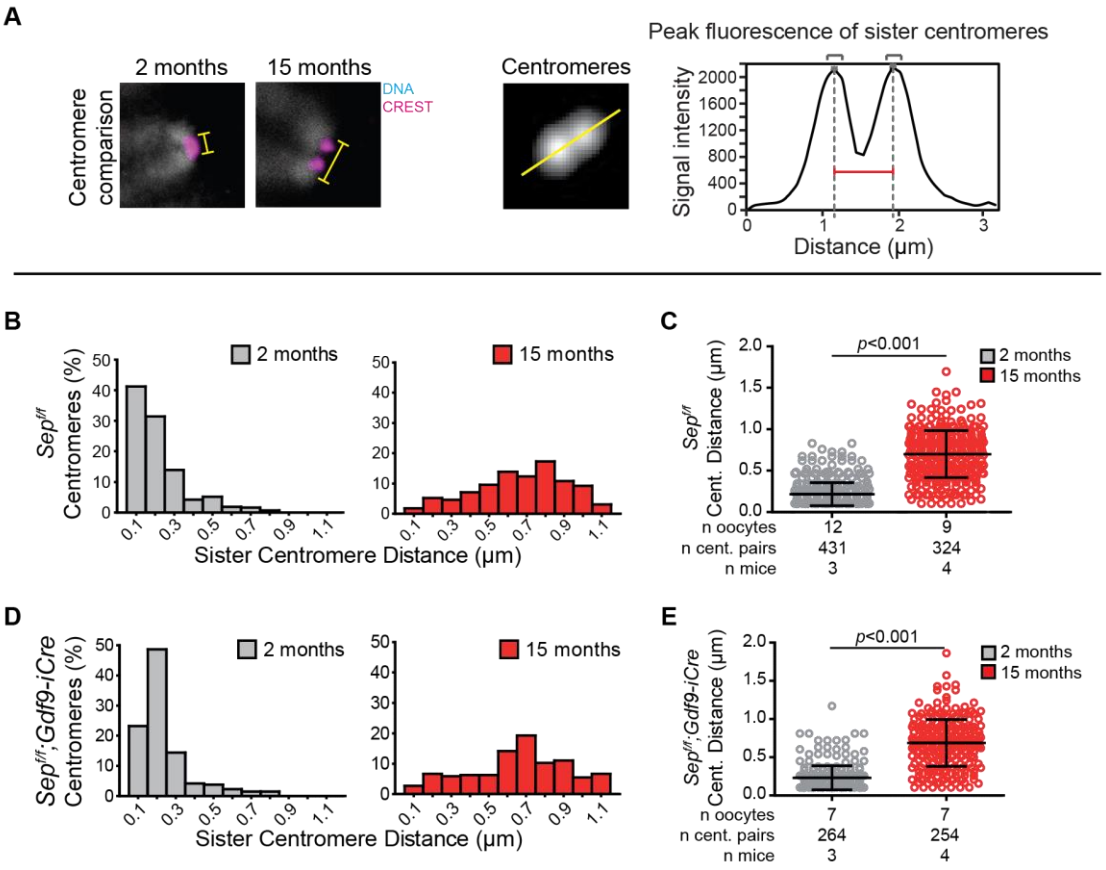

Figure 4.6 Distance between sister centromere increases during ageing in *Sep$^{f/f}$;Gdf9-iCre* oocytes

A Images show examples of the centromere configuration in bivalent chromosomes at GVBD+5hrs which were stained for DNA (DAPI) and CREST. A unified configuration in 2-month-old and non-unified in 15-month-old. The distance between the two peaks of maximum intensity in the core of the centromeres was measured by tracing a line-scan **B** The histograms show the frequency distribution of centromeric distances in oocytes from young and old *Sep$^{f/f}$* females. Sister Centromeres apposition (<0.3µm) is conserved in the majority of (>40%) bivalent chromosomes from 2-months-old *Sep$^{f/f}$* oocytes. Less than the 15% of sister centromeres in bivalents from 15-month-old *Sep$^{f/f}$* oocytes conserve their apposition (<0.3µm).

Figure legend continues on next page

C The dot plot shows measurements of the inter-centromere distances in oocytes from young and old *Sep$^{f/f}$* females, comparing the mean distance between both ages, error bars represents the ± s.d. **D** Comparison of the frequency distribution of centromeric distances between young and old *Sep$^{f/f}$;Gdf9-iCre* females. The pattern in the distribution is similar as in *Sep$^{f/f}$*. **E** Graph compares the mean of inter-centromere distances in oocytes from young and old *Sep$^{f/f}$;Gdf9-iCre* females. Each data point represents the distance between a pair of sister centromeres; error bars represents the ± s.d. The n numbers are shown in the graphs

4.5. Deregulated separase activity is not the cause of the age-related cohesin depletion.

Disruption of the bivalent chromosome structure in association with depletion of cohesin has been proposed as hallmark effects of female reproductive ageing (Lister *et al.*, 2010). The data presented above indicate that deterioration of the bivalent chromosome architecture during female ageing is comparable between wild-type and *separase-deleted* oocytes. We next asked whether the observed disruption of bivalent structure in aged *separase*-deleted (*Sep$^{f/f}$;Gdf9-iCre)* oocytes is also associated with cohesin depletion.

To address this question I used the same strategy implemented to determine the extent of disruption on bivalent chromosomes during ageing. To make our experiment comparable, I fixed oocytes chromosomes at GBVD+5hr from young and old female mice on the same slide for *Sep$^{f/f}$* and *Sep$^{f/f}$;Gdf9-iCre*.

According to our current understanding, only Rec8-containing cohesin complexes loaded onto the chromosomes loaded early during oogenesis can confer cohesion to stabilise the bivalent during the prolonged period of prophase arrest (Tachibana-Konwalski *et al.*, 2010). Therefore, for detecting chromosome-associated cohesin I used a Rec8 antibody generously provided by Maureen Eijpe (Eijpe *et al.*, 2003). Additionally, I labelled centromeres with CREST and DNA with DAPI.

Consistent with previous studies in wild-type mouse oocytes (Chiang *et al.*, 2010; Lister *et al.*, 2010), confocal imaging revealed a marked reduction in chromosome-associated Rec8 in 15-month-old *Sep*$^{f/f}$ oocytes compared to 2-month-old *Sep*$^{f/f}$ (Figure 4.7, A). To test the hypothesis that this is caused by deregulated separase activity, I performed parallel experiments using *Sep*$^{f/f}$*;Gdf9-iCre* oocytes. However, immunofluorescence images of *Sep*$^{f/f}$*;Gdf9-iCre* oocytes chromosomes reveal that fluorescence intensity of Rec8 is also reduced from chromosomes in aged *separase-deleted* oocytes (Figure 4.7, B). In both genotypes, Cohesin appeared to be reduced on arms and at centromeres.

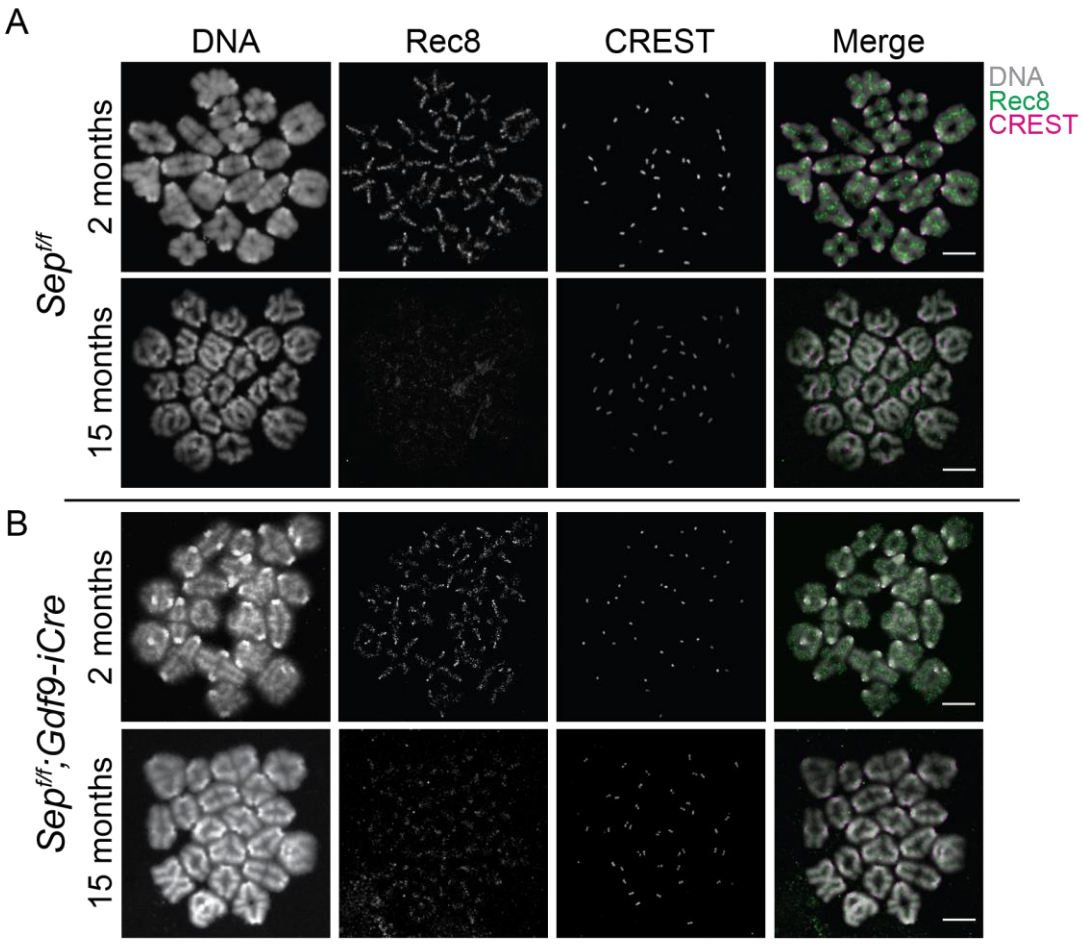

Figure 4.7 Age-related depletion of Cohesin occurs in *Sep$^{f/f}$;Gdf9-iCre* oocytes

Figure show maximum projections of representative chromosomes spread from oocytes cultured to GVBD+5hrs stained for DNA (DAPI), Rec8 and CREST. **A** Panel compares oocyte chromosomes from 2-month-old and 15-month-old *Sep$^{f/f}$* females. There is a marked reduction of Rec8 cohesin subunit from chromosome arms and centromeres in 15-month-old (scale bars 10µm) **B** The panel is a comparison of cohesin levels on the chromosomes in separase deleted oocytes from young and old females. Oocyte chromosome from 15 months old *Sepf/f;Gdf9-iCre* females show a marked depletion of Rec8 from chromosome arms and centromeres (scale bars 10µm).

Quantification of chromosomal cohesin is very difficult due to the difference of its organisation between young and aged oocytes. In oocytes from young females, cohesin localises to the inter-chromatid axis and is generally detectable from the centromeres to the telomeres. By contrast, cohesin in oocytes from aged mice appears to have a less well-defined distribution, frequently appearing to be randomly distributed on the chromatin rather than in the inter-chromatid domain making it difficult to perform signal segmentation on any 3D software analysis. Furthermore, the structural differences related to destabilisation of chiasmata makes it difficult to compare arm cohesin in the two age groups.

I, therefore, focused on quantification of cohesin at the centromere. The confocal microscope allows us to acquire images suitable for 3-dimensional analysis. The surface selection tool incorporated in Imaris software facilitates the segmentation of a region of interest (ROI) using a determined fluorescence signal (Figure 4.8). I calculated the fluorescence of centromeric Rec8 using the CREST signal to define the centromeres as the ROI.

To treat all centromeres under the same conditions, firstly, I define the average centromeric diameter of a given oocyte. Secondly, I used this diameter to establish dimensional and pixel intensity thresholds. The surface mask to wrap the whole 3D structure of each centromeric pair was created using these thresholds, which were equally applied to all the oocytes fixed within the same slide.

Imaris software finds the intensity values for all the different channels of each volumetric pixel (voxel) that has been wrapped and reports independently the values for each one of the segmented areas within the image. In consequence, I obtained per oocyte a file containing 40 measurements per channel, which correspond to the forty centromeric pairs of each oocyte.

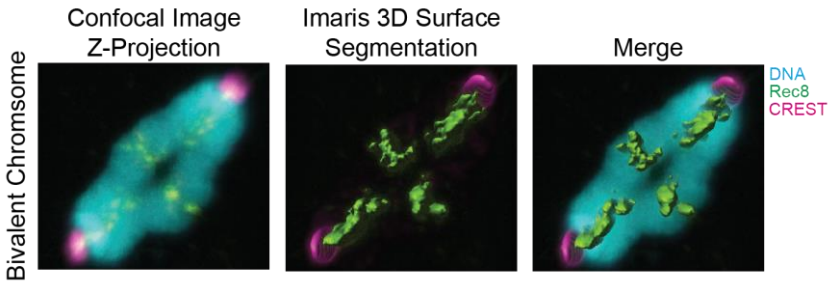

Figure 4.8 Imaris surface segmentation in a bivalent chromosome

The panel shows a bivalent chromosome after being prepared for image analysis On Imaris software. It illustrates an example of the 3-dimentional mask that Imaris software applies over the signal of interest after adjusting the voxel dimension and intensity threshold to create surface segmentation in the region of interest. For illustration proposes Rec8 (green) and CREST (Magenta) have been segmented, the DNA.

As mentioned above oocytes from young and aged females were fixed on the same slide. As a starting point, I, therefore, plotted the fluorescence intensity measurements for centromeric Rec8 and CREST for individual oocytes on each slide and normalised the Rec8 signal to the CREST signal. As can be seen in both genotypes (Figure 4.9 and Figure 4.11), the CREST signal is generally reduced in oocytes of aged mice. This is consistent with previous reports (Lister et al, 2010; Yun et al, 2014) and suggests that oocytes from aged mice have smaller centromeres. The molecular basis for this is currently under investigation by another PhD student in the lab. For my purposes, the reduced CREST signal makes it an imperfect internal control; the Rec8:CREST ratio (Figure 4.10 and Figure 4.12) is likely to underestimate the extent of cohesin depletion during female ageing. This is especially evident in Figure 4.9 in which the data for oocytes from *Sep*$^{f/f}$ young and aged females indicate that the CREST signal for most of the aged oocytes is very much reduced relative to the young oocytes. Figure 4.9 and Figure 4.10 show data for oocytes from young and aged *Sep*$^{f/f}$. Figure 4.11 and Figure 4.12 show data for *Sep*$^{f/f}$*;Gdf9-iCre*.

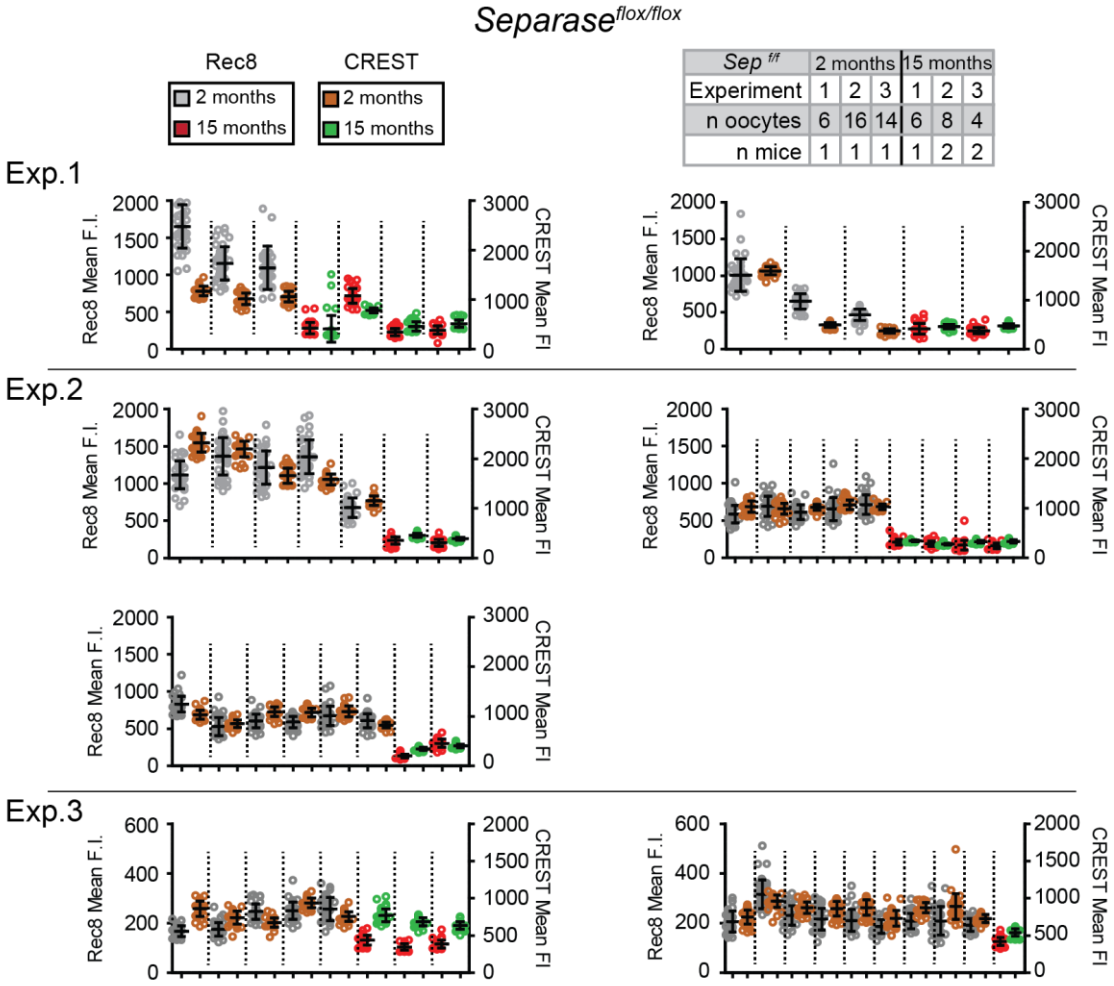

Figure 4.9 Comparison of Rec8 and CREST levels in chromosomes of individual oocytes from young and old *Sep*$^{f/f}$ females

Graphs show mean F.I. for Rec8 and CREST signals obtained from confocal images of air-dried chromosome spreads prepared from oocytes harvested from 2-months-old and 15-month-old *Sep*$^{f/f}$ females. Oocytes from both ages were spread on the same slide at GVBD+5 hrs. Each graph represents an individual slide, corresponding to a single experiment. Each data point represents the F.I. measurement from individual centromere within a given oocyte. Data from different oocytes are separated by broken lines and F.I. values of Rec8 and CREST for individual oocytes are plotted next to each other. Error bars represent the mean ± s.d. for each oocyte. The number of oocytes and mice used in each experiment is explained in the convention table on top of the figure.

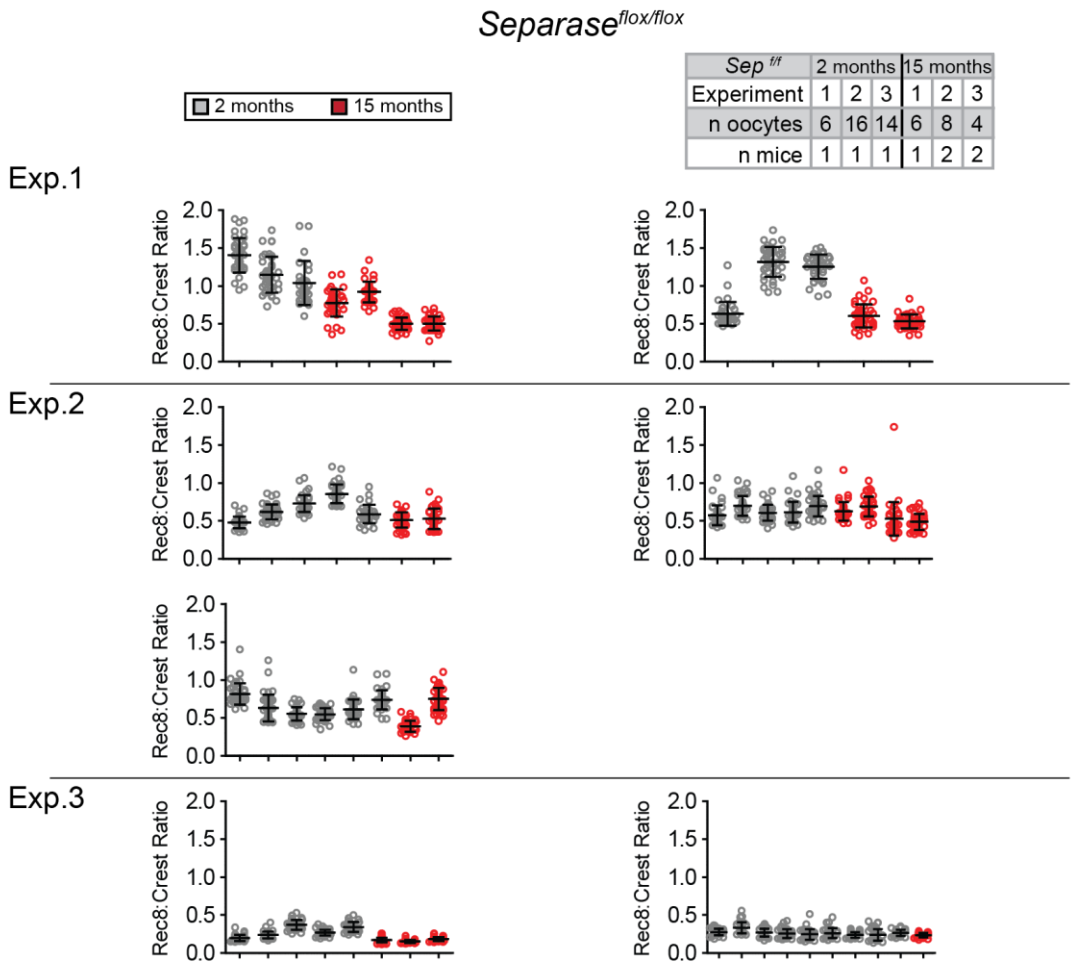

Figure 4.10 Ratios of Rec8:CREST calculated from values presented in Figure 4.9, Comparison between young and aged *Sep*$^{f/f}$ chromosomes

Graphs showing the ratio of Rec8:CREST in oocytes from 2-month-old and 15-month-old *Sep*$^{f/f}$ females calculated from the F.I. data shown in figure 4.9. Each data point represents the Rec8:CREST ratio at individual centromeres. Each dataset represents all centromere measurements obtained from an individual oocyte. Error bars show the mean ± s.d. of the ratios within each oocyte. The number of oocytes and mice used in each experiment is explained in the convention table on top of the figure.

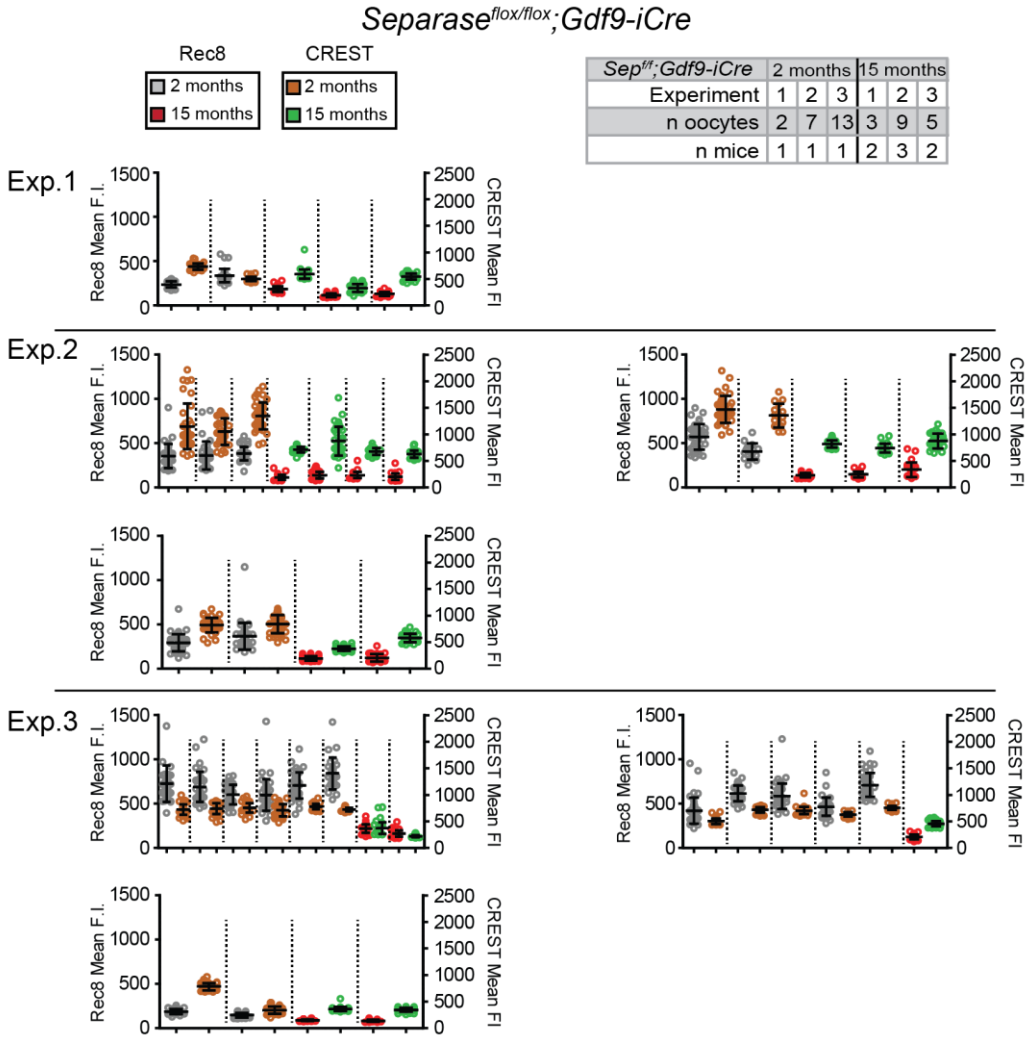

Figure 4.11 Comparison of Rec8 and CREST levels in chromosomes of individual oocytes from young and old *Sep$^{f/f}$;Gdf9-iCre* females

Graphs show mean F.I. for Rec8 and CREST signals obtained from confocal images of air-dried chromosome spreads prepared from oocytes harvested from 2-months-old and 15-month-old *Sep$^{f/f}$;Gdf9-iCre* females. Oocytes from both ages were spread on the same slide at GVBD+5 hrs. Each graph represents an individual slide, corresponding to a single experiment. Each data point represents the F.I. measurement from individual centromere within a given oocyte. Data from different oocytes are separated by broken lines and F.I. values of Rec8 and CREST for individual oocytes are plotted next to each other. Error bars represent the mean ± s.d. for each oocyte. The number of oocytes and mice used in each experiment are shown in the convention table on top of the figure.

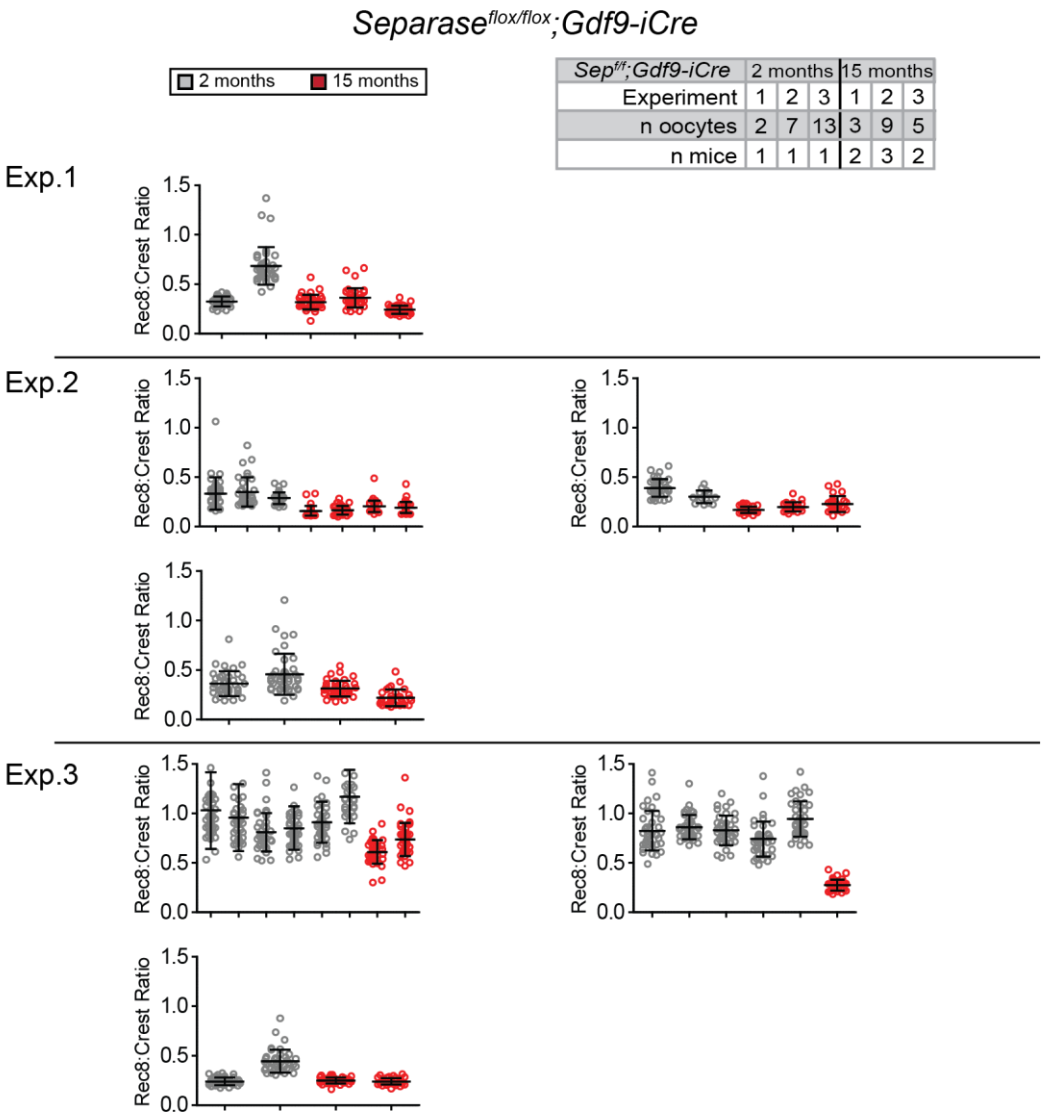

Figure 4.12 Ratios of Rec8:CREST calculated from values presented in Figure 4.11, Comparison between young and aged *Sep$^{f/f}$;Gdf9-iCre* chromosomes

Graphs showing the ratio of Rec8:CREST in oocytes from 2-month-old and 15-month-old *Sep$^{f/f}$;Gdf9-iCre* females calculated from the F.I. data shown in figure 4.11. Each data point represents the Rec8:CREST ratio at individual centromeres. Each dataset represents all centromere measurements obtained from an individual oocyte. Error bars show the mean ± s.d. of the ratios within each oocyte. The number of oocytes and mice used in each experiment are shown in the convention table on top of the figure.

To compare all my experiments together I calculated the means of means for the Rec8:CREST ratio by calculating the mean of all centromere per oocyte and then obtaining the mean for all the oocytes. The resulting graphs show a great dispersion of the data points with no significant difference in cohesin levels between young and old in *Sep*$^{f/f}$ (p=0.314, two sample t-test). This is likely to be at least in part due to the particularly low CREST levels in oocytes from aged *Sep*$^{f/f}$ females. Comparison between young and aged *Separase-deleted* oocytes indicated a significant reduction in cohesin levels in oocytes from older females (p<0.000, Mann-Whitney U Test. Figure 4.13)

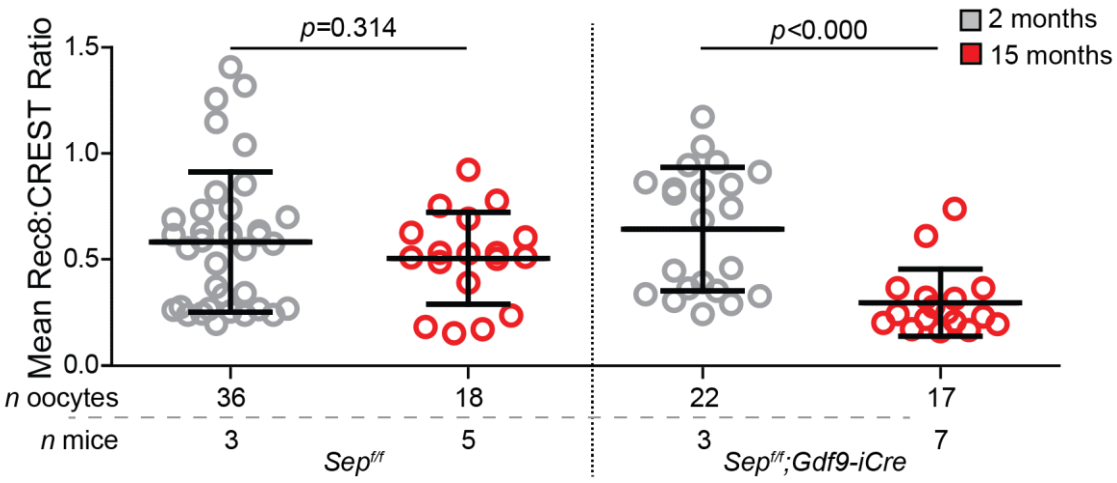

Figure 4.13 Combined analysis of Rec8:CREST ratio in *Sep*$^{f/f}$ and *Sep*$^{f/f}$*;Gdf9-iCre*

The graph shows a parallel comparison of the means of means for the Rec8:CREST ratio obtained from Figure 4.10 and Figure 4.12 compiling the data from young and aged oocytes for *Sepf/f* and *Sepf/f;Gdf9-iCre* in all experiments. Each data points represent the mean Rec8:CREST ratio of all centromere pairs of a given oocyte, error bars represents the ± s.d. The n numbers are shown in the graphs.

I next analysed the data by normalising the Rec8:CREST ratio of aged oocytes to the mean Rec8:CREST ratio of the young oocytes for each slide and then I grouped them by experiment. I found that this approach reduced the spread of the data and indicated that oocyte chromosomes from 15-month-old *Sep*$^{f/f}$ mice show decreased mean Rec8:CREST ratio compared to 2-month-old *Sep*$^{f/}$ across all experimental repeats (Figure 4.14, top row). Similarly, *Sep*$^{f/f}$*;Gdf9-iCre* oocytes from 15-month-old females also showed reduced Rec8:CREST ratios when normalised to those of 2-month-old oocytes. Again, this was consistent between all experiments Figure 4.14, bottom row).

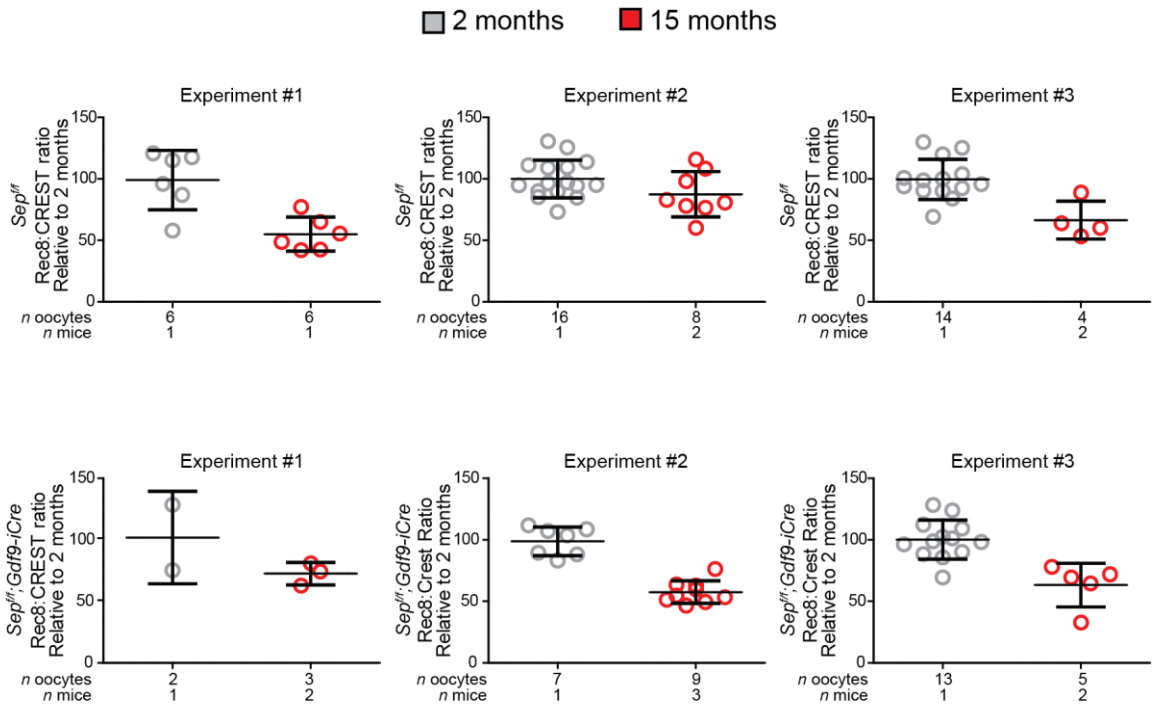

Figure 4.14 Normalisation of the Rec8:CREST ratio from aged oocytes to young per slide for both genotypes, *Sep$^{f/f}$* and *Sep$^{f/f}$;Gdf9-iCre*

Dot plots show the comparison of Rec8:CREST ratios between 2-month-old and 15-month-old. *Sep$^{f/f}$* (top row) and *Sep$^{f/f}$;Gdf9-iCre* (bottom row). Only oocytes within the same slide were used to normalise the values in relation to two-month-old. Each data point represents the mean value of Rec8:CREST ratio relative to two months of all centromeres pairs for a given oocyte. Graphs represent the results for each independent repeat of the experiment. The number of oocytes and mice used for each experiment are located in the X axis (Total, n= 36 oocytes from 3 two-month-old *Sep$^{f/f}$* mice, n= 18 oocytes from 5 fifteen-month-old *Sep$^{f/f}$* mice. n= 22 oocytes from 3 two-month-old *Sep$^{f/f}$;Gdf9-iCre* mice, n= 17 oocytes from 7 fifteen-month-old *Sep$^{f/f}$;Gdf9-iCre* mice)

The Rec8:CREST fluorescence intensity ratio for all our experiments indicate a significant decrease (p=0.000, two sample T-test) in the levels of centromeric Rec8 in 15-month-old *Sep*$^{f/f}$ mouse oocytes (n= 18 oocytes, five mice) compared to 2-month-old *Sep*$^{f/f}$ oocytes (n= 36 oocytes, three mice). Similarly, Centromeric Rec8 is significantly reduced (p=0.000, two sample T-test) in oocytes from 15-month-old *Sep*$^{f/f}$*;Gdf9-iCre* (n= 629 Cent. Pairs from 16 oocytes, seven mice) compared to 2-month-old *Sep*$^{f/f}$*;Gdf9-iCre* oocytes (n= 822 Cent. Pairs from 22 oocytes, three mice, Figure 4.15)

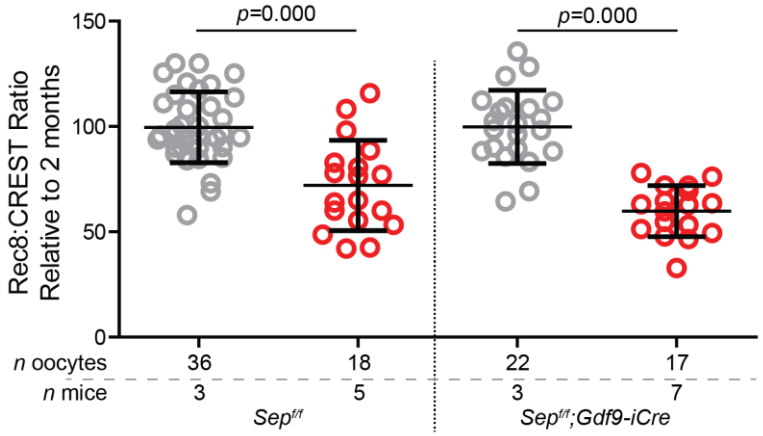

Figure 4.15 Centromeric cohesin depletes with age in *separase-deleted* oocytes

The graph displays the mean values of Rec8:CREST ratios calculated in Figure 4.10 and Figure 4.12 in relation to two months comparing in parallel young vs. old *Sep*$^{f/f}$ and *Sep*$^{f/f}$*;Gdf9-iCre* mouse oocytes. Each data point represents the mean value for all centromeres of a given oocyte. Error bars represent the ± s.d. The levels of centromeric cohesin in old mouse oocytes from both genotypes is significantly reduced compared to two months (*Sep*$^{f/f}$: p=0.000, two sample t-test. *Sep*$^{f/f}$*;Gdf9-iCre*: p=0.000, two sample t-test). n= 36 oocytes from 3 two-month-old *Sep*$^{f/f}$ mice, n= 18 oocytes from 5 fifteen-month-old *Sep*$^{f/f}$ mice. n= 22 oocytes from 3 two-month-old *Sep*$^{f/f}$*;Gdf9-iCre* mice, n= 17 oocytes from 7 fifteen-month-old *Sep*$^{f/f}$*;Gdf9-iCre* mice.

These results indicate that cohesin becomes depleted from oocytes chromosomes during ageing even in the absence of separase. I, therefore conclude that leaky inhibition of separase is not the cause of the age-related depletion of cohesin in the oocytes.

4.6. Cohesin in distally associated homologues

Interestingly, I observed that distally associated homologues remain attached by small traces of cohesin at the telomeres. This raises the possibility that cohesin at mouse telomeres may be resistant to the mechanisms responsible for cohesin depletion during ageing. This would explain the marked absence of prematurely separated homologues in studies on WT mice (Lister, et al 2010; Chiang et al, 2010).

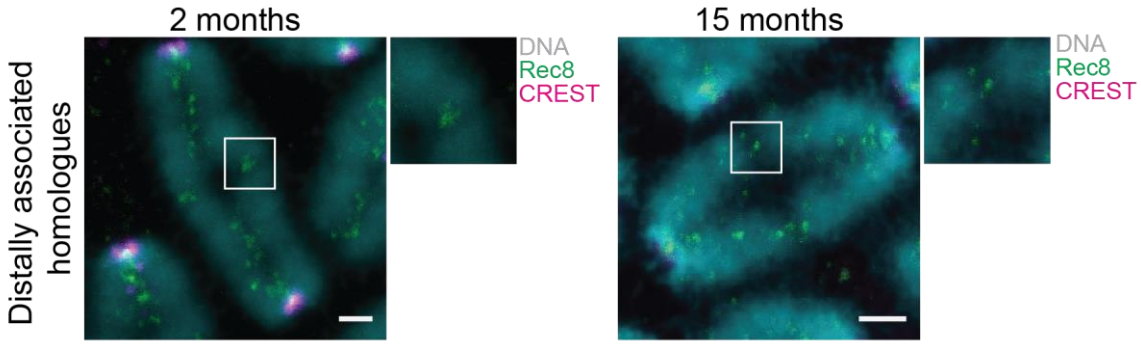

Figure 4.16 Traces of cohesin remain at the telomeres in distally associated homologues

The panel shows representative images of bivalent chromosomes with distally associated homologues from oocytes cultured to GVBD+5hrs comparing 2-month-old vs. 15-month-old. Insets amplify the distal telomere region which remains held by traces of cohesin (scale bars 2µm).

4.7. Cohesin depletion at the centromeres correlates with increasing distance between sister centromeres in *Separase*-deleted oocytes

Consistent with previous findings (Lister *et al.*, 2010), the data shown in Figure 4.6 indicate that the distance between sister centromeres is increased in oocytes from aged *Sep$^{f/f}$* and in *Sep$^{f/f}$;Gdf9-iCre* oocytes. To determine whether the distance between sister centromeres is correlated with the levels of centromeric cohesin, I generated scatter plots for individual oocytes in *Sep$^{f/f}$* and *Separase*-deleted oocytes, show that from data 2-months-old clusters at bottom-centre of the graph while the data from 15-month-old groups towards the top left (Figure 4.17,A for *Sep$^{f/f}$* and Figure 4.18,A for *Sep$^{f/f}$;Gdf9-iCre*). Plots by age of these values indicate a slight negative correlation but disperse with a deficient trend for the 2-month-old *Sep$^{f/f}$* (p=0.161 Least Square, Figure 4.17,B) and 15-month-old *Sep$^{f/f}$;Gdf9-iCre* (p=0.535 Least Square, Figure 4.18,B). The absence of a trend in this analysis might be predictable as we should not be expecting to see major changes in the centromeric distance or the levels of cohesin within the same age group.

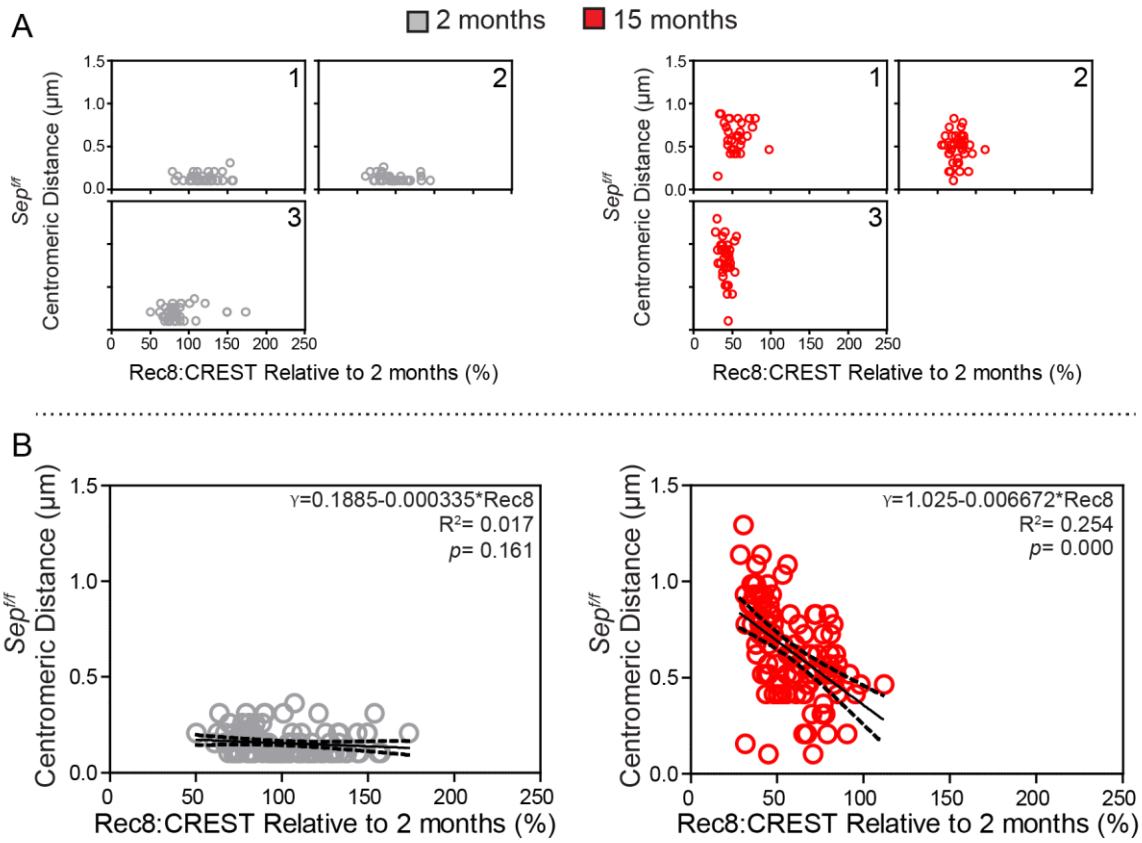

Figure 4.17 Analysis of distance between sister centromeres and cohesin depletion separately by age in *Sep$^{f/f}$* oocytes

In this figure each data point represents the values of a sister centromere pair from bivalent chromosomes in oocytes cultured to GVBD+5hrs **A** The scatter plots show the correlation of the distance between sister centromeres (y-axis) and Rec8:CREST ratio (x-axis), each data point is a centromeric pair and each one of the boxes represent one oocyte **B** Graphs show the compilation of all centromeric values separated by age. The broken black line shows the linear trend. On the top right of each graph are located: i) The equation for the prediction line. ii) The coefficient of determination (R^2) and iii) the significance of the linear regression test. (n= 118 centromeric pairs from two 2-month-old females, and n= 106 centromeric pairs from two 15-month-old females)

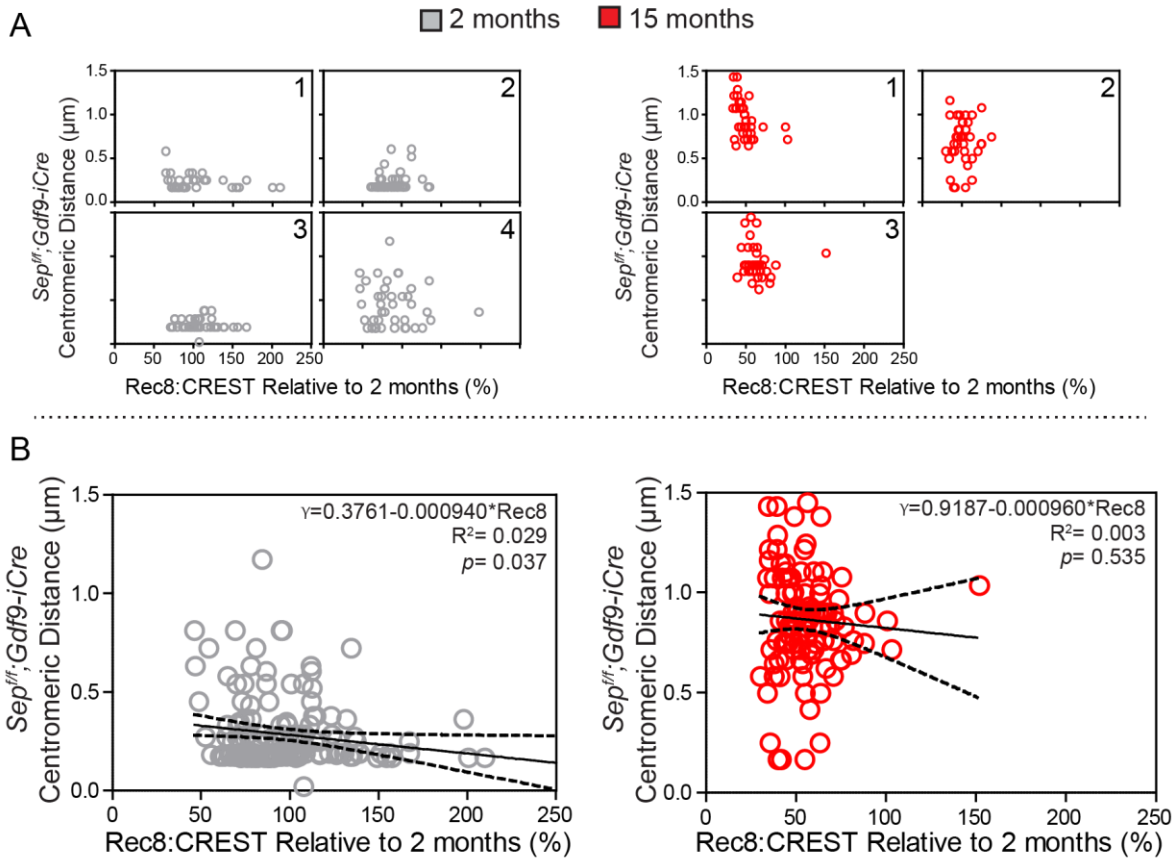

Figure 4.18 Analysis of distance between sister centromeres and cohesin depletion separately by age in *Sep$^{f/f}$;Gdf9-iCre* oocytes

In this figure each data point represents the values of a sister centromere pair from bivalent chromosomes in oocytes culture to GVBD+5hrs **A** The scatter plots show the correlation of the distance between sister centromeres (y-axis) and Rec8:CREST ratio (x-axis), each data point is a centromeric pair and each one of the boxes represent one oocyte **B** Graphs show the compilation of all centromeric values separated by age. The black line among the data points shows the linear trend. On the top right of each graph are located: i) The equation for the prediction line. ii) The coefficient of determination (R^2) and iii) the significance of the linear regression test. (n= 152 centromeric pairs from two 2-month-old females, and n= 117 centromeric pairs from two 15-month-old females)

To be able to analyse a trend, I incorporated both ages on the same scatter plot for each genotype. Least Square analysis for this graph shows that the Rec8:CREST values (x-axis) can predict the distance between sister centromeres (y-axis) in both genotypes (p=0.000, Figure 4.19,A).

The analysis also indicates a negative correlation between sister centromeric distance and centromeric Rec8 that can be predicted in the 47% of the cases in *Sep*$^{f/f}$ (R^2=0.479) and 30% in *Sep*$^{f/f}$*;Gdf9-iCre* (R^2=0.303) (Figure 4.19,A). Data dispersion in the scatter plot for both genotypes attempts to describe a curve. Consequently, I reanalyzed the graphs using exponential non-linear regression equation. The coefficient of prediction increased in relation to the linear regression to a 59% in *Sep*$^{f/f}$ (R^2= 0.5933) and 40% in *Sep*$^{f/f}$*;Gdf9-iCre* (R^2=0.4021) (Figure 4.19,B).

These results indicate that increase is the distance between sister centromeres can be associated with cohesin depletion during ageing. Also, the exponential increase of centromeric distance in relation to the reduction of cohesin levels might suggest that centromeres tolerate a certain degree of cohesin depletion before losing their juxtaposition. It would be interesting to analyse other ages in between 2 and 15 months to see if the exponential increase in distance is maintained and perhaps determine how much cohesin sister centromeres can lose.

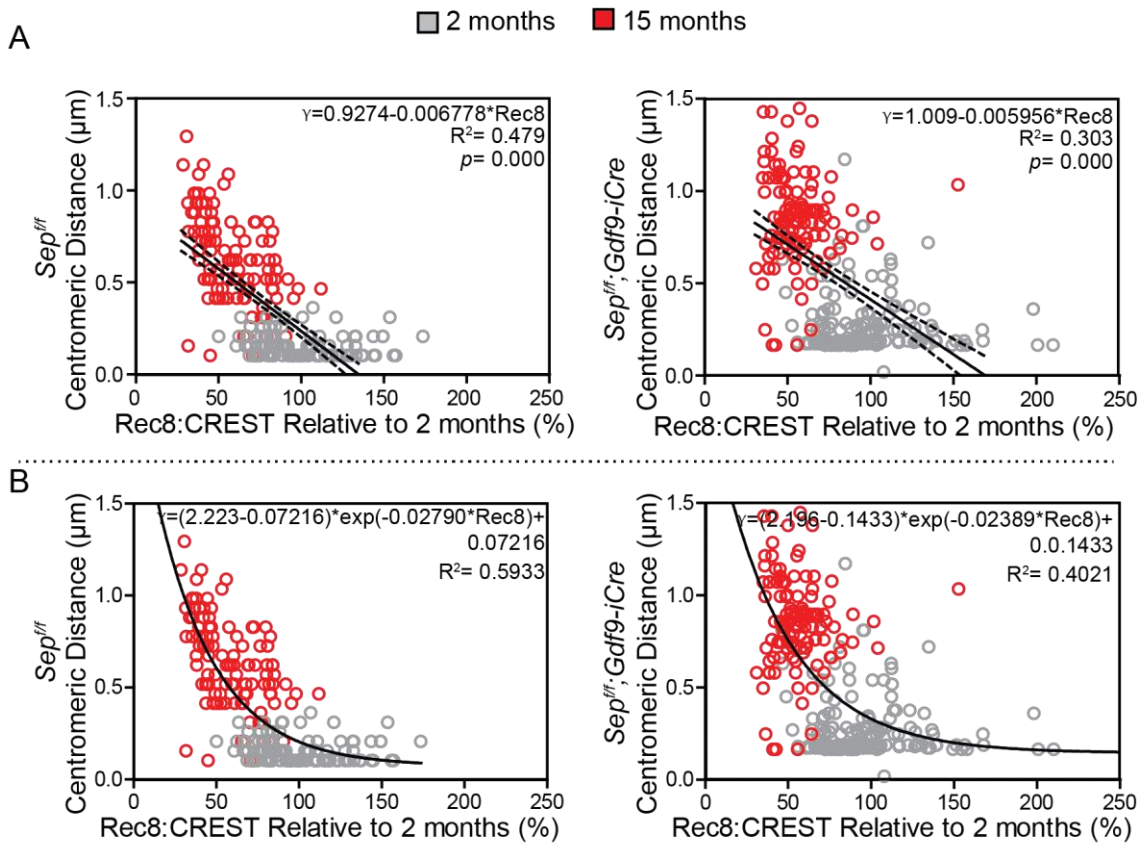

Figure 4.19 Distance between sister centromeres correlates with cohesin depletion and increases in an exponential manner in *Sep$^{f/f}$* and *Sep$^{f/f}$;Gdf9-iCre* mouse oocytes

In this figure each data point represents the values of a sister centromere pair from bivalent chromosomes in oocytes culture to GVBD+5hrs **A** Least Square linear regression analysis for correlation of centromeric distance and Rec8:CREST ratio in young and aged for *Sep$^{f/f}$* and *Sep$^{f/f}$;Gdf9-iCre* mouse oocytes, The black line among the data points shows the linear trend. The equation for the prediction line, the coefficient of determination (R^2) and the significance of the linear regression test. Are located on the top right of each graph **B** Non-linear regression (curve fitting) for exponential analysis in young and aged oocytes from both genotypes. The equation for the prediction line and the coefficient of determination (R^2) are on the top right of each graph; R^2 shows that exponential analysis is better to predict the variation of the distance between centromeres in relation to the variation in centromeric cohesin.

4.8. Discussion

A number of independent studies of MI oocytes have reported that oocyte chromosomes become depleted of the meiosis–specific cohesin subunit Rec8 during female ageing (Chiang *et al.*, 2010; Lister *et al.*, 2010). It has also been reported that this is accompanied by destabilisation of chiasmata, leading to an increase in the proportion of distally-associated homologues (Lister *et al.*, 2010), which could be explained by depletion of arm cohesin. Similarly, depletion of centromeric cohesin is accompanied by an increased distance between sister kinetochores (Chiang *et al.*, 2010; Lister *et al.*, 2010). Together, these structural defects are likely to predispose bivalents to missegregation during anaphase I.

Despite its likely functional significance, progress in identifying the mechanisms underlying age-related cohesin depletion has been very limited. Chiang et al. reported that oocytes from aged females are more susceptible to prematurely activated separase (Chiang *et al.*, 2011). However, it was not clear whether premature activation of oocyte separase is a feature of female ageing. To address this question we aim to specifically delete separase in oocytes from the primordial-stage. To do so, I used mice whose separase peptidase domain has been flanked by *loxP* sites (Wirth *et al.*, 2006) and drove the *Cre recombinase* activity using the *GDF-9* promoter. Deletion of *Separase* in oocytes has been carried out in oocytes during the growing phases using the ZP3 promoter (Kudo *et al.*, 2006), however, this deletion has never attempted from the resting pool of primordial-stage oocytes. Consistent with the absence of separase, I found that anaphase I was inhibited in *Sep*$^{f/f}$;*Gdf9-iCre* oocytes (Figure 4.4).

A problem of studying aged mice is that they gain weight as a result of the long confinement period, frequently becoming obese. Thus, metabolic effects of obesity could confound studies on the effects of ageing. To reduce this risk, I provided an enriched cage environment for mice included in this study. This included igloos, chewing sticks sunflower seeds and cardboard tubes to keep them entertained and away from increasing their food intake as result of boredom. For cost reasons, I did not perform a controlled experiment to measure the effects. However, I observed that none of the females became obese under these conditions. Therefore, the effects

we observe are likely to be specifically due to ageing rather than other metabolic effects related to the body mass.

To test the prediction that cohesin depletion could be prevented by deletion of separase from the time primordial follicles are formed, I harvested oocytes from the ovaries of young (2-month-old) and old (15-month-old) females from the wild-type (*Sep*$^{f/f}$) and *Separase* knockout (*Sep*$^{f/f}$;*Gdf9-iCre*) females. To minimise artifactual effects, oocytes from young and old females were spread on the same slide, for both genotypes, after culturing to GVBD+5hrs.

The prevalence of homologous pairs with tenuous telomeric linkages (distally associated homologues) in cohesin deficient oocytes (Hodges et al, 2005) and in oocytes from aged females (Lister et al, 2010) has been attributed to destabilisation of chiasma (Hodges *et al.*, 2005; Lister *et al.*, 2010). Given that chiasma correspond to the sites of reciprocal DNA exchange between homologues, it is difficult to envisage a mechanism for the destabilisation of the crossover sites themselves. A more likely explanation is that loss of arm cohesin distal to the crossover sites results in premature resolution of chiasma. Analysis of bivalent configuration revealed that the proportion of distally associated homologues increase in aged *Separase*-deleted oocytes. Indicating that chiasma destabilisation is prevalent even when separase has been absent during the extended period of prophase arrest. Interestingly, these findings do not coincide with the structural changes in the chromosomes that this mouse model attempted to prevent.

Cohesion is necessary to maintain the apposition of sister centromeres. Concomitantly, the unified structure of the centromeres is fundamental for establishing the monopolar kinetochore-microtubule attachment essential for the reductional division (Hauf and Watanabe, 2004). The model for separase deletion in oocytes aims to maintain the levels of cohesin, which is who provides chromosome cohesion, at centromeres and as well as in the chromosomes arms. With this model, we hypothesised that the unified structure of sister centromeres would be preserved during the protracted prophase arrest undergone by aged oocytes. However, this results suggest that deletion of separase do not preclude the loss of close proximity between sister centromeres in aged oocytes.

After I observed that the changes in the bivalent structure that can prompt oocyte aneuploidy after meiosis I persist in aged Separase-deleted oocytes (Chiang *et al.*, 2010; Lister *et al.*, 2010; Sakakibara *et al.*, 2015), I next questioned whether these changes obey to age-related cohesin depletion in oocytes from *Separase* knockout mouse. Using the same experimental approach as before, I stained oocytes spread at GVBD+5hr for Rec8 cohesin subunit and CREST as a centromere marker.

Our hypothesis postulated that leaky inhibition of separase is the cause of age-related depletion of cohesin. In consequence, if the protease separase is deleted from the pool of oocytes at the primordial-stage then cohesin will not deplete from the chromosomes. However, contrary to our hypothesis, confocal imaging revealed a marked decline in Rec8 during females ageing in both genotypes. This was evident in arms and at centromeres.

Quantification of chromosomal cohesin is very difficult due to the difference of its organisation between young and aged oocytes. In young oocytes, cohesin is located and perfectly organised between homologue chromosomes all along from the centromeres to the telomeres while in their older counterpart cohesin appear to be randomly distributed not only between homologues but also on them. This random distribution of cohesin in oocytes chromosomes from older mice can generate unreliable signal segmentation on any 3D software analysis. To solve the problem on how to measure chromosomal cohesin prometaphase I oocytes I used the CREST signal to segment the region on Imaris software. From these regions, I obtain the values for Rec8 fluorescence intensity. As a result of this measurements, The Rec8:CREST Ratio show that cohesin depletes with age in $Sep^{f/f}$ and this is consistent with finding previously reported (Chiang *et al.*, 2010; Lister *et al.*, 2010). However, contrary to our hypothesis Rec8:CREST ratio shows cohesin depletion in oocytes from old $Sep^{f/f}$*;Gdf9-iCre* females.

These results were evident from the raw values of centromeric Rec8, which remained relatively consistent across all the slides. To make comparable between all our slides I normalised the Rec8 values the CREST. Interestingly, I observe that CREST levels also deplete with age to the point that could make the Rec8:CREST value very high. After renormalizing the Rec8:CREST values of 15-month-old to the corresponding 2-month-old of the slide I obtain that the Rec8:CREST values were

still significantly lower. By normalising it to CREST indicate that cohesin depletes from oocyte chromosomes during age by a separase-independent mechanism and that the depletion of cohesin can be underestimated in the Rec8:CREST ratio.

We interestingly observed that distally associated homologues remain attached by small traces of cohesin at the telomeres. Moreover, cohesin along the arms of distally associated homologues in oocytes from older females appears significantly reduced but a small portion of cohesin remains at the telomere. Why the entire bulk of cohesin is not removed? I correlated the centromeric distance to the corresponding levels of Rec8:CREST ratio to determine whether the increase in the distance between sister centromeres associated to cohesin depletion. Consistent with previous findings (Lister *et al.*, 2010), centromeric distance increase as levels of cohesin drop in the centromere. Interestingly, the distance between sister centromeres increases exponentially according to the cohesin levels decay. Could this implicate that changes on the architecture of bivalent chromosomes become evident only when cohesin rings located at key positions are removed? I speculate that if this is the case, then cohesin should be organised in two strata; one that provides the foundation of cohesion and a second that establish support to the foundation.

Although it has been suggested that cohesin could migrate from the chromosome arm towards the telomere, I personally do not think this possible in meiosis as the displacement of the cohesin ring could severely alter the condensation of the chromosome. It also could be possible that in meiosis cohesion at the telomeres has a different regulation. In mitosis, SA1-depleted cells are unable to maintain cohesion at the telomeres, while SA2-depleted cells can maintain cohesion at the telomere but lose centromeric cohesion (Canudas and Smith, 2009).

If my speculation is true, then what we might be seeing in distally associated homologues in oocytes from older females could be a reflection of the “cohesion destroyer” inability to reach the deepest stratum of cohesin in this region. A theory of stratified organisation of the cohesion infrastructure could explain why some chromosomes are more susceptible to missegregation than others. Three-dimensional super-resolution microscopy with an adequate telomere marker should provide new insights on how the cohesion infrastructure is configured at this region.

Together these findings provide conclusive evidence that depletion of cohesin is not due to leaky inhibition of separase. Chiang *et al.,* (2011) showed that both inhibitory mechanisms, CDK1-Cyclin B1 and securin, have to be suppressed simultaneously for separase to become active (Chiang *et al.*, 2011). They also showed that oocytes from older mice are more susceptible to loss of cohesion when injected with mutated-separase immune to inhibition. According to my results, it is unlikely that the proteins controlling separase (Stemmann *et al.*, 2001; Herbert *et al.*, 2003) prior anaphase I lose their inhibitory capability during ageing. Possibly, the increased susceptibility of cohesion loss observed after injection of mutated separase (Chiang *et al.*, 2011) can be attributed to the weakness of cohesion infrastructure of the chromosomes in aged mouse oocytes.

To demonstrate that effective separase deletion occurred during the primordial-stage oocyte, the absence of the protease separase at this stage has to be proved. Several times we attempt to do this by immunofluorescence. However, in this mouse model, the separase protease has been truncated by removing the peptidase domain which is coded from exons 24 to 31. Unfortunately, all commercially and non-commercially antibodies that are available to date also recognise the non-truncated part of separase, which gives a positive separase staining in primordial-stage oocytes. To solve this problem, we order the production of an antibody that exclusively targets the separase peptidase domain (exons 24 to 31) to a company in Australia, but this antibody is expected to arrive during the first semester of 2017. This constitutes an important caveat on this part of my work and the assumptions I made on this chapter are subject to further confirmation of the absence of separase in primordial-stage oocytes upon the arrival of the new antibody.

Further investigation is required to determine who might be the culprit of cohesin depletion during female ageing. Other possible candidates include WAPL, which opens the cohesin ring at the kleisin-Smc3 interface during the prophase pathway (Nasmyth, 2011). Although, it is unclear if the prophase pathway also occurs in mammalian oocytes as centromeric cohesin is protected by Sgo2-PP2A (Kitajima *et al.*, 2006) while arm cohesin is removed by separase (Kudo *et al.*, 2006). Imbalance of other cohesin regulators or defective clearance of damaged proteins are other

potential subjects in the study of age-related cohesin depletion which are under further investigation in our laboratory.

Chapter 5. Results: When during oogenesis is cohesin lost?

5.1. Oocyte development

Oogenesis in female mammals commences during fetal life. Upon arrival to the primitive gonad, migrating germ cells form cysts by undergoing several rounds of mitotic divisions before entering into meiosis (de Cuevas *et al.*, 1997; Pepling and Spradling, 1998). Replicated DNA strands produced during premeiotic S-Phase are tethered by cohesin rings, which can create stable interaction with the DNA when ESCO1 (eco1 in yeast) acetylates the Smc3 cohesin subunit (Zhang *et al.*, 2008a). Entering into meiosis, germ cells, which are now called oocytes, arrest at meiotic prophase after maternal and paternal homologues undergo reciprocal recombination to form bivalent chromosomes (Borum, 1961; Baudat *et al.*, 2013).

The invasion of the prophase-arrested oocyte cysts by somatic cells, which occurs during fetal life in humans (Maheshwari and Fowler, 2008) and the first two days post-birth in mice (Pepling and Spradling, 2001), results in the formation of primordial follicles (Tingen *et al.*, 2009). Widespread oocyte death accompanies the process of primordial follicle formation (Pepling and Spradling, 2001). This process dramatically reduces the number of oocytes present in the ovary, in humans, their number is estimated in about 7 million at the moment cyst-breakdown and reduces to 1 million at birth (te Velde *et al.*, 1998). Similarly, in mice, around 20,000 oocytes are present in the cyst at 13.5 dpc (days post coitum) but reduces to 7000 at 2 dpp (days postpartum) (McClellan *et al.*, 2003).

During female reproductive lifespan the number of oocytes at primordial stage becomes depleted and represents the combined of effect of the following three fates: i) remain in the quiescent state ii) succumb to death through atresia either in the primordial stage or after being selected for growth iii) be recruited for growth, develop and ovulate after puberty (Adhikari and Liu, 2009). Oocytes that survive to ovulation spend most of their lifecycle in a non-growing state enclosed in primordial follicles. Furthermore, oocytes from older females are distinguished from their younger counterparts by an extended duration at the primordial stage. During the intervening period, only Rec8-containing cohesin complexes can confer the cohesion required to

maintain intact bivalent chromosomes (Tachibana-Konwalski *et al.*, 2010). Moreover, evidence from mice suggests that cohesive cohesin cannot be reloaded during prophase arrest (Tachibana-Konwalski *et al.*, 2010; Burkhardt *et al.*, 2016).

While our lab, and others (Chiang *et al.*, 2010), have previously shown that fully grown M-phase and prophase-arrested (GV) oocytes show an age-related reduction in cohesin (Lister *et al.*, 2010), it remains to be determined whether this occurs during the relatively quiescent primordial stage. An alternative possibility is that cohesin complexes become vulnerable to damage during the period of intense metabolic activity associated with the remarkable increase in volume during the oocyte growth phase (Sternlicht and Schultz, 1981; Fair *et al.*, 1997). This can last about 10 days in mice (Picton, 2001) and 220 days in women (McGee and Hsueh, 2000).

To gain new insights into the mechanisms underlying depletion of chromosomal cohesin during female ageing, it is important to determine when during oogenesis cohesin becomes depleted from oocyte-chromosomes

5.2. Strategies for the study of cohesin during oogenesis: *TG Rec8-Myc* mouse model

Investigation of cohesin levels in primordial-stage oocytes requires IF of ovarian sections, which can be notoriously difficult to interpret due to non-specific staining. In addition, labelling of cohesin on the chromosomes is particularly difficult as not many antibodies are successful at targeting the cohesin subunits (Waizenegger *et al.*, 2000; Kudo *et al.*, 2006). The insertion of Myc-tag at the C-terminus of the α-kleisin was previously reported for detecting this cohesin subunit when antibodies have failed (Waizenegger *et al.*, 2000). A transgenic *Rec8-Myc* mouse (*TG Rec8-Myc*) was created to determine if separase-mediated cleavage of Rec8 resolves bivalent chromosomes during meiosis I (Kudo *et al.*, 2006). The *TG Rec8-Myc* mouse was generated by replacing all the endogenous Rec8 with a Rec8-transgene containing nine copies of human Myc-tag using a *Rec8* knockout mouse (Xu *et al.*, 2005). The *TG Rec8-Myc* mouse was subsequently useful for studying the cleavage sites of Rec8 protein (Kudo *et al.*, 2009). Due to the existing difficulties for labelling Rec8

cohesin subunits in ovarian section and the shortage of the anti-Rec8 antibody we use this *TG Rec8-Myc* mouse.

To validate the *TG Rec8-Myc* mouse, we cultured to GVBD+5hrs oocytes from 2-month-old wild-type CD1 and *TG Rec8-Myc.* To control IF artefacts, we spread the chromosomes on the same slide and stained them for anti-Rec8 antibody (Eijpe *et al.*, 2003) and anti Myc-tag antibody (Millipore UK). Imaging reveals that in oocytes from the wild-type CD1 mouse, Rec8 cohesin subunit is located at the interchromatid axis and between sister centromeres; there was no signal detected from the anti Myc-tag antibody. In contrast, prometaphase I oocytes (GVBD+5hrs) from the *TG Rec8-Myc* mouse show staining for anti Rec8 and anti Myc-tag antibodies following the same staining pattern as wild-type CD1 mouse oocytes (Figure 5.1).

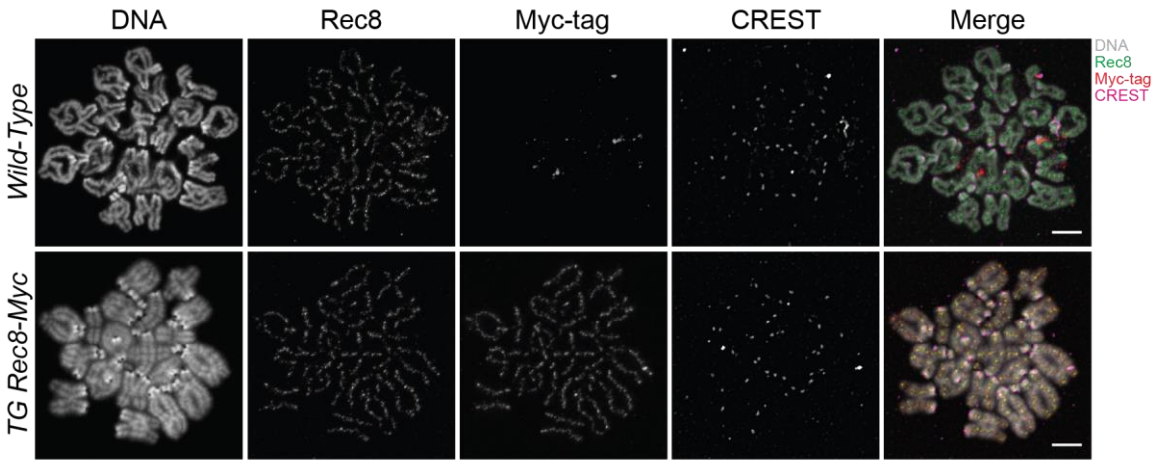

Figure 5.1 Antibody specificity test for Rec8 and Myc-tag

Panel illustrates representative images of oocytes cultured to GVBD+5hrs and stained for anti-Rec8 and anti Myc-tag antibodies in wild-type and *TG Rec8-Myc* mice. Oocytes from wild-type CD1 mouse show no staining for anti-Myc-tag antibody while the staining patterns of anti Rec8 and anti Myc-tag antibodies are similar in *TG Rec8-Myc* oocytes (scale bars 10µm). This validation was performed in collaboration with Daniel Cooney.

5.2.1. *Do aged TG Rec8-Myc mouse oocyte chromosome show hallmark effects of female ageing?*

The *TG Rec8-Myc* mouse carries a genetic modification on the meiotic-specific cohesin α-kleisin subunit which works as the exit gate of the cohesin ring (Nasmyth, 2011). In addition, the TG mouse carries multiple copies of *Rec8* and may, therefore, be more resistant to depletion and its consequences during female ageing. Therefore, it is important to determine whether the *TG Rec8-Myc* mouse oocytes exhibit the hallmark effects of ageing previously described from studies of prometaphase I and MII oocytes (Chiang *et al.*, 2010; Lister *et al.*, 2010). To test this, I cultured oocytes from 2-month-old and 15-month-old *TG Rec8-Myc* mouse to GVBD+5hrs. Also, to minimise the influence of artefacts during the IF procedures, I prepared air-dried chromosome spreads from oocytes of young and old females on the same slide and stained them for Rec8-Myc and CREST. Confocal images show that the Rec8-Myc fluorescence intensity of in oocyte chromosomes from 15-month-old females is lower at the centromeres and chromosome arms compared to two months (Figure 5.2).

Following the same strategy I used in my previous chapter (Chapter 4, Mechanisms of cohesin depletion), I analysed the chromosome spread images obtained by the confocal microscope on Imaris using surface segmentation tool on the CREST signal.

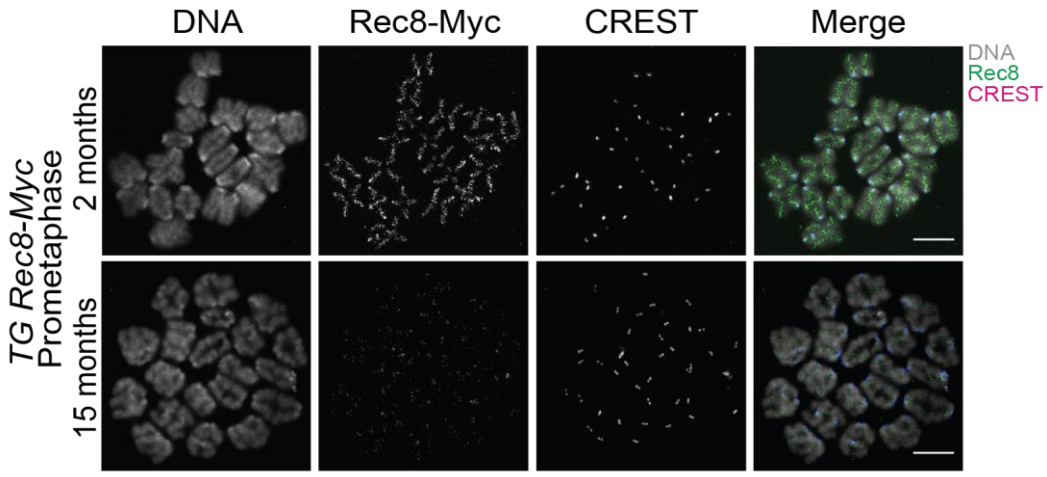

Figure 5.2 Comparison of Rec8-Myc fluorescence intensity in oocytes chromosomes from young and old *TG Rec8-Myc* females

Panel show maximum projections of representative oocytes chromosomes spread from 2-month-old and 15-month-old *TG Rec8-Myc* females cultured to GVBD+5hrs and stained for DNA (DAPI), Rec8 and CREST. Oocytes chromosomes from15-month-old females show a significant reduction in Rec-Myc fluorescence intensity from centromeres and chromosome arms compared to 2 months (Scale bars 10µm)

Imaris measurements reveal that the mean fluorescence intensity of centromeric Rec8-Myc is reduced in the majority of 15-month-old *TG Rec8-Myc* females compared to oocytes from 2-month-old (Figure 5.3). I also obtained the values for the levels of CREST and observed that the signal is generally reduced in oocytes from 15-month-old *TG Rec8-Myc* (Figure 5.3). Thus, quantification by calculating the Rec8-Myc:CREST ratio for individual centromeres underestimates the extent of the cohesin depletion in oocytes from old females as seen in (Figure 5.4). Nonetheless, normalisation of the Rec8-Myc:CREST ratio for each centromere to the average of the ratio for all centromeres from the 2-month-old for the same slide indicated that centromeric Rec8 is significantly reduced ($p=0.008$, Mann-Whitney U test) in aged oocytes (Figure 5.5). I, therefore, conclude that *TG Rec8-Myc* females show an age-related decline of cohesin.

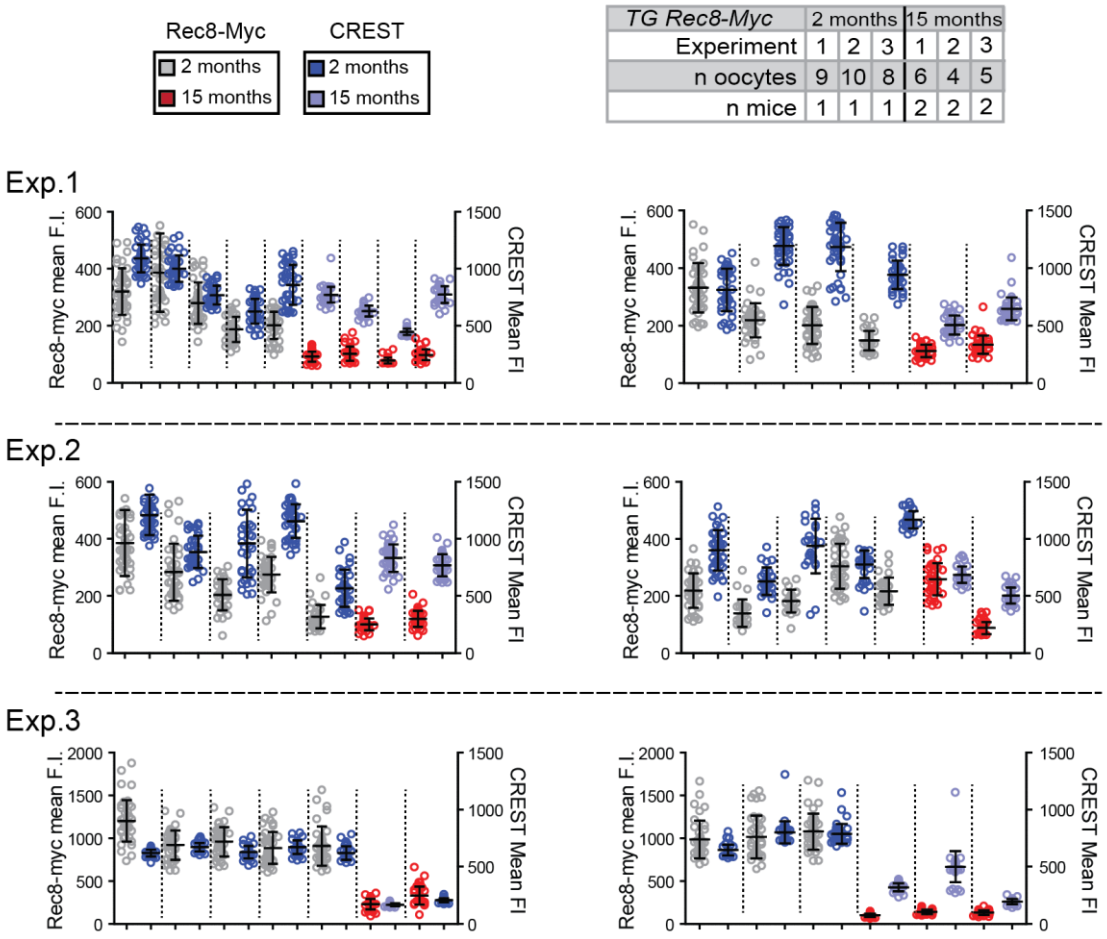

TG Rec8-Myc	2 months			15 months		
Experiment	1	2	3	1	2	3
n oocytes	9	10	8	6	4	5
n mice	1	1	1	2	2	2

Figure 5.3 Comparison of Rec8-Myc in oocytes from young and old TG Rec8-Myc females

Graphs show mean F.I. for Rec8-Myc and CREST from confocal images of air-dried chromosome spreads prepared from oocytes harvested from 2- and 15-month-old TG Rec8-Myc mice and spread on the same slide at GVBD+5 hrs. Each graph represents an individual slide. Each data point represents the F.I. measurement from individual centromere. Broken lines separate Rec8 and CREST FIs from individual oocytes. Error bars represent the mean ± s.d. for each oocyte. The number of oocytes and mice used in each experiment is shown in the table.

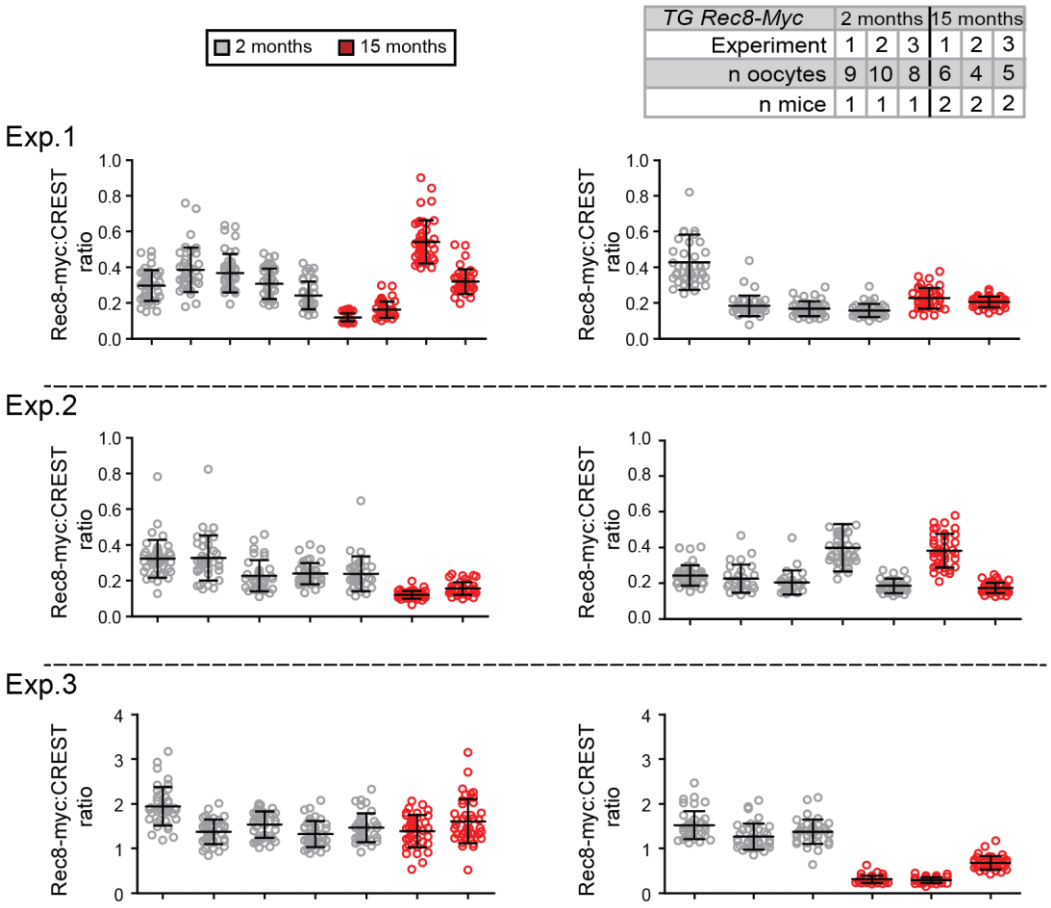

Figure 5.4 Rec8-Myc:CREST ratio by individual oocytes comparing young vs old *TG Rec8-Myc* females

Graphs showing the ratio of Rec8-Myc:CREST in oocytes from young and old females calculated from the F.I. data shown in Figure 5.3. Each data point represents the Rec8-Myc:CREST ratio at individual centromeres. Each dataset represents all centromere measurements obtained from an individual oocyte. Error bars show the mean ± s.d. of the ratios within each oocyte. The number of oocytes and mice used in each experiment is shown in the table.

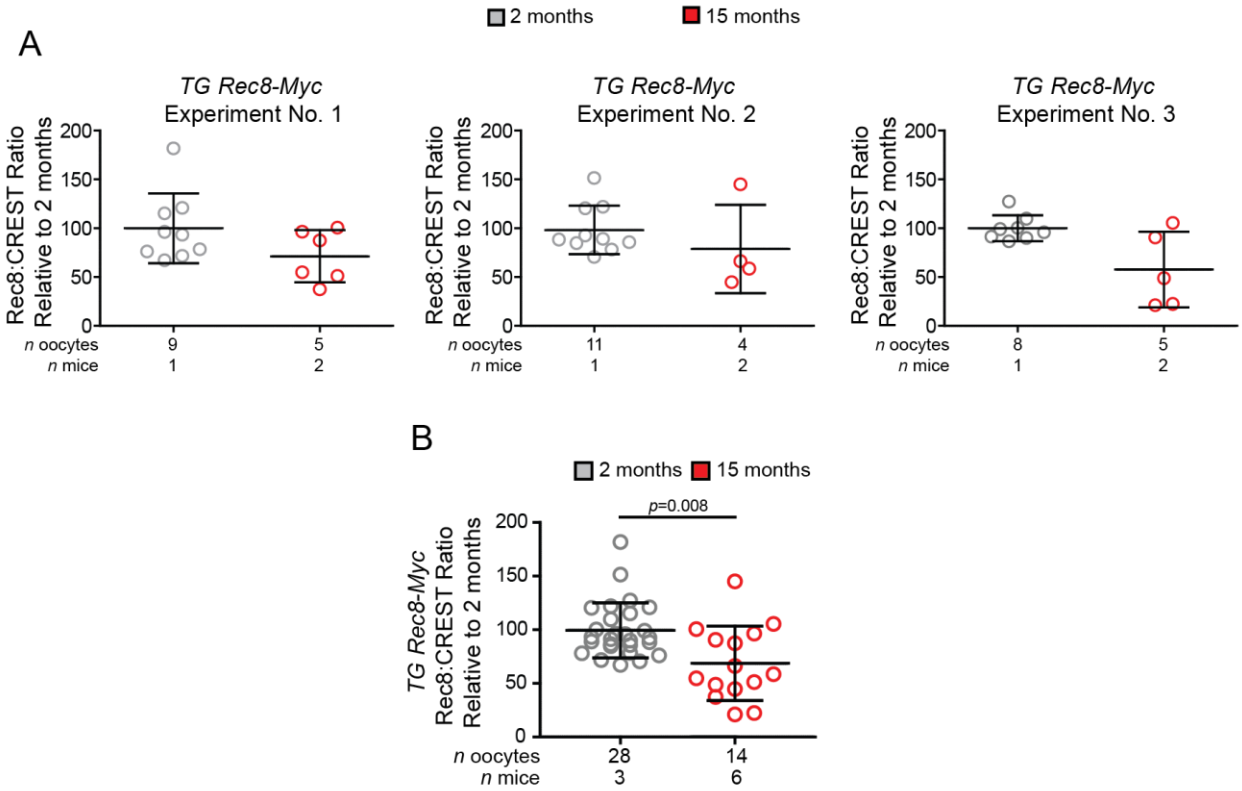

Figure 5.5 Depletion of cohesin is prevalent in aged TG Rec8-Myc oocytes

A Dot-plots show Rec8:CREST ratios relative to two months comparing young vs. aged oocytes from *TG Rec8-Myc* females, separated by experiments. Each data point represents the mean Rec8:CREST ratio of all centromeres of a single oocyte. Error bars represent the mean ± s.d. for each oocyte. The number of oocytes and mice are shown under each graph. **B** The graph shows Rec8:CREST ratios relative to 2 months combining all experiments. Error bars represent the mean ± s.d. for each oocyte. There is a significant depletion in the levels of centromeric cohesin in aged *TG Rec8-Myc* mouse oocytes (p=0.008 Mann-Whitney U test). The number of oocytes and mice are indicated in the graph.

To determine whether the consequences of cohesin depletion are consistent between *TG Rec8-Myc* oocytes and those from other mouse strains (Chiang *et al.*, 2010; Lister *et al.*, 2010), I scored bivalents according to with the number of visible chiasmata (<1 visible chiasma; single chiasma: and >1 chiasma) as previously reported (Lister *et al.*, 2010). Consistent with previous findings (Lister et al 2010; Chiang et al, 2010) and my own findings for the separase null (Chapter 4 – Results: Mechanisms of cohesin depletion), I observed bivalents in which homologues appeared to be closely connected at the telomeres, but without a visible chiasma. These, which are referred to as distally associated homologues, were significantly increased in oocytes from 15 months compared with 2-month-old *TG Rec8-Myc* mice ($p<0.001$, χ^2; Figure 5.6, A). The proportion of bivalents in which single, or multiple chiasmata were observed was not significantly different between the two age groups (Figure 5.6, A). The finding that the increase in distally associated homologues was not accompanied by a concomitant reduction in those with single chiasma differs from our previous findings (Lister *et al.*, 2010).

We previously hypothesised that because bivalent stability is dependent on cohesin distal to the chiasma, single-chiasmata bivalents may be particularly susceptible to cohesin depletion. My findings indicate that this is not universally the case. Moreover, the proportion of distally associated homologues observed in oocytes from aged females was also reduced (25% *vs.* 35%) compared with our previous work (Lister *et al.*, 2010). One possibility is that this reflects a protective effect of multiple copies of *Rec8-Myc* in the TG oocytes.

To further investigate the effects of cohesin depletion at centromeres of TG*Rec8-Myc* oocytes, I measured the distance between sister centromeres. This is important because the loss of the “unified structure” of sister centromeres may compromise monopolar attachment of sisters, and hence make it difficult to achieve stable bi-orientation of bivalent chromosomes on the MI spindle. To measure inter-centromere distances, I followed the same procedure used in my previous chapter (Chapter 4 – Mechanisms of cohesin depletion), where I determined the distance by detecting the brightest point in the core of the CREST signal. The result of these measurements shows that sister centromeres are significantly further apart in bivalent chromosomes

of oocytes from 15-month-old compared to 2-month-old *TG Rec8-Myc* mice (Figure 5.6, B). This is consistent with previous findings (Lister *et al.*, 2010).

In conclusion, these results indicate that similar to oocytes from old wild-type females (Lister *et al.*, 2010) the *TG Rec8-Myc* mouse shows the hallmark effect of ageing. While the consequence of cohesin depletion on bivalent stability may be less severe compared with previous strains studied, my findings offer a good indication that *TG Rec8-Myc* mouse strain is useful for the study of female reproductive ageing.

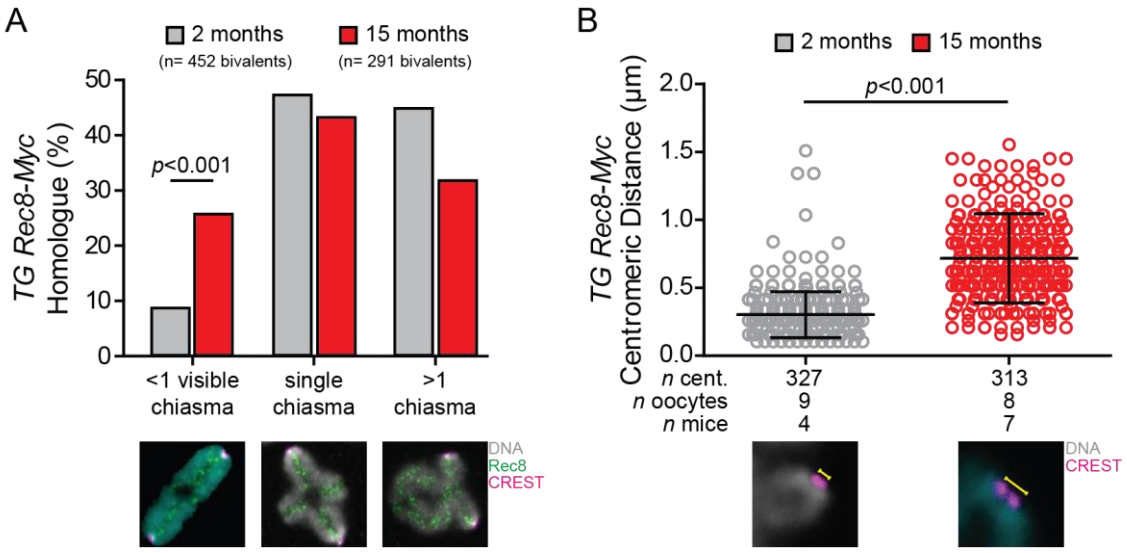

Figure 5.6 Effect of female age on bivalent structure in *TG Rec8-Myc* oocytes

A The bar chart shows the homologues linkages classified according to the number of visible chiasma (no visible chiasma, single chiasma, or >1 chiasma) in oocytes from 2-month-old (n= 27 from 4 females) and 15-month-old (n= 16 from 7 females) *TG Rec8-Myc* mice. The analysis is based on bivalents that could be unambiguously classified (n= 452 from 2-month-old oocytes; n= 291 from 15-month-old oocytes). Images show representative bivalents for each category. Comparison of oocytes from 2 and 15-month oocytes indicated a significant increase in the proportion of bivalents with no visible chiasma ($P<0.001$; χ^2 test). **B** Dot plot shows the distance between sister centromere measured by line scan in 2 months (n=327 centromere pairs, 9 oocytes from 4 females) and 15-month oocytes (n=313 centromere pairs, 8 oocytes from 7 females). Each data point represents a single centromere pair. Errors bars show the mean ± s.d. Comparison of the distance between sister centromere pairs indicates a significantly increased distance in oocytes from 15-month-old females ($p< 0.001$. χ^2 test) Images show typical examples of unified and separated centromeres.

5.2.2. *Do aged TG Rec8-Myc oocytes exhibit premature sister separation during meiosis I?*

Cohesin depletion during female ageing associated with disruption of bivalent chromosomes provides a plausible explanation for the age-related increase in oocyte aneuploidy (Chiang *et al.*, 2010; Lister *et al.*, 2010; Chiang *et al.*, 2011; Sakakibara *et al.*, 2015). In consequence, I asked whether the oocytes from old *TG Rec8-Myc* females exhibit premature sister separation during anaphase I. To answer this question, I cultured oocytes from 2-month-old and 15-month-old *TG Rec8-Myc* mice for 16 hours (overnight) to metaphase II and fixed them on the same slide. Anaphase I converts bivalents into dyad chromosomes, and anaphase II converts dyad chromosomes to single chromatids. Thus, in metaphase II-arrested oocytes from both ages, I looked at the proportion of oocytes that display premature separation of chromatids. I found that 40% of the oocytes from the *TG Rec-Myc* mice aged 15 months contain single chromatids (n=17 oocytes from five mice). In contrast, all oocytes (100%) from 2-month-old *TG Rec-Myc* mice contain only dyad chromosomes (n=34 oocytes from five mice) (Figure 5.7). With this experiment, we conclude that similar to aged wild wild-type mouse oocytes (Lister *et al.*, 2010) the *TG Rec8-Myc* mouse also exhibits premature separation of sister centromeres.

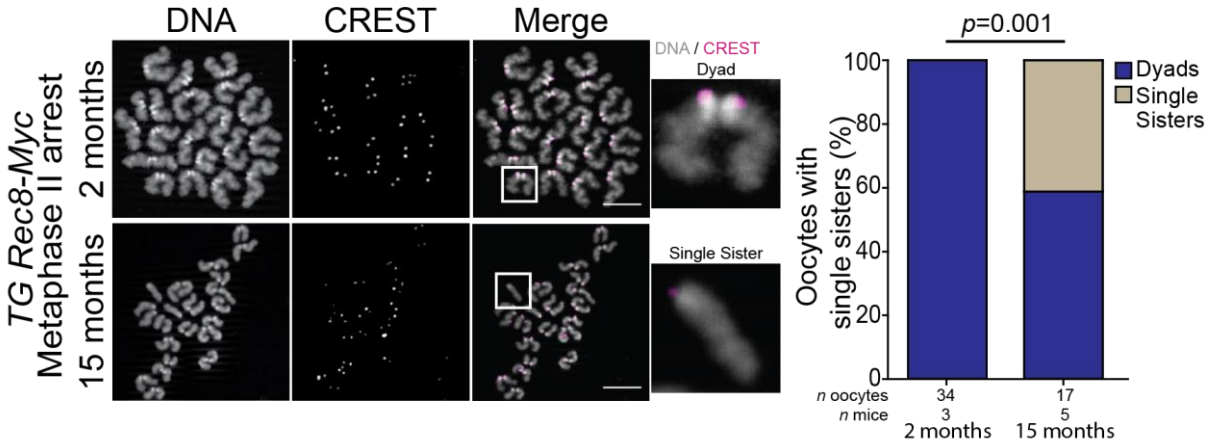

Figure 5.7 Aged oocytes from the *TG Rec8-Myc* mouse exhibit premature separation of sister centromeres

The panel shows representative images of air-dried oocyte chromosome spread after overnight culture from 2-month-old and 15-month-old *TG Rec8-Myc* mouse. The Insets show an example of a dyad chromosome (top row) and a single chromatid (bottom row) from young and aged *TG Rec8-Myc* mouse oocytes respectively (Scale bars 10µm). The bar chart compares the proportion of oocytes containing dyads and single chromatids from young and old *TG Rec8-Myc* mice. Only oocytes from old females contain single chromatids (P=0.001; χ^2 test)

Together, these results on the characterization of the effects of female age on bivalent chromosomes indicate that the effect of reproductive ageing in *TG Rec8-Myc* females is similar to that observed in wild-type female mice, which have been previously used to investigate age-related chromosome segregation errors (Chiang *et al.*, 2010; Lister *et al.*, 2010). In conclusion, the findings suggest that *TG Rec8-Myc* females provide a valid model for investigating the molecular basis of cohesin depletion during female reproductive ageing.

5.3. Strategies for the study of cohesin during oogenesis: Identification of primordial-stage oocytes

The progressive decline in the number of primordial-stage oocytes during female ageing (Gosden *et al.*, 1983; Faddy and Gosden, 1996) makes the study of female reproductive ageing very challenging. Chromatin immunoprecipitation (ChIP) after high purity isolation of oocytes via FACS is possibly the most suitable technique to investigate the levels of chromosome-associated cohesin. However, due to the depletion of oocytes during ageing, FACS analysis would require a very large number of aged mice to meet the minimum requirements for cell sorting. In response to this challenge, we use histological techniques.

To appropriately use histological techniques, we first need to learn how to look at the ovary under the microscope. The different stages of follicular development are well defined by the morphology and number of cells surrounding the oocyte (Pedersen and Peters, 1968; Picton, 2001). Primordial follicles, which are the earliest stage of follicular development, contain the resting pool of oocytes. Histological characteristics of this type of follicle consist of a prophase-arrested oocyte in a relatively quiescent state with approximately 10µm in diameter surrounded by a single layer of flattened cells (Rajareddy *et al.*, 2007) (Figure 5.8).

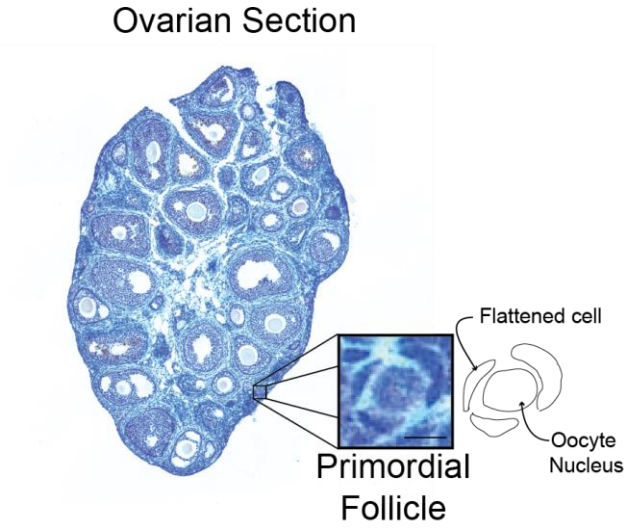

Figure 5.8 Primordial follicle in comparison to the ovarian section
The image shows an example of a 2-month-old mouse ovarian section stained for hematoxylin-eosin illustrating the small is the size of a primordial follicle in relation to the whole ovary. The inset shows a magnified image of an individual primordial follicle located at the ovarian cortex; the schematic shows the different compartments of the primordial follicle (Scale bar 5µm).

Recognition of mouse primordial follicles is very difficult due to their small size. We, therefore, used the transcription factor Foxo3A for training proposes and to convince myself that I was able to identify primordial-stage oocytes using fluorescence microscopy (Figure 5.9). Foxo3A is a downstream effector of the PTEN-PI3K-AKT pathway (Tran *et al.*, 2003) which prevents activation of primordial-stage oocytes (Castrillon *et al.*, 2003) and is highly expressed in the nucleus of primordial-stage oocytes (Liu *et al.*, 2007).

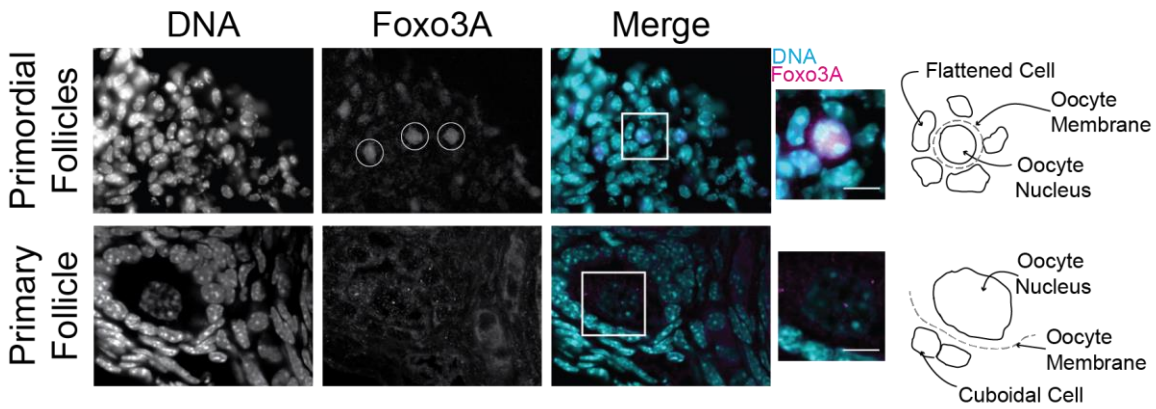

Figure 5.9 Identification of primordial follicles using Foxo3A in fluorescence microscopy

The panel shows a comparison of Foxo3A nuclear expression between oocytes at primordial stage (top row) and growing phase (bottom row). White circles in Foxo3A image indicate oocytes expressing high levels of the transcription factor. Insets show magnified images of the oocyte nucleus at the primordial stage (top panel) and at the growing phase (bottom panel), in which nuclear localisation of Foxo3A is very much reduced compared with primordial-stages (Scale bars 5µm).

To test the specificity of the anti-Myc antibody, I performed immunohistochemistry on ovarian sections from 2-month-old *TG Rec8-Myc* and wild-type mice that were loaded onto the same slide. Rec8 is a meiotic-specific α-kleisin cohesin subunit (Molnar *et al.*, 1995; Uhlmann *et al.*, 1999). In consequence, when we target the Myc-tag in the *TG Rec8-Myc* ovaries, only the oocytes within the section are labelled. We identified primordial-stage oocytes and observed that Rec8-Myc was localised only in the nucleus while surrounding pre-granulosa cell nucleus and other somatic cells in the tissue did not show any staining (Figure 5.10, top row). Also, the phenotype of the staining in oocyte nucleus from the *TG Rec8-Myc* mouse shows a punctuated pattern which is enriched at the heterochromatin regions. Oocyte nucleus in the ovarian section from wild-type mouse shows no staining for the anti-Myc

antibody and only auto-fluorescence from the tissue can be detected (Figure 5.10, bottom row).

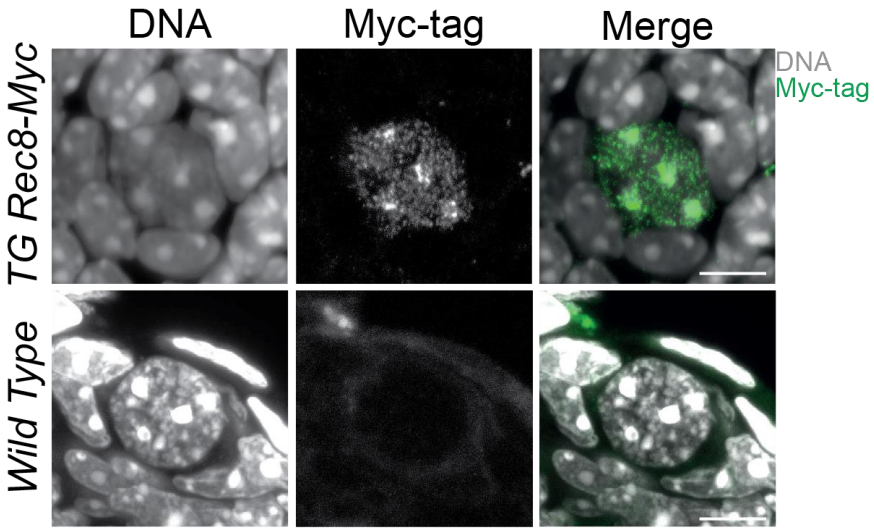

Figure 5.10 Specificity of anti-Myc antibody

The panel shows representative images of primordial-stage oocytes from the *TG Rec8-Myc* and wild-type mice that were fixed on the same slide and immunolabeled using anti-Myc tag antibody clone 4A6 conjugated with Alexa Fluor 488 (Millipore). Wild-type primordial-stage oocyte shows no nuclear staining (Scale bars 5µm).

5.4. Chromosome-associated cohesin is reduced in primordial stage oocytes from aged females

The prevalence of cell death due to follicular atresia represents a potential confounding factor in the assessment of cohesin levels in primordial-stage oocytes. To avoid measuring cohesin in oocytes that were undergoing atresia, I stained the ovarian section with TUNEL (TdT-mediated dUTP-biotin nick end labelling), which is an assay for cell death identification that has been widely used (Gavrieli *et al.*, 1992). To learn how to interpret TUNEL staining in primordial stage oocytes, I co-stained TUNEL with active caspase caspase-3 in ovarian sections. I found that oocytes at primordial stage expressing active caspase-3 did not always express TUNEL and vice versa (Figure 5.11, A). However, oocytes with high levels of active caspase-3 were associated with high TUNEL expression. Conversely, I also observed oocytes with high expression of TUNEL, but not active caspase-3. The need to permeabilize the ovarian sections for assessment of oocyte cohesin dictated the use of TUNEL alone to distinguish between dying and healthy primordial stage oocytes. My subsequent analyses are based only on TUNEL-negative oocytes (Figure 5.11, B).

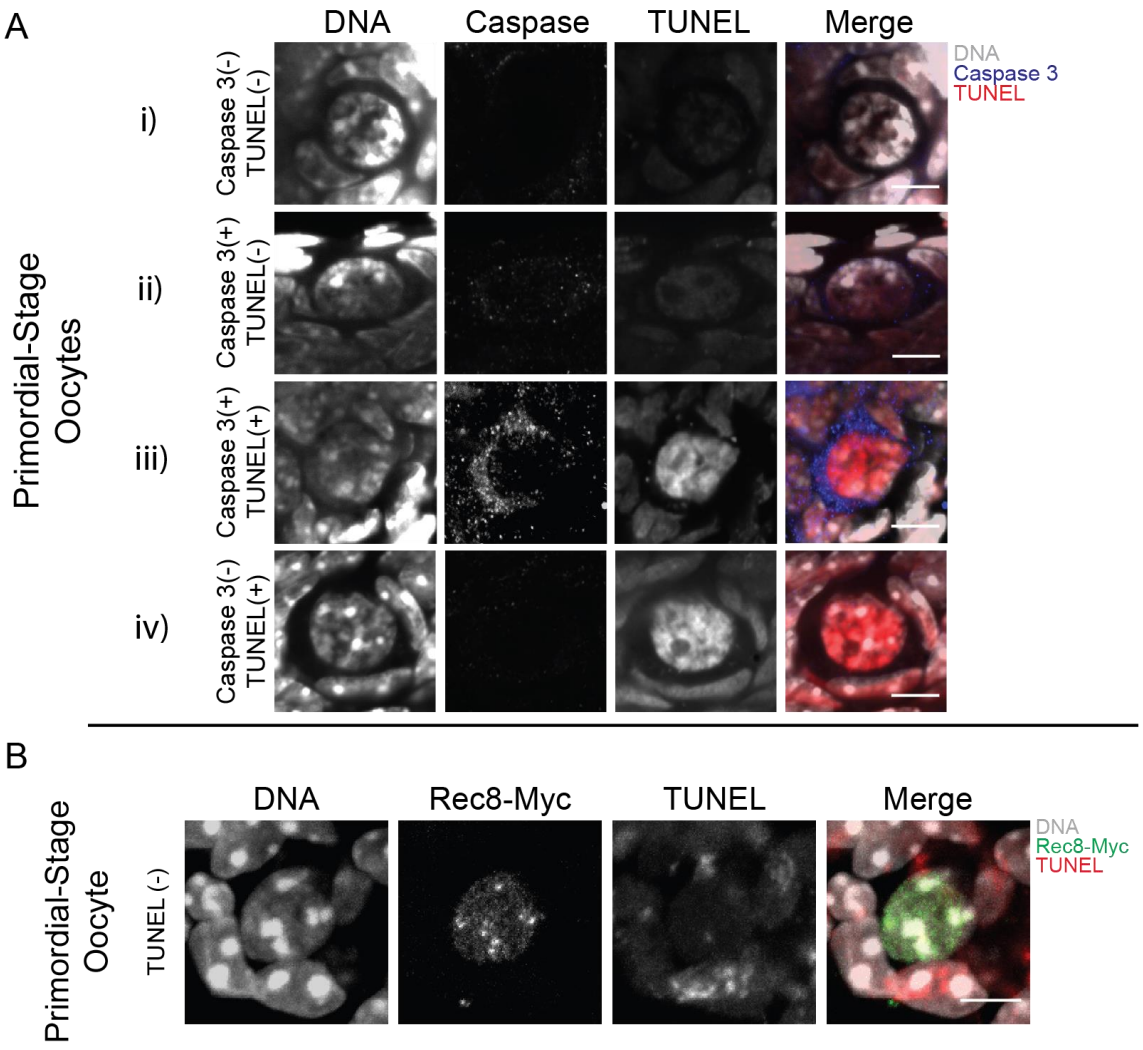

Figure 5.11 Recognition of dead primordial-stage oocytes using TUNEL

A. Images show representative primordial stage oocytes stained for active caspase-3 and TUNEL in ovarian cryosections (scale bars 5µm). i) not expressing caspase-3 nor TUNEL. ii) expressing of caspase-3 but not TUNEL. iii) expressing caspase-3 and TUNEL. iv) expressing TUNEL but not caspase3. TUNEL positive oocytes have either high levels of active caspase-3 or none. **B** Panel show images of a representative oocyte at the primordial stage which is TUNEL negative and co-stained with Rec8-Myc.

The staining for Rec8-Myc in prophase-arrested oocytes is characterised by a very distinctive punctuated pattern over the chromatin and enriched in the areas of heterochromatin (Figure 5.12, A), which is consistent with a previous report in *drosophila melanogaster* (Oliveira *et al.*, 2014). This observation is important because it implies that Rec8-Myc distribution is not uniform in the nucleus, and can lead to a misinterpretation if the analysis is based on images containing an incomplete nucleus. To solve this problem, I cut the ovarian tissue at 30µm thick to increase the probability of finding primordial-stage oocytes with an intact nucleus within the section and used the confocal microscope to create the z-stacks (Figure 5.12, B). Another important challenge of working with ovarian sections from 15-month-old mice is that the reserve of primordial follicles is almost depleted, making it practically impossible to find them using fluorescence microscopy. I, therefore, use ovarian sections from 12-month-old *TG Rec8-Myc* females as my old group. To minimise external variables, I loaded on the same slide ovarian sections from young (2-month-old) and old (12-month-old) *TG Rec8-Myc* females.

Somatic cells that could be on top and bottom of the section can obstruct the visualisation of the nucleus of the primordial-stage oocyte, making imprecise the use of segmentation tools on Imaris. Therefore, I used Volocity software because it allows me to segment regions of interest visualising the z-stack frame by frame and also ensuring that the oocyte nucleus is complete (Figure 5.12, C).

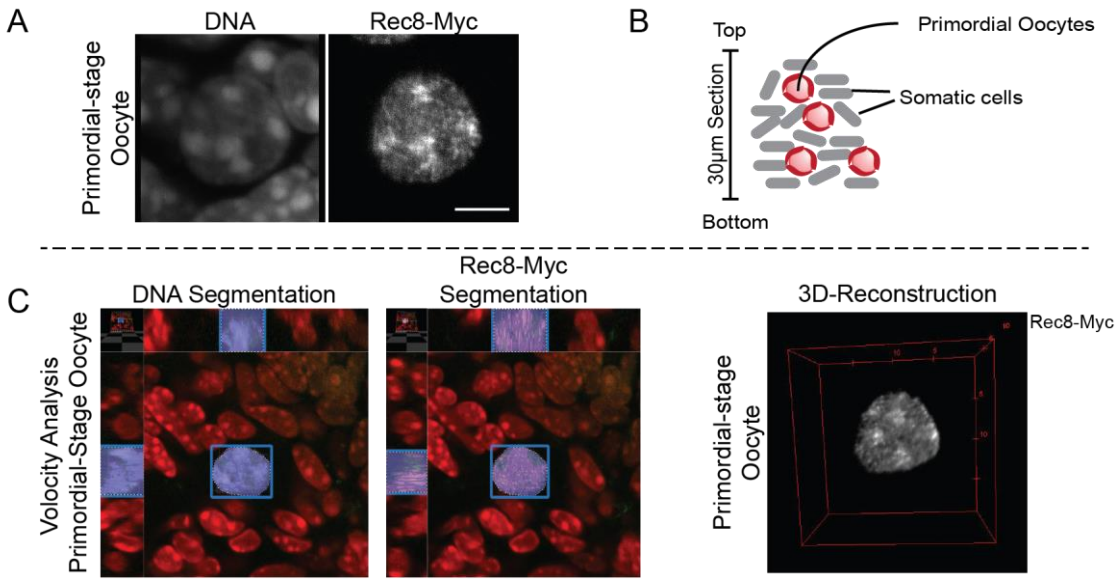

Figure 5.12 Strategies for acquiring and analysing images of primordial-stage oocytes

A Images show a primordial-stage oocyte stained for Rec8-Myc on ovarian cryosections. The Rec8-Myc staining shows a punctate pattern in the nucleus, which appears to be enriched in areas of heterochromatin (Scale bar= 5µm). **B** Schematic illustrating the rationale for cutting ovarian sections at 30µm thick to increase the probability of finding more primordial-stage oocytes with an intact nucleus. **C** Panel shows how Volocity allows DNA and Rec8-Myc segmentation visualising X-Y and Z projections, also a 3-D reconstruction to visualise that the whole nucleus of the oocyte was intact.

To only measure chromosome associated cohesin, I permeabilized the ovarian sections using 1% Triton X-100 in PBS pre-fixation and 1% lipsol in PBS post-fixation. For labelling Rec8 I used the already validated anti Myc-tag antibody. The DNA was labelled with TO-PRO3, which successfully stains DNA in ovarian sections, it does not do so in air-dried chromosome spreads. Because TO-PRO3 binds stoichiometrically to double-stranded DNA (Bink *et al.*, 2001) it provides a means of normalising Rec8-Myc F.I. values in the nucleus.

To determine whether chromosomal cohesin becomes depleted in primordial-stage oocytes, I used ovarian sections from 2-month-old and 12-month-old mice. I chose 12-month-old because of the very low numbers of primordial follicles in ovaries of older females. Firstly, I segmented the nucleus of the primordial-stage oocytes and compared the values of total TO-PRO3 between young and aged *TG Rec8-Myc* to determine whether I could use it to normalise the values of chromosome-associated Rec8. I analysed each experiment separately and found that the total fluorescence levels of TO-PRO3 are not significantly different between primordial stage oocytes from young and old *TG Rec8-Myc* in any of the experiment (Figure 5.13, A). (Experiment 1, p=0.4845 Mann-Whitney U test; n oocytes= 17 young and 8 aged. Experiment 2 p=0.1006 Mann-Whitney U test; n oocytes = 13 young and 4 aged. Experiment 3 p= 0.258 Two-Sample t-Test; n oocytes = 9 young and 14 aged).

I next segmented all Rec8-Myc foci that were overlapping TO-PRO3 to obtain the total fluorescence intensity of Rec8-Myc (Figure 5.13, B), and obtained the ratio using the corresponding total TO-PRO3 fluorescence for each primordial-stage oocyte (Figure 5.13,C). Consistently through all our experiments, the Rec8-Myc:TO-PRO3 ratio in 12-month-old primordial-stage oocytes is significantly lower compared to 2-month-old. (Experiment 1, p<0.001 Two-Sample t-Test; n oocytes = 17 young and 8 aged. Experiment 2 p=0.003 Two-Sample t-Test; n oocytes = 13 young and 4 aged. Experiment 3 p= 0.004 Two-Sample t-Test; n oocytes = 9 young and 14 aged).

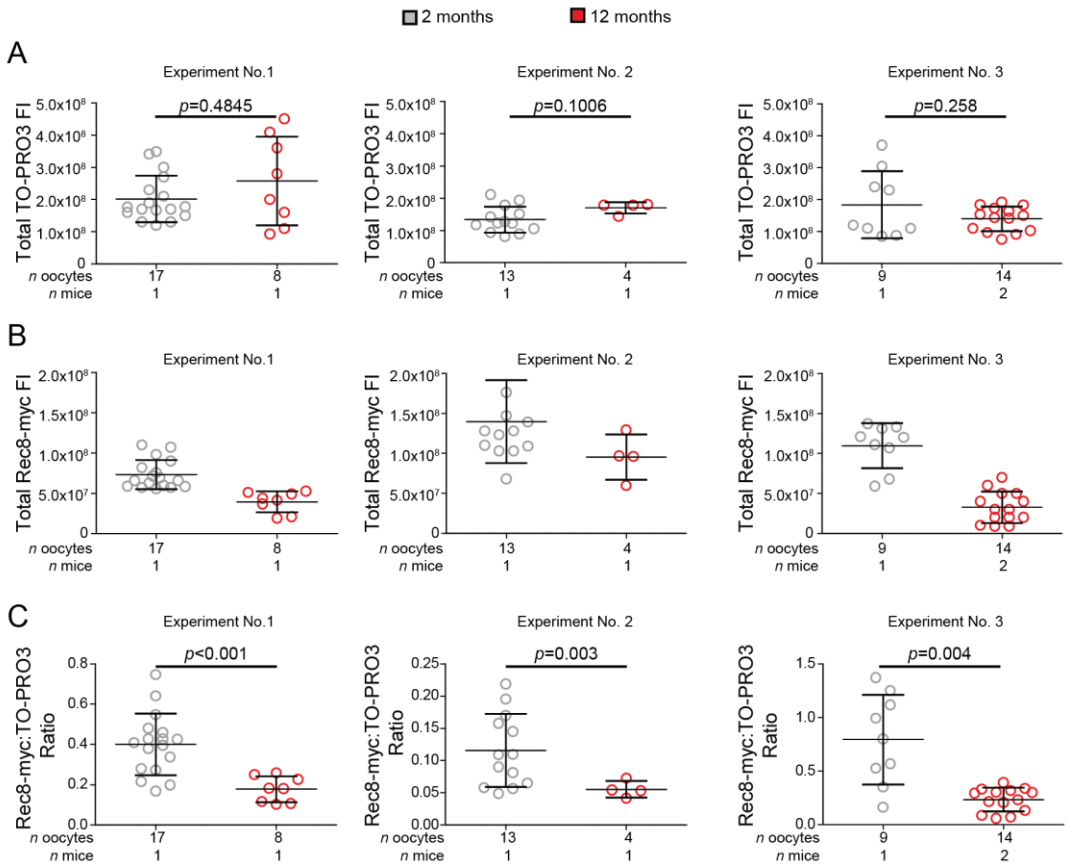

Figure 5.13 Comparison of DNA-associated Rec8-Myc in the nuclei of primordial-stage oocytes from 2 and 12-month-old mice

Data in this figure represents measurements in primordial-stage oocytes from young (2-month-old) and aged (12 month-old) *TGRec8-Myc* females. **A** The dot-plots show levels of TO-PRO3 between young and aged oocytes. Each graph represents a separate experiment and each datapoint represents the F.I. measurement in the nucleus of a primordial-stage oocyte. Comparison of the TO-PRO3 F.I. shows no significant difference between both group ages in any of the experiments (Mann-Whitney U test; P values shown). **B** Graphs show the F.I. of chromosome-associated Rec8-Myc from the same oocytes in "A" comparing young vs aged oocytes. **C** Graphs show the Rec8-Myc:TO-PRO3 ratio for each oocyte nucleus in 3 separate experiments. All experiments show a significant depletion in the ratio of Rec8-Myc:TO-PRO3 between oocytes from 2 and 12 month-old mice (P values are shown; Two-Sample t-test)

Confocal imaging reveals that distribution Rec8-Myc foci are condensed and bright in 2 months while reduced and more diffuse in primordial-stage oocytes from 12-month-old females (Figure 5.14). Also, confocal images show that there is a reduction in Rec8-Myc fluorescence intensity in the heterochromatin regions in oocytes from 12-month-old females. All our experiments together indicate that chromosome-associated Rec8-containing cohesin complexes show a 0.6-fold reduction in primordial-stage oocytes between the ages of 2 and 12 months *TG Rec8-Myc* ($p<0.001$, Two-Sample t-Test; n primordials= 39 young and 26 aged from 3 and 4 females respectively). These results indicate that the relatively quiescent prophase-arrested pool of primordial stage oocytes is vulnerable to depletion of cohesin.

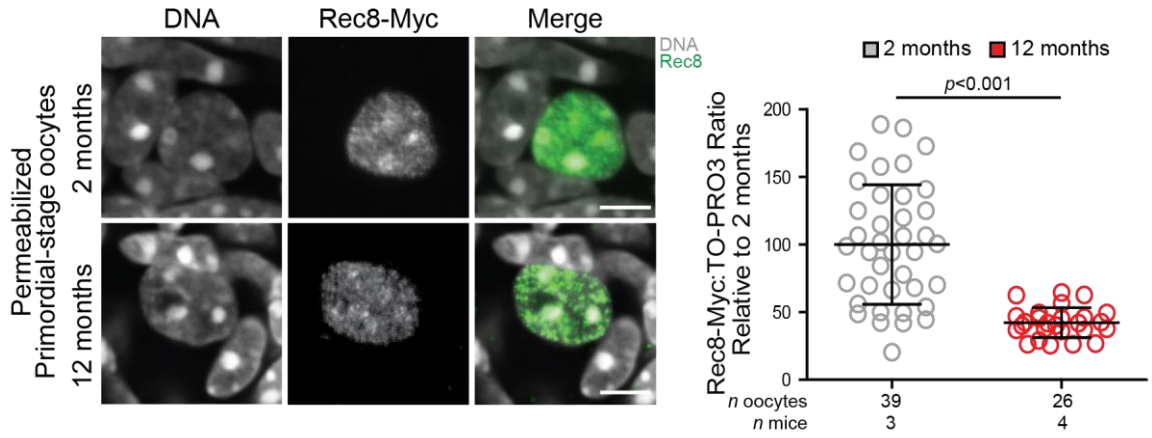

Figure 5.14 Chromosome-associated cohesin is depleted in aged primordial-stage oocytes from *TG Rec8-Myc* mice

Images show maximum projections of representative primordial-stage oocytes in ovarian cryosections and stained for Rec8-Myc and TO-PRO3. The panel compares Rec8-Myc staining between young and old *TG Rec8-Myc* female mice (Scale bars 5µm). The graph shows that a comparison of the Rec8-Myc:TO-PRO3 ratio in primordial stage oocytes from 2 and 12-month-old females, normalised to the mean ratio calculated for 2-month-old mice in each experiment. Each data point represents the measurements of a single oocyte at the primordial stage. Error bars show means ± s.d. There is a significant difference between the mean ratios from old and young ($p<0.001$, Two-Sample t-Test); the levels of chromosome-associated cohesin in primordial-stage oocytes from old *TG Rec8-Myc* females undergo a 0.6-fold reduction compared to young females. The number of oocytes and mice are indicated in the graph.

5.5. Is there any further depletion during the growing phases?

To determine whether there is an additional loss of cohesin during oocyte growth, I spread the nucleus from fully-grown prophase-arrested GV-stage oocytes obtained from 2 and 12-month females. Nuclear spreads from young and old females were prepared in the same slide, stained for Rec8-Myc and DAPI and imaged by confocal microscopy to generate z-stacks. Unfortunately, the TO-PRO3 dye is ineffective in this type of preparation. I, therefore, used the DAPI signal to segment the chromatin on Imaris software and obtain the values for total F.I. of Rec8-Myc.

According to my previous results in the primordial-stage oocytes, we should expect a significant reduction in the levels of total fluorescence of Rec8-Myc in the fully-grown oocyte. This was indeed evident from the confocal images and the levels of total fluorescence intensity (Figure 5.15, A. $p<0.001$ Mann-Whitney U test; n= 24 oocytes 2-month-old, n=14 oocytes 12-month-old; from 3 and 3 females respectively). However, comparison of the fold change between young and old at the primordial and fully grown stage indicates that the reduction is greater in primordial oocytes (0.6 fold in primordial stage *vs* 0.36 fold in fully grown) (Figure 5.15, B). These results suggest that depletion of cohesin from the chromosomes occurs predominantly during the primordial-stage.

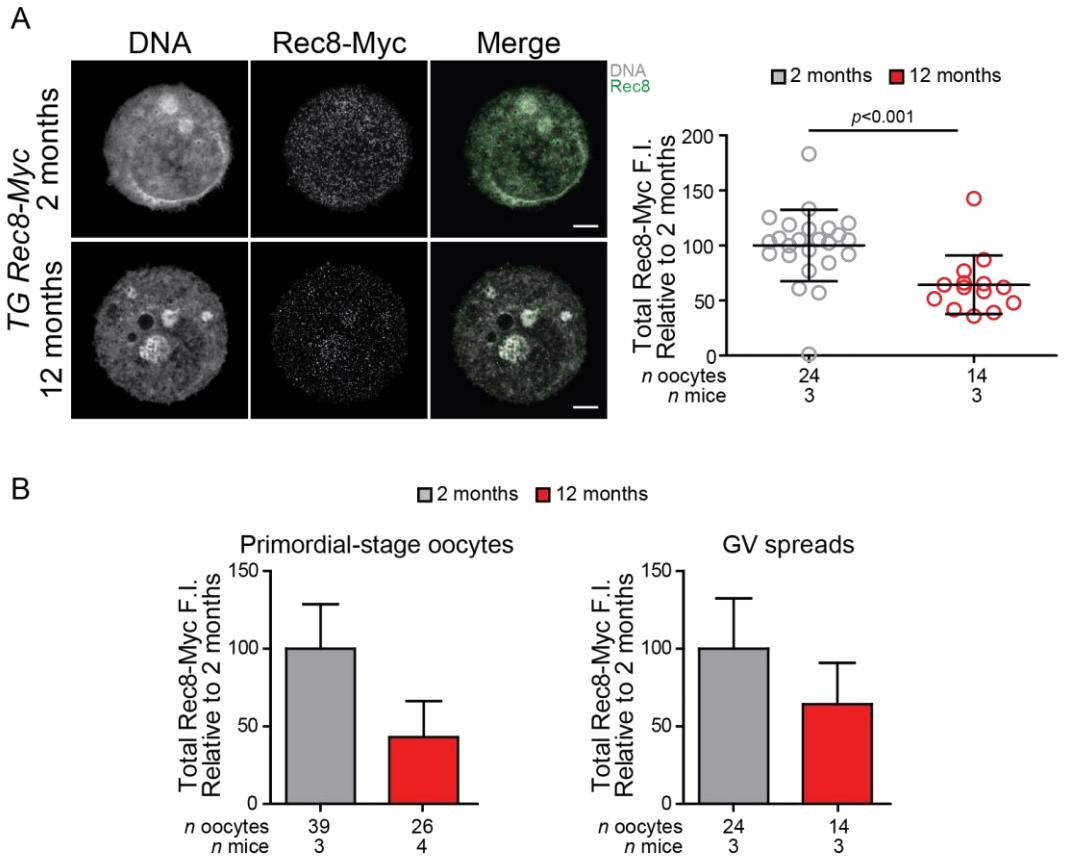

Figure 5.15 Rec8-Myc levels deplete primarily during the non-growing phase of primordial-stage oocyte

A Images show maximum projections of representative nuclei from fully-grown GV oocytes from 2 and 12-month-old *TG Rec8-Myc* females. Nuclear spreads were stained for Rec8-Myc and DNA using DAPI (Scale bars 10µm). The graph on the right shows the total chromosome-associated Rec8-myc values from the GV spreads. Each data point represents individual oocyte and error bars show ± s.d. There is a significant depletion of total Rec8-Myc F.I. in 12-month-old fully-grown GV oocytes compared to 2-month-old ($p<0.001$ Mann-Whitney U test; n= 24 oocytes 2-month-old, n=14 oocytes 12-month-old; from 3 and 3 females respectively). **B** Bar charts compare in parallel the extent of the depletion of cohesin during ageing in the resting pool of primordial-stage oocyte and after all phases of oocyte growth (fully-grown GV). This comparison points that cohesin depletes mostly during the primordial stage.

5.6. Levels of soluble cohesin do not decline markedly in primordial oocytes during female ageing.

Because my primary question related to the decline in chromosome-associated cohesin, the data presented above were obtained from permeabilized ovarian sections using a protocol designed to reduce soluble cohesin from the nucleus. However, I was also interested in determining whether soluble cohesin declined in parallel with chromosomal cohesin. I, therefore, compared primordial-stage oocytes from 2 and 12-month-old ovaries using non-permeablized ovarian sections from *TG Rec8-Myc* females. As above, 30µm thick sections were stained for Rec8-Myc for cohesin and TO-PRO3 for the DNA. In the procedure for this staining, I excluded the permeabilization step (1% Triton X-100 pre-fixation) and imaged by confocal microscopy. As for permeabilized sections, the analysis was performed using Volocity to segment the DNA and also the foci of Rec8-Myc and normalised them to TO-PRO3 to calculate the total levels of Rec8 in the nucleus of the primordial-stage oocyte (Figure 5.16)

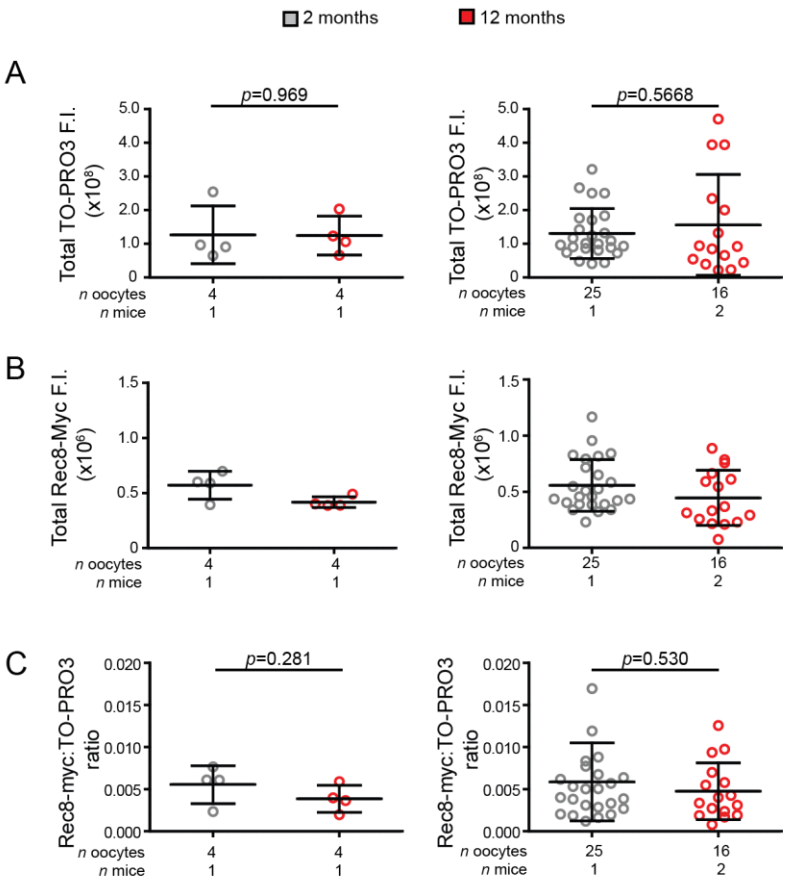

Figure 5.16 Values of TO-PRO3 and Rec8-Myc for comparative analysis of total cohesin in non-permeabilized primordial-stage oocytes

Data represents measurements in primordial-stage oocytes from non-permeabilized ovarian sections. **A** The dot-plots compare the levels of TO-PRO3 between young and aged oocytes showing no significant difference between both age groups in any of the experiments (Exp.1, p=0.969 Two-Sample t-test; n= 4 young and 4 aged from 1 and 1 females respectively. Exp2 p=0.1006 Mann-Whitney U test; n= 13 young and 4 aged from 1 and 1 females respectively). **B** Graphs show the values of total Rec8-Myc from the same oocytes in "A" comparing young vs aged oocytes. **C** Rec8-Myc:TO-PRO3 ratio show no significant depletion in the levels of chromosome-associated cohesin in twelve-month-old oocytes; this is constant between all experiments (Exp1, p=0.281 Two-Sample t-Test. Exp2 p=0.530 Mann-Whitney U test).

Interestingly, my results indicate that there is no significant difference in the level of total cohesin detected in primordial-stage oocytes from young and old mice (Figure 5.17, *p*=0.3726 Mann-Whitney U test; n= 29 oocytes 2-month-old, n=20 oocytes 12-month-old; from 2 and 3 females respectively). These findings suggest that the level of soluble Rec8 present in primordial stage oocytes does not decline markedly during female ageing. Thus, together with the data shown in Figure 5.14, my findings suggest that Rec8 is present but cannot remain associated with the chromosomes.

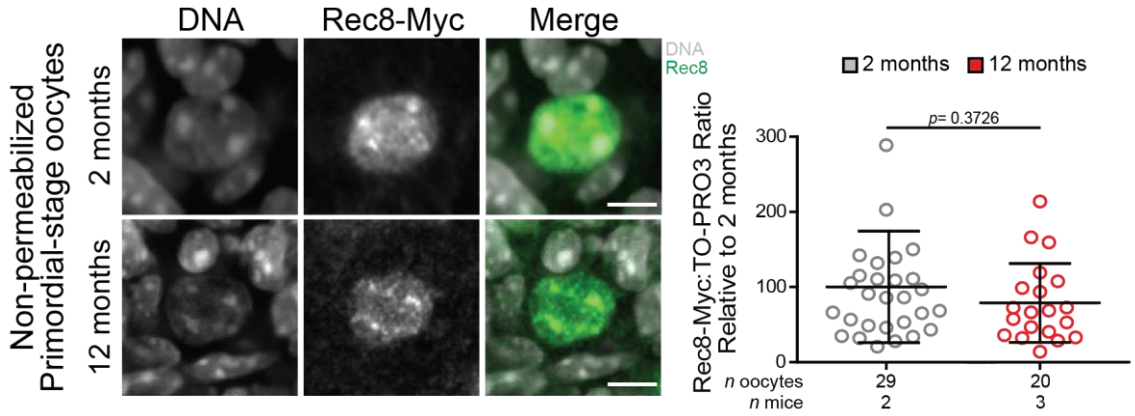

Figure 5.17 Total cohesin remains relatively content in age primordial stage oocytes from TG Rec8-Myc mice

Panel show maximum projections of representative primordial-stage oocytes comparing cohesin staining in young and old TG Rec8-Myc female mice in non-permeabilized ovarian cryosections (Scale bars 5µm). The graph compares the Rec8-Myc:TO-PRO3 ratio between young and aged oocytes from *TG Rec8-Myc* females. Each data point corresponds to an individual oocyte nucleus and the error bars represent the ± s.d. The graph shows that levels of total cohesin remain relatively constant between 2 and 12-month-old TG Rec8-Myc females (p=3726, Two-Sample t-Test) the number of oocytes and mice are shown in the graph

5.7. Discussion

Establishing the stage of oocyte development in which cohesin is depleted from the chromosomes is crucial. This can help to find other possible culprits of cohesin depletion during ageing and also is useful in informing the likely success and implementation of new therapeutic strategies to reduce reproductive risk during maternal ageing. To determine when during oogenesis is cohesin depleted from oocyte chromosomes, I used the *TG Rec8-Myc* mouse which facilitates the detection Rec8 and has been widely utilised for the study of cohesin regulation (Kudo *et al.*, 2006; Kudo *et al.*, 2009; Tachibana-Konwalski *et al.*, 2010). We validated detection of Rec8 in this mouse doing parallel experiments with wild-type CD1 mice were we stained oocytes fixed at prometaphase I with anti Myc-tag and anti Rec8 (Eijpe *et al.*, 2003) antibodies. This experiment shows that wild-type oocytes only stain for Rec8 but not for the anti-Myc tag. Furthermore staining for Myc-tag in *TG Rec8-Myc* oocytes shows a similar pattern to that obtained with the anti-Rec8 antibody.

Since the *TG Rec8-Myc* mouse carries a transgene on the meiotic-specific α-kleisin (Rec8) subunit of cohesin, it was important to determine whether this mouse line exhibits the hallmark effects of female ageing and might, therefore, be useful for the study of the molecular basis for age-related oocyte aneuploidy. In parallel experiments comparing young (2-month-old) and old (15-month-old) *TG Rec8-Myc* oocytes cultured to GVBD+5hrs, I determined the levels of centromeric cohesin and analysed the integrity of the bivalent chromosome structure. Using the same analysis strategy as in my previous chapter (Chapter 4 – Mechanisms of cohesin depletion), applying Imaris surface segmentation to the CREST signal I measured Rec8-Myc levels at the centromeres. Confocal imaging and quantification confirm that chromosomal Rec8-Myc levels become depleted with advancing female age in *TG Rec8-Myc* oocytes. The significantly increased proportion of distally associated homologues in oocytes from old *TG Rec8-Myc* females most likely reflects substantial destabilisation of bivalent chromosomes during ageing in this mouse line. However, this destabilisation is less severe in comparison to our previous work in naturally aged wild-type mouse oocytes (Lister *et al.*, 2010). I speculate that this could be a protective effect produced by the extra copies of Rec8-Myc. Consistent with previous findings (Chiang *et al.*, 2010; Lister *et al.*, 2010), *TG Rec8-Myc* oocytes

aged 15 months show that the unified structure of sister centromeres is lost. In addition, I found that 40% of metaphase II oocytes from 15-month-old females contained some single chromatids compared with none in oocytes from 2-month-old females. Together, all of these results provide robust evidence that the *TG Rec8-myc* exhibit all features of female ageing and therefore this mouse line is useful as a model for the study of female reproductive ageing.

In general, any study at a molecular level in mammalian primordial-stage oocyte is very difficult due to its tight relationship with the pregranulosa cells, and also its difficult accessibility. These challenges are compounded when we attempt to study the effect of ageing because the population of primordial follicles declines (Faddy and Gosden, 1996) as female mammals get older making it difficult to study sufficient numbers of oocytes. Learning how to identify primordial follicles effectively is key to their study during ageing. To do so, I used the transcription factor Foxo3A which has been found to be highly expressed in nuclei of primordial-stage oocytes (Liu *et al.*, 2007).

Following extensive characterization and optimisation, I determined the levels of cohesin in primordial-stage oocytes in young and old *TG Rec8-Myc* females. However, the challenges did not stop there. The initial pool of oocytes in the ovary depletes with age by recruitment for growth or death by atresia. The process of cell death can alter the integrity of the DNA in the oocytes and might, therefore, be a confounding factor, which may affect cohesin's ability to remain stably associated with chromatin due to an age-independent effect. Therefore, to reliably compare the levels of cohesin in primordial-stage oocytes, I excluded oocytes undergoing cell death.

In response to oocyte DNA damage, TAp63 mediates activation of PUMA and NOXA (Kerr *et al.*, 2012) which results in initiation of the process of cell death (Suh *et al.*, 2006; Chen *et al.*, 2015). Because cell death is a very complex process with many activator and effectors (Hengartner, 2000) identifying a lone cell marker that detects primordial-stage oocytes in the process of atresia is difficult. I, therefore, decided to use a TUNEL assay, which labels double-strand DNA breaks and is considered to be an end-stage marker of cell death and is suitable for use in permeabilized ovarian sections. TUNEL-positive oocytes were excluded from the analysis.

Rec8 foci are distributed irregularly across the nucleus and are enriched in the heterochromatic areas. This creates a further challenge because the fluorescence intensity values can differ depending on where the nucleus was cut. I, therefore, developed a protocol for immunohistochemistry in 30µm thick ovarian sections to increase the probability of finding primordial-stage oocytes with an intact nucleus. To determine the level of chromosome-associated cohesin, I developed a protocol to permeabilize ovarian sections with 1%Triton and 1% Lipsol aiming to remove all soluble cohesin. During the optimisation process for this protocol, I observed that soluble Rec8-Myc located in the cytoplasm of the oocytes were not longer detectable in permeabilized sections while only nuclear Rec8-Myc was detected after this protocol. This reflects that the Rec8-Myc immunostaining is more likely to be chromosome-associated Rec8. Confocal imaging and whole nucleus measurements in Volocity show that chromosome-associated cohesin is depleted in primordial-stage oocytes from old *TG Rec8-Myc* females.

Using fluorescence microscopy, Tsutsumi *et al*. (2014) previously reported that in human ovarian oocytes, whose stage of development was not specified, there was a non-significant trend towards reduced cohesin is ovarian tissue from older women (Tsutsumi *et al.*, 2014). However, they did not take into consideration that cohesion is dependent only on those complexes that are associated with chromosomes. Levels of total cohesin and chromosome-associated cohesin might be different. In support of this, I found that total cohesin did not decline during female ageing the *TG Rec8-Myc* primordial-stage oocytes. It was, therefore, essential to develop a methodology to effectively permeabilize the ovarian tissue and to use fluorescence microscopy that has been adapted to the specific distribution of Rec8 in the chromatin. My results indicate that cohesin depletion from oocyte chromosomes during ageing begins from the primordial stage and does not appear to be due to a deficiency in the level of soluble cohesin in the nucleus.

After being recruited for growth, the size of the oocyte and the follicle dramatically increase. This process demands an intense metabolic activity shared between the oocyte and the follicle (Su *et al.*, 2009). To determine whether further cohesin depletion occurs during the growing phases as a result of this intense metabolic activity in aged oocytes, I compared Rec8-Myc levels in fully-grown GV spreads from

2-month-old and 12-month-old. The results indicate that although the levels of Rec8-Myc in GVs from old *TG Rec8-Myc* females were significantly lower than GVs from young females, the extent of depletion in aged GVs does not exceed that in aged primordial-stage oocytes. I, therefore, conclude that cohesin is predominantly depleted from oocyte chromosomes during the primordial stage. It remains to be established whether this is due to protein damage affecting the integrity of the cohesin complex or due to age-related changes to chromatin structure. In support of the latter, a number of studies have reported that altered chromatin structure is a common feature of general senescence (Lopez-Otin *et al.*, 2013). This possibility is currently being investigated by another PhD student in the lab.

Chapter 6. Results: Is there a mechanistic link between ovarian ageing and cohesin depletion?

6.1. Ovarian ageing

The findings presented in chapter 5 (When during oogenesis is cohesin lost) indicate that age-related cohesin depletion occurs predominantly at the primordial stage in a gradual manner. It would, therefore, appear that cohesin depletion occurs in parallel with the well-established decline in the ovarian population of primordial follicles. We, therefore, wished to test the idea that ovarian ageing and cohesin depletion might be mechanistically linked. In support of this idea, it has recently been reported that the risk of chromosome missegregation is increased in cases of ovarian insufficiency (Haadsma *et al.*, 2010). This raises the possibility that factors secreted by neighbouring primordial follicles might contribute either directly, or indirectly to the maintenance of chromosome structure in primordial-stage oocytes. If this is the case, then cohesin level will deplete from oocyte chromosomes as the resting pool of primordial-stage oocyte depletes from the ovary.

Primordial-stage oocytes are held at the non-growing phase via the Pten-AKT-mTOR pathway, which is compounded by many inhibitors and effectors (Reddy *et al.*, 2008). Activation of mTOR will promote cellular growth (Yang and Guan, 2007) and survival resulting in activation for growth of primordial-stage oocytes (Adhikari and Liu, 2009). AKT can release mTOR from its inhibitor (TSC1/TSC2) only if Pten allows AKT phosphorylation by PI3P (Reddy *et al.*, 2010). Exon 5 deletion of *Pten* creates a chain reaction that unleashes mTOR resulting in a widespread activation of primordial-stage oocytes (Reddy *et al.*, 2008), female mice exhaust completely their ovarian reserve and become infertile within 13 weeks. We, therefore, used this model for investigating the effect of primordial follicle depletion on chromosome-associated cohesin in oocytes independent of female ageing.

6.2. Strategy to accelerate the recruitment for growth of primordial follicles using the *Pten* knockout model

To accelerate recruitment for growth in primordial-stage oocytes and induce premature ovarian ageing, we used a *Pten* knockout mouse. In this mouse *Pten* exon 5 has been flanked by *LoxP* sites (*Pten*$^{f//f}$) (Jackson Laboratories). Tamoxifen-inducible Cre recombinase (Cre-ERT2) activity was driven from the Vasa promoter (Ddx4). To induce the deletion of *Pten* in oocytes (*Pten*$^{-/-}$), I injected *Pten*$^{f/f}$*;Ddx4-CreERT2* females aged 2 weeks with tamoxifen (75mg/kg body weight) via intraperitoneal (I.P.) once a day for 5 consecutive days. The strategy to induce the deletion of *Pten* in oocytes using tamoxifen is explained in Figure 6.1. I compared the effects of the *Pten* deletion with control females (*Pten*$^{f/f}$) that were also injected with tamoxifen at 2 weeks post birth.

As an additional control to validate the phenotype seen in the *Pten*$^{-/-}$ females, I also injected 2-week-old *Pten*$^{f/f}$ and *Pten*$^{f/f}$*;Ddx4-CreERT2* females with the drug-vehicle (corn oil) used to dilute tamoxifen. Ovaries from both treatments (tamoxifen and drug-vehicle) were dissected at one and eleven weeks post injections, oocytes were harvested only from ovaries after 11 weeks post injections.

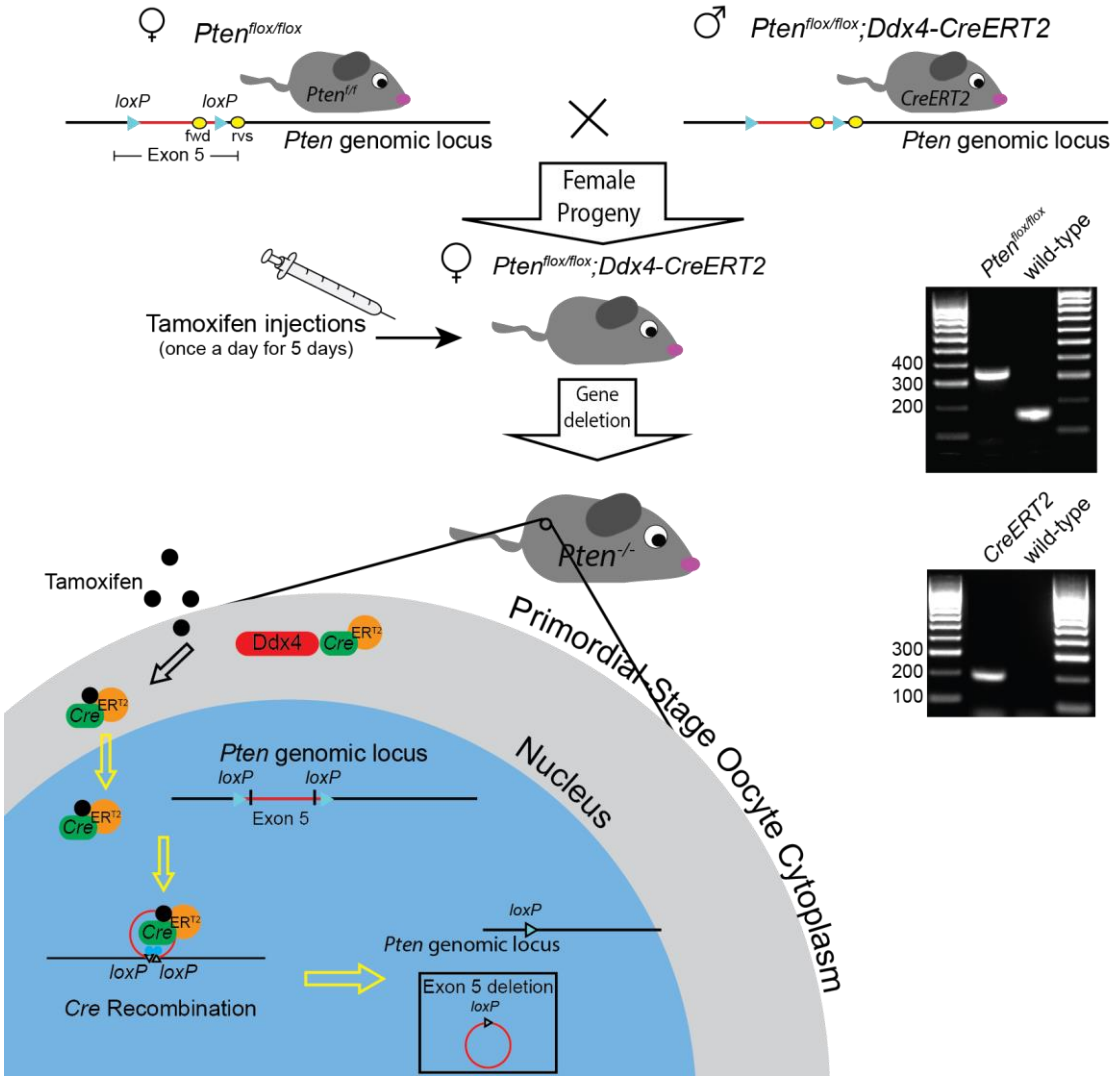

Figure 6.1 Strategy to induce *Pten* deletion from oocyte to accelerate recruitment of primordial follicles

Schematics illustrate the strategy to induce *Pten* deletion in female mice. At the top of the figure, cartoons represent the cross between a *Pten*$^{f/f}$ female and a male *Pten*$^{f/f}$*;Ddx4-CreERT2*, the line beneath the mice, is a representation of the location of the of the *loxP* (small triangles) at exon 5 of the *Pten* genomic locus and PCR primers (yellow ovals). The resulting progeny from this cross will have *Pten*$^{f/f}$*;Ddx4-CreERT2* females. To generate *Pten* knockout (*Pten*$^{-/-}$) female are injected with tamoxifen. The big half circles on the bottom left represent the cytoplasm (grey) and nucleus (blue) of a primordial-stage oocyte.

Figure legend continues on next page

Tamoxifen penetrates to the cytoplasm and bind to CreERT2, which travels to the nucleus and recombine the *loxP* to excise exon 5 from the *Pten* genomic locus. Gels from DNA PCR show that *Pten* flanked by *loxp* sites is 328bp while wild-type is 156bp, *CreERT2* is 200bp and wild-type mice do not have *Cre*.

To determine whether females carrying *Pten*$^{-/-}$ oocytes had increased rate of primordial follicle recruitment, I performed follicular counts in mouse ovaries one-week after the treatment (tamoxifen and drug-vehicle injections) and also at 11 weeks post-injection. In the latter case, I allocated one ovary from each female (tamoxifen group: *Pten*$^{f/f}$ n= 3, *Pten*$^{-/-}$ n=4. Drug-vehicle group: *Pten*$^{f/f}$ n= 3, *Pten*$^{f/f}$*;Ddx4-CreERT2* n=4) for the harvest of oocytes from antral follicles and one for sectioning to perform primordial follicle counts. For this propose, I grouped the type of follicles into two categories: i) Primordial follicles, consisting by an oocyte of about 10µm in diameter, surrounded by a single layer of flattened cells. ii) Growing follicles, consisting by an oocyte larger than 15µm in diameter surrounded by one or more layers of cuboidal cells.

Only oocytes on the section that had a clear nucleus were counted. Growing follicles can contain nucleus up to 30µm in diameter. Therefore, to prevent counting growing follicles more than once I cut ovarian section at 8µm and counted the follicles on every 5th section. Follicles are not evenly distributed throughout the ovary and with this method, I am missing the primordial follicles in between every 5th section (counted sections). Hence, I counted the follicles throughout the entire ovary and calculated the total number of primordial follicles in the ovary using an already developed and validated equation for this counting system (McClellan *et al.*, 2003) (see equation in materials and methods).

Haematoxylin-eosin staining of ovarian sections after one week of tamoxifen injections revealed that ovaries containing *Pten*$^{-/-}$ oocytes are considerably larger than *Pten*$^{f/f}$ (Figure 6.2, A). In addition, although after 11 weeks of tamoxifen injection ovaries from both genotypes seem to have the same size, sections from ovaries containing *Pten*$^{-/-}$ oocytes appeared to contain an increased number of corpora lutea (Figure 6.2, A). After performing follicular counts one week after treatment (tamoxifen

and drug-vehicle) the average for calculated number of primordial follicles were above 500 follicles for all genotypes and treatments (Tamoxifen: *Pten*$^{f/f}$=571; *Pten*$^{-/-}$ =743. Drug-vehicle: *Pten*$^{f/f}$= 735*; Pten*$^{f/f}$*;Ddx4-CreERT2*= 690*)*. At this same time point, only the ovaries from *Pten*$^{-/-}$ females contain in average 240 growing follicles while ovaries from *Pten*$^{f/f}$ females treated with tamoxifen, *Pten*$^{f/f}$ and *Pten*$^{f/f}$*;Ddx4-CreERT2* females treated with drug vehicle had respectively 104, 104, 120 growing follicles (tamoxifen group: *Pten*$^{f/f}$ n= 3, *Pten*$^{-/-}$ n=4. Drug-vehicle group: *Pten*$^{f/f}$ n= 3, *Pten*$^{f/f}$*;Ddx4-CreERT2* n=3).

At eleven weeks post treatment, the average calculated number of primordial follicles in *Pten*$^{f/f}$ females treated with tamoxifen, *Pten*$^{f/f}$ and *Pten*$^{f/f}$*;Ddx4-CreERT2* females treated with drug vehicle were respectively 347, 333 and 358. Only ovaries from *Pten*$^{-/-}$ females contained 59 primordial follicles in average (tamoxifen group: *Pten*$^{f/f}$ n= 3, *Pten*$^{-/-}$ n=4. Drug-vehicle group: *Pten*$^{f/f}$ n= 3, *Pten*$^{f/f}$*;Ddx4-CreERT2* n=4). The average number of growing follicles in the ovaries from *Pten*$^{f/f}$ and *Pten*$^{-/-}$ females treated with tamoxifen, *Pten*$^{f/f}$ and *Pten*$^{f/f}$*;Ddx4-CreERT2* females treated with drug vehicle at this time point was 81, 61, 76, 68 respectively.

While one-week after the treatments (Tamoxifen and drug-vehicle) the calculated total number of primordial follicles is similar for both genotypes in both treatments, the number of growing follicles is two-fold greater in ovaries *Pten*$^{-/-}$ females compared to *Pten*$^{f/f}$ and ovaries from mice treated with drug-vehicle (Figure 6.2, C). In addition, at 11-weeks-post injection ovaries from *Pten*$^{-/-}$ females contain 3 times less primordial follicles than ovaries from *Pten*$^{f/f}$ females and drug-vehicle treated females (p=0.004, ANOVA. Figure 6.2, B). My finding that there was no differences in the number of follicles in the group of females treated with drug-vehicle indicates that this effect is specifically due to deletion of *Pten* as I found no effect of the vehicle used to prepare the tamoxifen injections.

These results are consistent with previous findings using mice with an oocyte – specific deletion of *Pten* in which *Cre* recombinase was driven from the Gdf9 promoter (Reddy *et al.*, 2008). As in that study, my findings indicate that the number of primordial follicles declines in ovaries from *Pten*$^{-/-}$ females as consequence of increased recruitment for growth. Thus, the tamoxifen-induced *Pten* knockout mouse

provides a useful model for investigating the effect of accelerated ovarian ageing on oocytes chromosomal cohesin.

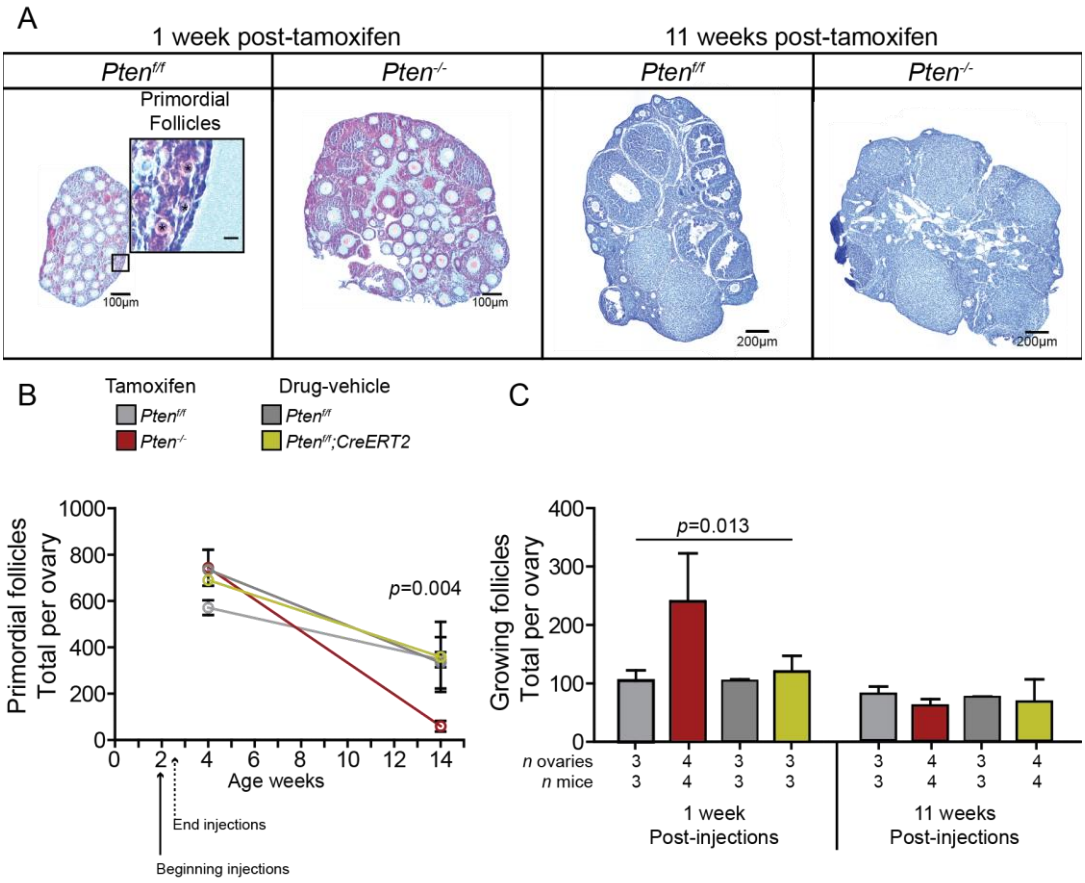

Figure 6.2 Increase in the recruitment of primordial follicles depletes the ovarian population of germ cells in *Pten*$^{-/-}$ females

A Panel of ovarian sections stained for haematoxylin-eosin compares ovaries from *Pten*$^{f/f}$ and *Pten*$^{-/-}$ females dissected at one and eleven weeks after tamoxifen injections. Inset for one-week post tamoxifen *Pten*$^{f/f}$ shows primordial follicles marked by asterisks, scale bar 10µm. *Pten*$^{-/-}$ ovary at one-week post tamoxifen shows size increase and an abundant number of growing follicles. (scale bars: 100µm). At weeks 11 post tamoxifen, ovaries from *Pten*$^{-/-}$ females have a reduced number of growing follicles and increased corpus luteum compared to *Pten*$^{f/f}$ (scale bars: 200µm). **B** Scatter plot shows the calculated total number of primordial follicles on week 1 and week 11 following injection of tamoxifen or drug-vehicle on day 14 for 5 consecutive days. Beginning and end of treatments are indicated by arrows on the X axis.

Figure legend continues on next page

Ovaries from *Pten*$^{-/-}$ (red line) show a significant reduction in the number of primordial follicles (p=0.004, ANOVA) compared to ovaries from *Pten*$^{f/f}$ and mice treated with drug-vehicle. **C** Bar chart shows total growing follicle number for both genotypes and treatments. *Pten*$^{-/-}$ ovaries at week-1 post-tamoxifen has a two-fold increase in growing follicles (p=0.013, ANOVA) compared with ovaries from *Pten*$^{f/f}$ and drug-vehicle treated females (n number for ovaries and mice for both graphs are indicated in the bar chart).

6.3. Cohesin depletion from oocyte chromosomes is a chronological event independent to the depletion of the germ cell pool

To ensure that the phenotype observed in oocytes from *Pten*$^{-/-}$ females is an effect of tamoxifen gene excision and no any other component on the vehicle used to dilute tamoxifen. I injected *Pten*$^{f/f}$ and *Pten*$^{f/f}$*;Ddx4-CreERT2* females with drug-vehicle. Eleven weeks after the treatment I harvested the oocytes and culture them to GVBD+5hrs. I spread the chromosomes of the oocytes from both genotypes on the same slide.

Imaging for 3-dimentional analysis of the chromosome spreads was performed in the confocal microscope. From the follicular counts we realised that there was no increased rate of primordial follicle recruitment in ovaries from *Pten*$^{f/f}$*;Ddx4-CreERT2* females when injected with drug vehicle. Therefore, ovaries from these females do not undergo accelerated ovarian ageing. We predict that cohesin levels should not be different between oocyte chromosomes from *Pten*$^{f/f}$ and *Pten*$^{f/f}$*;Ddx4-CreERT2* females injected with drug-vehicle. As predicted, analysis of confocal images indicated that Rec8 is not reduced from at the centromeres nor at the chromosome arms in drug-vehicle injected *Pten*$^{f/f}$*;Ddx4-CreERT2* compared to *Pten*$^{f/f}$ (Figure 6.3).

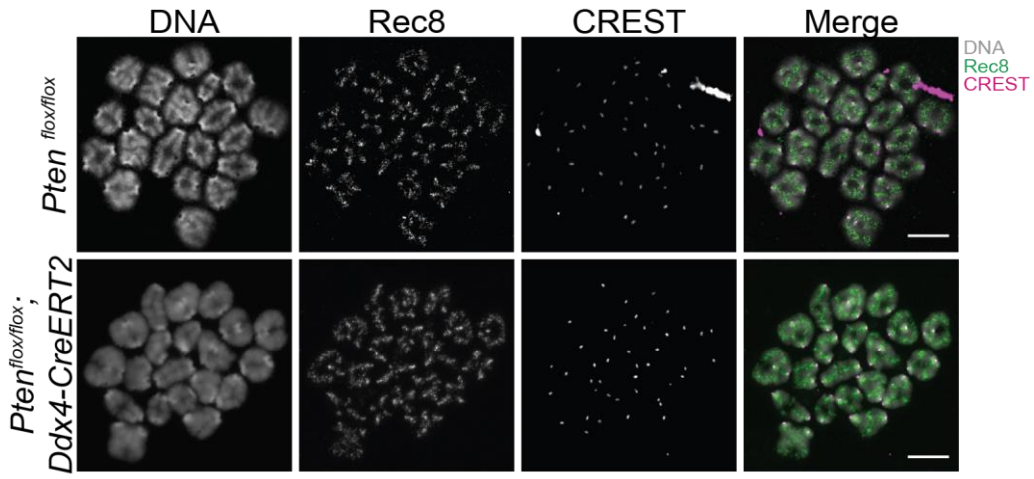

Figure 6.3 Levels of centromeric cohesin do not change in drug-vehicle injected *Pten$^{f/f}$;Ddx4-CreERT2* compared to *Pten$^{f/f}$*

Panel illustrates maximum projections of representative oocyte chromosomes fixed at GVBD+5hrs from *Pten$^{f/f}$* and *Pten$^{f/f}$;Ddx4-CreERT2* females after 11 weeks post drug-vehicle injection. Chromosomes were stained for Rec8 and CREST. Images show that levels of Rec8 do not reduce in oocyte chromosomes from *Pten$^{f/f}$;Ddx4-CreERT2* females compared to *Pten$^{f/f}$* (Scale bars: 10µm).

Comparison of individual oocytes measurements for Rec8 and CREST (Figure 6.4) obtained from the image analysis on Imaris surface segmentation show that Rec8 levels at the centromeres remain at similar levels between both genotypes. Figure 6.4 also shows CREST levels remain similar between oocyte chromosomes from *Pten$^{f/f}$* and *Pten$^{f/f}$;Ddx4-CreERT2* after culture to GVBD+5hrs. To obtain the Rec8:CREST ratio I divided the values of Rec8 in the values of CREST corresponding to the same centromere pair (Figure 6.4,B).

	Pten $^{f/f}$	*Pten* $^{flox/flox}$*;Ddx4-CreERT2*
Experiment	1 2 3	1 2 3
n oocytes	2 5 2	1 8 5
n mice	1 1 1	1 1 1

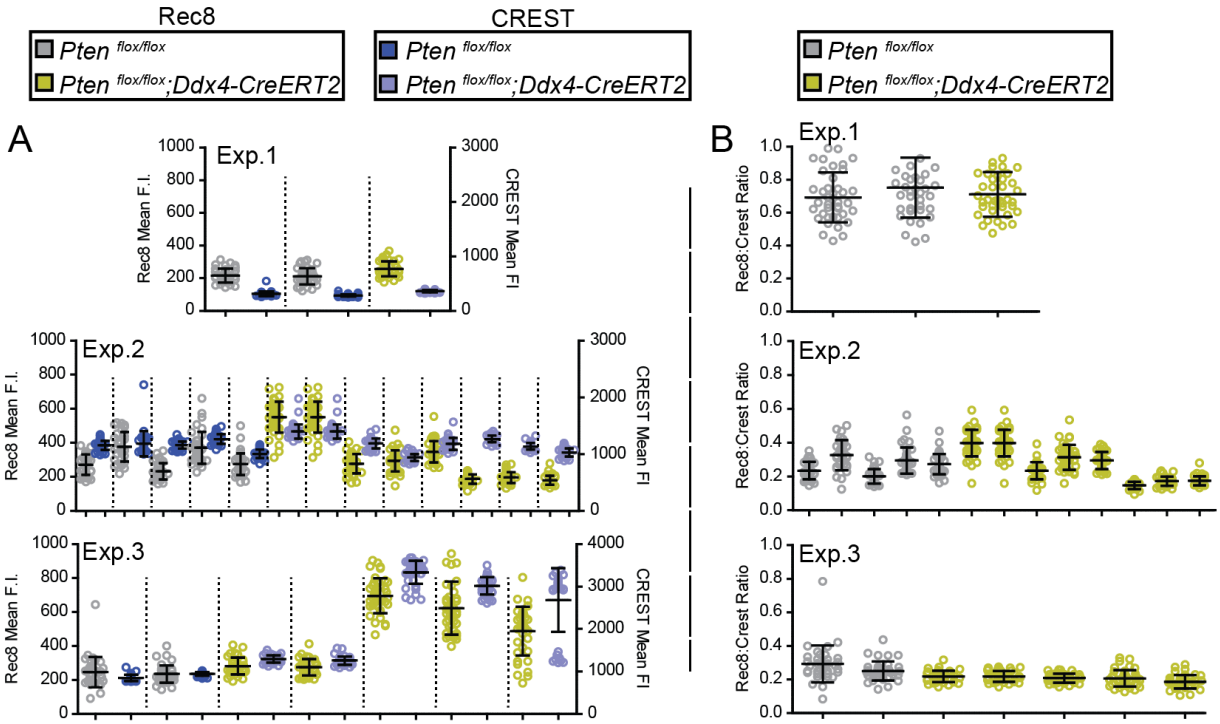

Figure 6.4 Comparison of Rec8 and CREST level between *Pten*$^{f/f}$ and *Pten*$^{f/f}$*;Ddx4-CreERT2* after 11 weeks of drug-vehicle injections

A Graphs show mean F.I. for Rec8 and CREST signals obtained from confocal images of air-dried chromosome spreads prepared from oocytes harvested from *Pten*$^{f/f}$ and *Pten*$^{f/f}$*;Ddx4-CreERT2* after 11 weeks of tamoxifen injections. Oocytes from both genotype females were spread on the same slide at GVBD+5 hrs. Each graph represents an individual slide, corresponding to a single experiment. Each data point represents the F.I. measurement from individual centromere within a given oocyte. Data from different oocytes are separated by broken lines and F.I. values of Rec8 and CREST for individual oocytes are plotted next to each other. Error bars represent the mean ± s.d. for each oocyte. The number of oocytes and mice used in each experiment is explained in the table on top of the figure. **B** Graphs showing the ratio of Rec8:CREST in oocytes from *Pten*$^{f/f}$ and *Pten*$^{f/f}$*;Ddx4-CreERT2* females calculated from the F.I. data shown in "A". Each data point represents the Rec8:CREST ratio at individual centromeres.

Figure legend continues on next page

Each dataset represents all centromere measurements obtained from an individual oocyte. Error bars show the mean ± s.d. of the ratios within each oocyte. The number of mice and oocytes are as shown in “A”.

I further normalised the Rec8:CREST ratio of oocyte centromere from *Pten$^{f/f}$;Ddx4-CreERT2* females injected with drug-vehicle to the mean Rec8:CREST ratio of all oocyte centromere from *Pten$^{f/f}$* and represented the normalised values as relative to wild-type. Using this approach, I detected no significant difference in the levels of centromeric cohesin in both phenotypes at 11 weeks after drug-vehicle treatment (Figure 6.5, p= 0.367, Two-sample t-test; n= 9 oocytes from three *Pten$^{f/f}$* females and n= 14 from three *Pten$^{f/f}$;Ddx4-CreERT2* females). These experiments indicate that the vehicle used for diluting the tamoxifen has no effect on the level of cohesin associated with oocyte chromosomes.

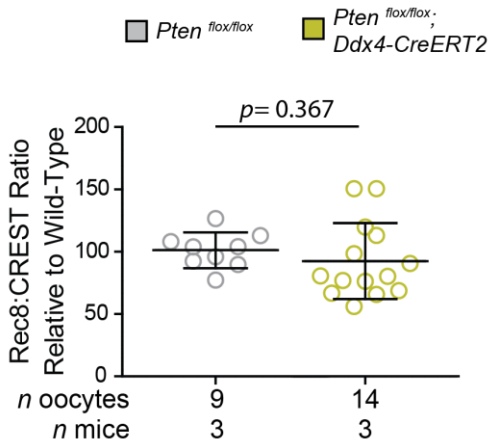

Figure 6.5 Levels of centromeric cohesin are not different between oocytes from *Pten$^{f/f}$* and *Pten$^{f/f}$;Ddx4-CreERT2* females injected with drug-vehicle

Graph shows the mean values of Rec8:CREST ratio normalized to the mean of all values obtained from *Pten$^{f/f}$* (wild-type) within the same experiment after 11week of drug-vehicle treatment. Error bars represent the mean ratio ± s.d. There was no significant difference in the levels of centromeric cohesin between oocytes from *Pten$^{f/f}$* and *Pten$^{f/f}$;Ddx4-CreERT2*. (p=0.367, Two-sample t-test; n= 9 oocytes from three *Pten$^{f/f}$* females and n= 14 from three *Pten$^{f/f}$;Ddx4-CreERT2* females).

To determine whether depletion of primordial follicles is associated with depletion of cohesin from oocyte chromosomes, I cultured to GVBD+5hrs oocytes from *Pten$^{f/f}$* and *Pten$^{-/-}$* after 11 weeks of tamoxifen treatment, which corresponds to a time of marked depletion of primordial follicles (Figure 6.2, B). After fixing the oocytes from both genotypes on the same slide, I stained them for Rec8 and CREST. Analysis of confocal images indicated that the chromosome-associated Rec8 is not reduced in *Pten$^{-/-}$* oocytes females compared with oocytes from *Pten$^{f/f}$* females. Centromeres and chromosomes arms in oocytes from both genotypes show strong staining for Rec8.

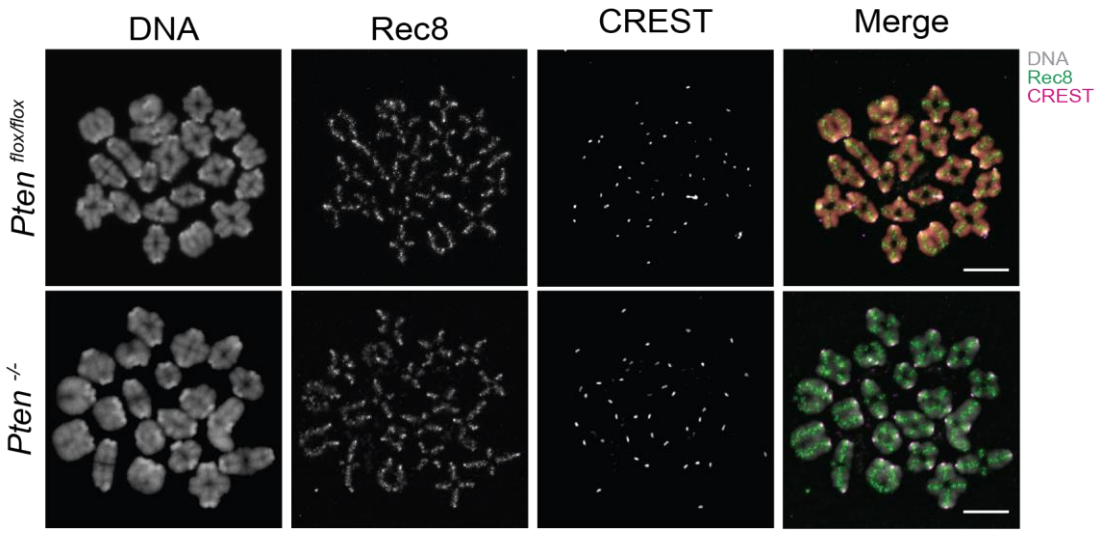

Figure 6.6 Rec8 cohesin do not deplete from the chromosomes after exhaustion of the ovarian reserve of primordial stage oocytes

Images show maximum intensity projections of representative chromosomes spread from oocytes cultured to GVBD+5hrs from *Pten*$^{f/f}$ and *Pten*$^{-/-}$ females 11 weeks following injection of tamoxifen for 5 days. Chromosomes were stained for Rec8 and CREST. Levels of Rec8 do not appear to be reduced from the chromosome arms or centromeres in oocytes from *Pten*$^{-/-}$ (Scale bars: 10µm).

Using the approach to quantification of centromeric Rec8 described above (Chapter 4, Section 4.5; Chapter 5, Section 5.2), I used surface segmentation on Imaris software to obtain the mean values of Rec8 and CREST for all centromeres in chromosome spreads from oocytes cultured to GVBD+5hrs (Figure 6.7). Unlike my previous experiments where I compared young vs aged mouse oocyte, here, using young mice, I compared oocytes from normal ovaries with ovaries from *Pten* deleted females, which showed a marked reduction in the number of primordial follicles (Figure 6.2, B). My findings indicate that levels of Rec8 are similar between oocyte chromosomes from *Pten*$^{f/f}$ and *Pten*$^{-/-}$ after 11 weeks of tamoxifen treatment (Figure 6.7). In addition, Figure 6.7 show that the levels of CREST between both genotypes remain similar.

To calculate the ratio, I divided the values of Rec8 by the corresponding values of CREST for each centromere (Figure 6.8). There was some variation between experiments, which may reflect differences between individual mice (Figure 6.8). However, by normalising the Rec8:CREST ratio for each oocyte centromere from *Pten*$^{-/-}$ females to the mean value of the ratio from all centromeres of *Pten*$^{f/f}$ females and represent them as relative to wild-type (Figure 6.9). I found that there is no significant difference in the levels of cohesin at the centromeres in oocytes from *Pten*$^{-/-}$ females after depletion of the ovarian reserve ($p=0.1014$, Mann-Whitney U test; n= 20 oocytes from five *Pten*$^{f/f}$ females and n= 24 from five *Pten*$^{-/-}$ females).

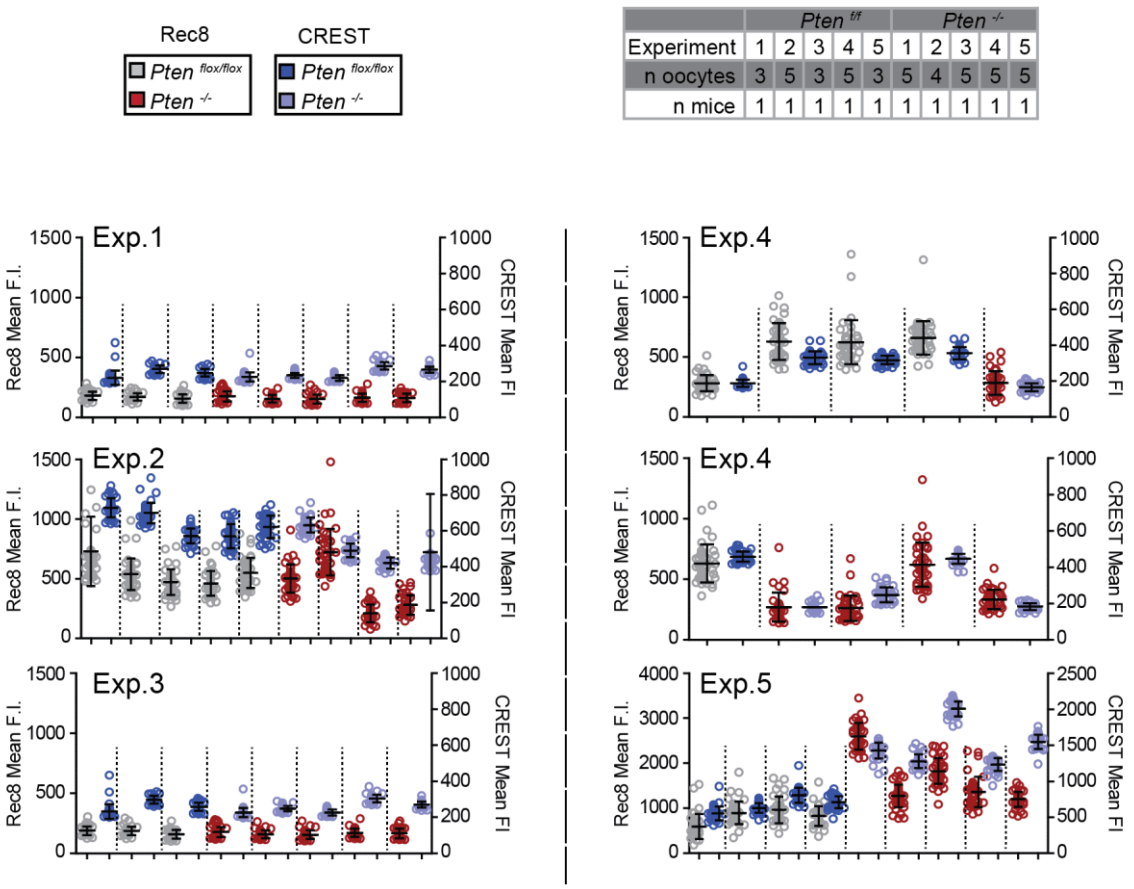

Figure 6.7 Comparison of Rec8 and CREST levels in chromosomes of individual oocytes from *Pten*$^{f/f}$ and *Pten*$^{-/-}$ females treated with tamoxifen

Graphs show mean F.I. for Rec8 and CREST signals obtained from confocal images of air-dried chromosome spreads prepared from oocytes harvested from *Pten*$^{f/f}$ and *Pten*$^{-/-}$ after 11 weeks of tamoxifen injections. Oocytes from both genotype females were spread on the same slide at GVBD+5 hrs. Each graph represents an individual slide, corresponding to a single experiment. Each data point represents the F.I. measurement from individual centromere within a given oocyte. Data from different oocytes are separated by broken lines and F.I. values of Rec8 and CREST for individual oocytes are plotted next to each other. Error bars represent the mean ± s.d. for each oocyte. The number of oocytes and mice used in each experiment is explained in the convention table on top of the figure.

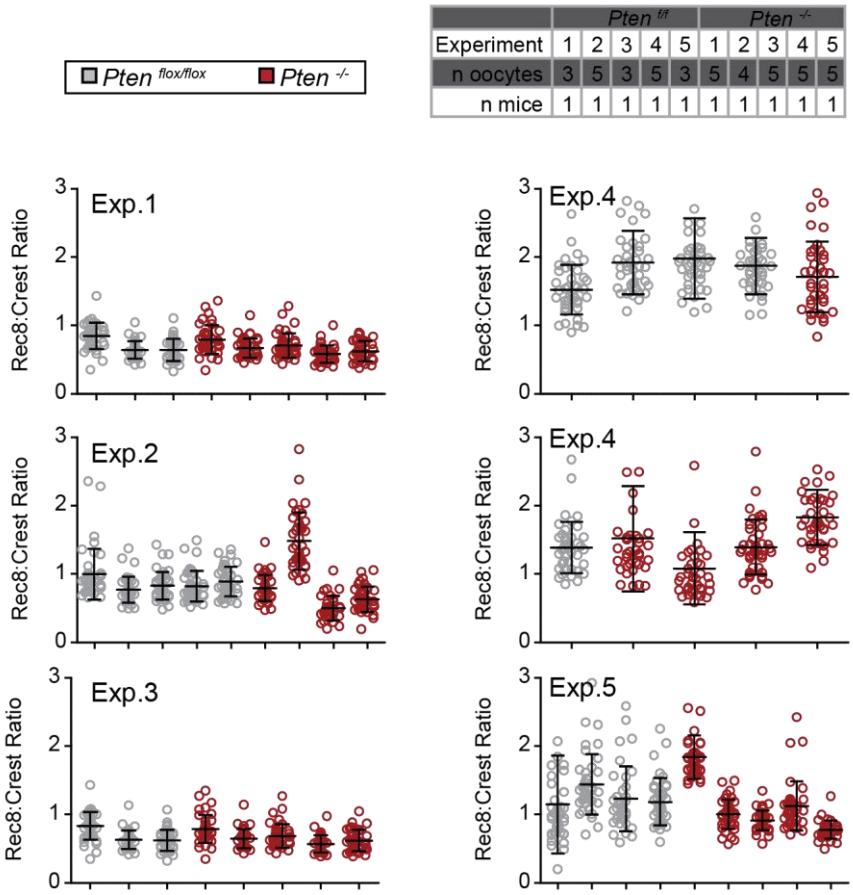

Figure 6.8 Ratios of Rec8:CREST calculated from values presented in Figure 6.7, Comparison between *Pten*$^{f/f}$ and *Pten*$^{-/-}$ chromosomes

Graphs showing the ratio of Rec8:CREST in oocytes from *Pten*$^{f/f}$ and *Pten*$^{-/-}$ females calculated from the F.I. data shown in Figure 6.7. Each data point represents the Rec8:CREST ratio at individual centromeres. Each dataset represents all centromere measurements obtained from an individual oocyte. Error bars show the mean ± s.d. of the ratios within each oocyte. The number of oocytes and mice used in each experiment is explained in the convention table on top of the figure.

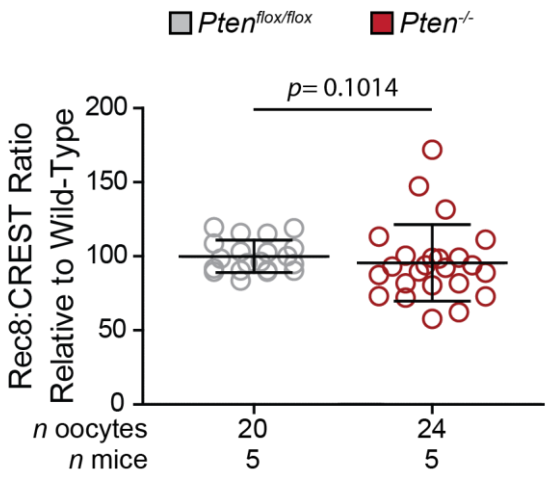

Figure 6.9 Centromeric Rec8 do not deplete from oocyte chromosomes after exhaustion of the primordial stage oocytes reserve in *Pten*$^{-/-}$ ovaries

Graph shows the mean values of Rec8:CREST ratio normalized to the mean of all values obtained from *Pten*$^{f/f}$ (wild-type) within the same experiment after 11week of tamoxifen injections. Error bars represent the mean ratio ± s.d. There was no significant difference in the levels of centromeric cohesin between oocytes from *Pten*$^{f/f}$ (normal ovarian ageing) and *Pten*$^{-/-}$ (accelerated ovarian ageing). (p=0.1014, Mann-Whitney U test; n= 20 oocytes from five *Pten*$^{f/f}$ females and n= 24 from five *Pten*$^{-/-}$ females).

Together, these experiments indicate that depletion of the pool of primordial follicles does not affect chromosomal cohesin and suggest that while age-related depletion of oocyte chromosomal cohesin occurs in parallel with the decline in the ovarian reserve of primordial follicles, there is no causal link between cohesin depletion and the decline in oocyte number.

6.4. Discussion

Primordial follicles, in which primordial-stage non-growing oocytes are maintained represent the reservoir of reproductive potential in mammals (McGee and Hsueh, 2000). Their use or demise, which is tightly regulated by autocrine, paracrine and hormonal signaling (Kumar *et al.*, 1997; Baker and Spears, 1999; Durlinger *et al.*, 1999; Adhikari and Liu, 2009; Reddy *et al.*, 2010), gradually reduce the oocyte number in the ovary leading to ovarian ageing which culminates in menopause (Faddy *et al.*, 1992; Faddy and Gosden, 1996).

A case-based report showed that trisomic pregnancies increase in patients with premature ovarian failure, which raises the possibility that cohesin depletion is linked to the depletion of the germ cell pool (Haadsma *et al.*, 2010). The aim of the work described in this chapter was to test the possibility that age-related depletion of oocyte chromosomal cohesin could be due to oocyte-extrinsic factors linked to the decline in the ovarian population of primordial oocytes, for example, through effects involving inter-follicular signalling (Campbell *et al.*, 2013). To test this, I used an oocyte-specific *Pten* deletion strategy to induce accelerated loss of primordial follicles in young mice and produce premature ovarian failure. Although mice and humans have differences in their reproductive cycles, the functionality of their organs and the molecular mechanisms that govern the cellular processes are similar. This makes the conditional *Pten* mouse a fine model to test the link between cohesin depletion and germ cell depletion.

To induce accelerated loss of primordial follicles in young females while allowing normal primordial follicle assembly in the ovary, I deleted *Pten* from oocytes using the tamoxifen-inducible Cre-ERT2 system driven from the Vasa (Ddx4) promoter. I generated *Pten* deleted oocytes ($Pten^{-/-}$) by injecting tamoxifen in 2-week-old $Pten^{f/f}$*;Ddx4-CreERT2* females. As a control for the tamoxifen treatment, I also injected females aged 2 weeks from both genotypes ($Pten^{f/f}$ and $Pten^{f/f}$*;Ddx4-CreERT2)* with the drug-vehicle I used for diluting tamoxifen. To test whether ovaries from $Pten^{-/-}$ females showed accelerated depletion of primordial follicles, I performed follicular counts at one week and eleven weeks after completion of 5 days of Tamoxifen injections. Follicular counts revealed that ovaries from $Pten^{-/-}$ females reduce the population of primordial follicles nearly to full depletion in comparison to

Pten$^{f/f}$ and mice from both genotypes in the control groups. In parallel with this, the ovaries from *Pten*$^{-/-}$ females showed a two-fold increase in the population of growing follicles indeed after one week of tamoxifen injection compared to *Pten*$^{f/f}$ and mice from both genotypes in the control groups. This indicates that the decline in primordials was due to increased recruitment and is consistent with previous reports where deletion of *Pten* from oocytes produces a widespread recruitment of primordial-stage oocytes leading to a premature ovarian failure in mouse aged 13 weeks (Reddy *et al.*, 2008). These results indicate that by deleting *Pten* using the tamoxifen-inducible Cre-ERT2, we can induce depletion of the ovarian reserve of primordial follicles in young mice.

To investigate whether depletion of cohesin occurs by a parallel but independent pathway to the depletion of primordial follicles in the ovary, I cultured to GVBD+5hrs oocytes from *Pten*$^{-/-}$ and *Pten*$^{f/f}$ females and spread the oocyte chromosomes from both genotypes on the same slide. Similarly, in the treatment control, I cultured to GVBD+5hrs oocytes from females (*Pten*$^{f/f}$ and *Pten*$^{f/f}$*;Ddx4-CreERT2*) that were injected with drug-vehicle and spread the chromosomes of both genotypes on the same slide. Three-dimensional images of chromosome spread stained for Rec8 and CREST acquired in the confocal microscope reveal that cohesin levels do not deplete from oocyte chromosomes of *Pten*$^{-/-}$ females after exhaustion of the ovarian reserve of primordial follicles. My findings indicate that changes in the ovarian signalling due to depletion of the ovarian pool of primordial oocytes are unlikely to contribute to the depletion of oocyte chromosomal cohesin observed during female ageing.

As women get older the risk of miscarriage and birth defects increases (Hunt and Hassold, 2010). For decades, since 1968 the explanations for the maternal age effect was built from the “line production” hypothesis (Henderson and Edwards, 1968). However, recent studies have provided new evidence for a plausible molecular mechanism involved in age-related chromosomes segregation errors (Chiang *et al.*, 2010; Lister *et al.*, 2010) and also that the “production line” hypothesis cannot explain increase of aneuploidy in advance maternal age (Rowsey *et al.*, 2014). Currently, it is considered the maternal age effect is caused by the protracted period of prophase arrest undergone by oocytes that will ovulate ~ 4 decades or more after birth. My research provides new evidence supporting the concept that cohesin depletion from

oocyte chromosomes observed in old naturally aged wild-type mice (Chiang *et al.*, 2010; Lister *et al.*, 2010) is more likely due to an oocyte-intrinsic factor determined by the duration of arrest in prophase of meiosis I.

Chapter 7. Discussion and Conclusions

Female reproductive lifespan is curtailed by exhaustion of the stock of oocytes established during fetal development, and by an increased incidence of chromosome segregation errors during meiosis, which results in birth defects, miscarriages, and infertility in older women (Herbert *et al.*, 2015). Birth defects were first associated with advanced maternal age back 1933 (Penrose, 1933). Despite this, progress in our understanding of the biological basis for this has, until recently, been very slow. However, the last 6 years has seen the emergence of cohesin, which holds sister chromatids together, as a plausible molecular candidate in the maternal age-effect. Work from our lab (Lister *et al.*, 2010) and others (Chiang *et al.*, 2010) reported that oocytes of naturally aged mice show a decline in the level of chromosomal cohesin during female ageing.

To explore the feasibility of intervention strategies to reduce the risk of oocyte aneuploidy and infertility in older women is essential to understand the causes of cohesin depletion during ageing. The separase-mediated cleavage of Rec8 during anaphase (Kudo *et al.*, 2006; Kudo *et al.*, 2009), and the increased susceptibility to premature loss of centromeric cohesin in the presence of constitutively active separase in oocytes from older female (Chiang *et al.*, 2011), make separase the prime suspect. To investigate whether leaky inhibition of separase during female ageing is the cause of cohesin depletion, I aimed to specifically delete *separase* from the primordial-stage oocyte. My results show that the deletion of *separase* does not prevent the age-related cohesin depletion when I culture oocytes from older mice to GVBD+5hrs. This indicates that up to prometaphase I (GVBD+5hrs), leaky inhibition of the protease separase is not the cause of cohesin depletion. I, therefore, conclude that depletion of cohesin from oocyte chromosomes during ageing occurs by a separase-independent mechanism.

My findings imply that the culprit of cohesin depletion from oocyte chromosomes during female ageing remains elusive. What are the other possible candidates? In mitotic cells, WAPL-mediated opening of the cohesin ring at the Smc3-Scc1 interphase removes the bulk of cohesin from the chromosome arms during the prophase pathway (Waizenegger *et al.*, 2000; Eichinger *et al.*, 2013). Moreover, the

dynamic loading and unloading of cohesin rings from the chromatin leading to the establishment of cohesion during S-phase is regulated by the antagonistic activities of WAPL and sororin (Nishiyama *et al.*, 2010; Ladurner *et al.*, 2016). Although studies in plants (*Arabidopsis thaliana*) suggest that WAPL is required to remove cohesin during prophase of meiosis I (De *et al.*, 2014), it is unclear whether the prophase pathway exists in mammalian meiocytes. Indeed, it would be argued that a removal of cohesin by a meiotic equivalent of the prophase pathway in oocytes would give rise to a precarious situation in which homologues would become susceptible to premature disjunction during the prolonged period of arrest in prophase of meiosis I. However, the possibility that cohesin is maintained by a balance of the counteracting forces of WAPL and sororin cannot be ruled out at this stage (Tedeschi *et al.*, 2013; Ladurner *et al.*, 2016). It is conceivable that a shift in the balance in favour of the "anti-establishment" activity of WAPL could underlie the depletion of cohesin during female ageing. It would, therefore, be interesting to investigate this further.

To gain further insight into the mechanisms underlying cohesion during female ageing, I investigated the timing, during oogenesis, when cohesin depletion occurs. As a strategy to detect oocyte cohesin in ovarian sections, I used a mouse model whose cohesin's α-kleisin subunit (Rec8) has attached Myc-tags. I aimed to determine whether cohesin depletion occurs during the primordial-stage oocytes, as a consequence of the extended period of prophase arrest; or during the growing phases, as a result of the intense metabolic activity. Personally, I predicted that cohesin will not be lost during the primordial-stage as a result of the reduced metabolism of this type of oocyte. Surprisingly, my results indicate that cohesin is predominantly depleted from oocyte chromosomes during the primordial stage. I was unable to detect any further depletion during oocyte growth. These findings suggest that failure of the mechanisms responsible for retaining cohesin on chromosomes occurs predominantly during the protracted period of meiotic prophase arrest.

According to our current understanding, Rec8-containing cohesin complexes loaded onto the DNA during foetal development are the only ones that can confer cohesion to stabilise the bivalent chromosomes without turnover during prophase arrest (Tachibana-Konwalski *et al.*, 2010; Burkhardt *et al.*, 2016). Interestingly, my results also indicated that only chromosome-associated cohesin depletes. I could not detect

significant depletion of total cohesin, which suggests that soluble cohesin does not decline during female ageing. This suggests that the limiting factor is not the supply of Rec8, but rather the ability of Rec8-containing cohesin complexes to remain associated with the chromatin. This could conceivably be due to protein damage affecting the ring conformation. An alternative possibility is age-related changes in the structure of the chromatin (Lopez-Otin *et al.*, 2013) could affect its ability to retain cohesin. This possibility is currently the subject of investigation in our laboratory by another PhD student.

Depletion of oocyte chromosomal cohesin during female ageing occurs in parallel with the decline in the lifetime stock of primordial-stage oocytes, culminating in the menopause. I, therefore, investigated the idea that depletion of cohesin from oocyte chromosomes could be mechanistically linked to depletion of the ovarian reserve, for example, due to changes in the inter-follicular signalling (Campbell *et al.*, 2013). To test this idea, I induced premature depletion of the ovarian reserve by specifically deleting *Pten* from oocytes (Reddy *et al.*, 2008).The strategy enabled me to distinguish between "ovarian ageing" from chronological ageing. My results indicate that premature exhaustion of the ovarian reserve does not result in depletion of chromosomal cohesin in oocytes from young mice. This implies that depletion of primordial oocytes and depletion of chromosomal cohesin occur by parallel but independent mechanisms. I, therefore, conclude that depletion of chromosomal cohesin occurs as a consequence of oocyte intrinsic factors related to the length of time that primordial-stage oocytes remain arrested in prophase of meiosis I.

Most of my work has been based on immunofluorescence and my attempts to quantify changes in cohesin are based on the ratio of Rec8 intensity to CREST, which labels a number of kinetochore components (Earnshaw and Cooke, 1989; Lister *et al.*, 2010). There are two major disadvantages associated with this approach. Firstly, it measures cohesin only a centromeres and not on chromosome arms. Secondly, consistent with previous findings (Lister *et al.*, 2010; Yun *et al.*, 2014), I found that the intensity of the CREST signal also declines with age. It is, therefore, likely that the Rec8:CREST ratio represents an underestimate of the extent of cohesin depletion during ageing. Further research on the ideal internal control for fluorescence analysis for cohesin is currently being investigated in our lab. One

promising approach includes the development of slides dotted with defined concentrations of uniformly oriented bacterial protein domains known to interact with antibodies. We are also testing Topoisomerase II-β, which stains centromeres and arms of bivalent chromosomes and, according to preliminary data, does not appear to decline with age. Despite the technical caveats, my data clearly confirm previous findings (Chiang *et al.*, 2010; Lister *et al.*, 2010; Yun *et al.*, 2014) that chromosomal cohesin declines as a function of female age.

Because Rec8 also has an important role in mediating recombination between parental homologues (Kugou *et al.*, 2009; Kim *et al.*, 2010), it has been difficult to formally prove a causal link between oocyte aneuploidy and the gradual decline in cohesin. Oocytes from mice heterozygous for loss of function mutations in the cohesin subunits Rec8 and SMC1b show an increased incidence of oocyte aneuploidy (Murdoch *et al.*, 2013). However, it is impossible to distinguish the contribution of defective and reduced cohesin during the prolonged prophase arrest. Nonetheless, I propose that cohesin depletion provides a plausible molecular explanation for the maternal age effect. This is based (i) on the essential role of Rec8-containing cohesin complexes in mediating bivalent stability during meiosis I and dyad stability during meiosis II (ii) on the finding in mice that Rec8-containing complexes are not reloaded after birth (Tachibana-Konwalski *et al.*, 2010; Burkhardt *et al.*, 2016), and (iii) on the finding that premature loss of centromeric cohesin shows a strong correlation with female age in humans and mice (Herbert *et al.*, 2015). A key next step in this research will be to determine the effect of female ageing on levels of cohesin and its protectors in human oocytes.

In conclusion, the work presented in my thesis extends current knowledge by determining that age-related depletion of oocyte chromosomal cohesin occurs by a separase-independent mechanism, predominantly during the primordial stage and independently of the decline in the pool of the primordial follicles. These findings have considerable clinical implications. First, the latter finding implies that young women with primary ovarian insufficiency (POI) might not necessarily be at increased risk of producing aneuploid oocytes, unless, of course, the POI is linked to impaired meiotic recombination. A corollary is that cohesin depletion is determined by the duration of arrest in prophase of meiosis I and that the risk of aneuploidy in older

women might not be averted by a good ovarian reserve. This calls into question, the value of commercially available “fertility kits” designed to determine the ovarian reserve by measuring biochemical markers such as inhibin (Lockwood, 2004). Most importantly, my findings argue against the possibility of restoring fertility of older women by artificially inducing activation of their remaining primordial-stage oocytes, for example using pharmacological inhibitors of Pten (Suzuki *et al.*, 2015). Based on my findings in the mouse, I propose that the only realistic strategy currently available for reducing the risk of age-related aneuploidy is for women to cryopreserve oocytes or ovarian biopsies while they are still young.

Abbreviations

APC/C	Anaphase promoting complex/cyclosome
ATP	Adenosine triphosphate
cAMP	Cyclic adenosine monophosphate
Cdc20	Cell-division cycle protein 20
Cdk	Cyclin dependent kinase
CENP	Centromere Protein
CO_2	Carbon dioxide
C-terminus	Carboxyl terminus
DAPI	4',6-diamidino-2-phenylindole
DNA	Deoxyribonucleic acid
DSBs	Double strand breaks
DTT	Dithiothreitol
FSH	Follicle stimulating hormone
g	Gram
GV	Germinal vesicle
GVBD	Germinal vesicle breakdown
IBMX	Isobutylmethylxanthine
IF	Immunofluorescence
IP	Intraperitoneal
L	Litre
LH	Luteinising hormone
M	Molar
mg	Milligram
MI	The first meiotic division/Metaphase I
MII	The second meiotic division/Metaphase II
MLH1	DNA mismatch repair protein
ml	Millilitre
mM	Milimolar
MQ	MilliQ
NaOH	Soduim Hydroxide
PB	Polar body

PBS	Phosphate buffered saline
pc	Post-coitum
PCR	Polymerase chain reaction
PFA	Paraformaldehyde
Plk1	Polo-like kinase 1
PP2A	Protein phosphatase 2A
Pten	Phosphatase and tensin homolog
s.d.	Standard deviation
Sgo	Shugoshin
SMC	Structural maintenance of chromosomes protein
µg	Microgram
µl	Microlitre
µM	Micromolar

Bibliography

Adhikari, D. and Liu, K. (2009) 'Molecular mechanisms underlying the activation of mammalian primordial follicles', *Endocr Rev*, 30(5), pp. 438-64.

Adhikari, D. and Liu, K. (2014) 'The regulation of maturation promoting factor during prophase I arrest and meiotic entry in mammalian oocytes', *Mol Cell Endocrinol*, 382(1), pp. 480-7.

Amann, R.P. (2008) 'The cycle of the seminiferous epithelium in humans: a need to revisit?', *J Androl*, 29(5), pp. 469-87.

Baker, S.J. and Spears, N. (1999) 'The role of intra-ovarian interactions in the regulation of follicle dominance', *Hum Reprod Update*, 5(2), pp. 153-65.

Baudat, F., Imai, Y. and de Massy, B. (2013) 'Meiotic recombination in mammals: localization and regulation', *Nat Rev Genet*, 14(11), pp. 794-806.

Baumans, V. (2005) 'Environmental enrichment for laboratory rodents and rabbits: requirements of rodents, rabbits, and research', *Ilar j*, 46(2), pp. 162-70.

Bayne, R.A., Kinnell, H.L., Coutts, S.M., He, J., Childs, A.J. and Anderson, R.A. (2015) 'GDF9 is transiently expressed in oocytes before follicle formation in the human fetal ovary and is regulated by a novel NOBOX transcript', *PLoS One*, 10(3), p. e0119819.

Bink, K., Walch, A., Feuchtinger, A., Eisenmann, H., Hutzler, P., Hofler, H. and Werner, M. (2001) 'TO-PRO-3 is an optimal fluorescent dye for nuclear counterstaining in dual-colour FISH on paraffin sections', *Histochem Cell Biol*, 115(4), pp. 293-9.

Borum, K. (1961) 'Oogenesis in the mouse. A study of the meiotic prophase', *Exp Cell Res*, 24, pp. 495-507.

Borum, K. (1967) 'Oogenesis in the mouse. A study of the origin of the mature ova', *Exp Cell Res*, 45(1), pp. 39-47.

Brar, G.A., Kiburz, B.M., Zhang, Y., Kim, J.E., White, F. and Amon, A. (2006) 'Rec8 phosphorylation and recombination promote the step-wise loss of cohesins in meiosis', *Nature*, 441(7092), pp. 532-6.

Buonomo, S.B., Clyne, R.K., Fuchs, J., Loidl, J., Uhlmann, F. and Nasmyth, K. (2000) 'Disjunction of homologous chromosomes in meiosis I depends on proteolytic cleavage of the meiotic cohesin Rec8 by separin', *Cell*, 103(3), pp. 387-98.

Burkhardt, S., Borsos, M., Szydlowska, A., Godwin, J., Williams, S.A., Cohen, P.E., Hirota, T., Saitou, M. and Tachibana-Konwalski, K. (2016) 'Chromosome Cohesion Established by Rec8-Cohesin in Fetal Oocytes Is Maintained without Detectable Turnover in Oocytes Arrested for Months in Mice', *Curr Biol*, 26(5), pp. 678-85.

Campbell, L., Trendell, J. and Spears, N. (2013) 'Identification of cells migrating from the thecal layer of ovarian follicles', *Cell Tissue Res*, 353(1), pp. 189-94.

Canudas, S. and Smith, S. (2009) 'Differential regulation of telomere and centromere cohesion by the Scc3 homologues SA1 and SA2, respectively, in human cells', *J Cell Biol*, 187(2), pp. 165-73.

Castrillon, D.H., Miao, L., Kollipara, R., Horner, J.W. and DePinho, R.A. (2003) 'Suppression of ovarian follicle activation in mice by the transcription factor Foxo3a', *Science*, 301(5630), pp. 215-8.

Chambon, J.P., Touati, S.A., Berneau, S., Cladiere, D., Hebras, C., Groeme, R., McDougall, A. and Wassmann, K. (2013) 'The PP2A inhibitor I2PP2A is essential for sister chromatid segregation in oocyte meiosis II', *Curr Biol*, 23(6), pp. 485-90.

Chen, H.-C., Kanai, M., Inoue-Yamauchi, A., Tu, H.-C., Huang, Y., Ren, D., Kim, H., Takeda, S., Reyna, D.E., Chan, P.M., Ganesan, Y.T., Liao, C.-P., Gavathiotis, E., Hsieh, J.J. and Cheng, E.H. (2015) 'An interconnected hierarchical model of cell death regulation by the BCL-2 family', *Nat Cell Biol*, 17(10), pp. 1270-1281.

Chiang, T., Duncan, F.E., Schindler, K., Schultz, R.M. and Lampson, M.A. (2010) 'Evidence that weakened centromere cohesion is a leading cause of age-related aneuploidy in oocytes', *Curr Biol*, 20(17), pp. 1522-8.

Chiang, T., Schultz, R.M. and Lampson, M.A. (2011) 'Age-dependent susceptibility of chromosome cohesion to premature separase activation in mouse oocytes', *Biol Reprod*, 85(6), pp. 1279-83.

Ciosk, R., Zachariae, W., Michaelis, C., Shevchenko, A., Mann, M. and Nasmyth, K. (1998) 'An ESP1/PDS1 complex regulates loss of sister chromatid cohesion at the metaphase to anaphase transition in yeast', *Cell*, 93(6), pp. 1067-76.

de Cuevas, M., Lilly, M.A. and Spradling, A.C. (1997) 'Germline cyst formation in Drosophila', *Annu Rev Genet*, 31, pp. 405-28.

De, K., Sterle, L., Krueger, L., Yang, X. and Makaroff, C.A. (2014) 'Arabidopsis thaliana WAPL is essential for the prophase removal of cohesin during meiosis', *PLoS Genet*, 10(7), p. e1004497.

Durlinger, A.L., Kramer, P., Karels, B., de Jong, F.H., Uilenbroek, J.T., Grootegoed, J.A. and Themmen, A.P. (1999) 'Control of primordial follicle recruitment by anti-Mullerian hormone in the mouse ovary', *Endocrinology*, 140(12), pp. 5789-96.

Durlinger, A.L., Visser, J.A. and Themmen, A.P. (2002) 'Regulation of ovarian function: the role of anti-Mullerian hormone', *Reproduction*, 124(5), pp. 601-9.

Earnshaw, W.C. and Cooke, C.A. (1989) 'Proteins of the inner and outer centromere of mitotic chromosomes', *Genome*, 31(2), pp. 541-52.

Eichinger, C.S., Kurze, A., Oliveira, R.A. and Nasmyth, K. (2013) 'Disengaging the Smc3/kleisin interface releases cohesin from Drosophila chromosomes during interphase and mitosis', *EMBO J*, 32(5), pp. 656-65.

Eijpe, M., Offenberg, H., Jessberger, R., Revenkova, E. and Heyting, C. (2003) 'Meiotic cohesin REC8 marks the axial elements of rat synaptonemal complexes before cohesins SMC1beta and SMC3', *J Cell Biol*, 160(5), pp. 657-70.

Faddy, M.J. and Gosden, R.G. (1996) 'A model conforming the decline in follicle numbers to the age of menopause in women', *Hum Reprod*, 11(7), pp. 1484-6.

Faddy, M.J., Gosden, R.G., Gougeon, A., Richardson, S.J. and Nelson, J.F. (1992) 'Accelerated disappearance of ovarian follicles in mid-life: implications for forecasting menopause', *Hum Reprod*, 7(10), pp. 1342-6.

Fair, T., Hulshof, S.C., Hyttel, P., Greve, T. and Boland, M. (1997) 'Nucleus ultrastructure and transcriptional activity of bovine oocytes in preantral and early antral follicles', *Mol Reprod Dev*, 46(2), pp. 208-15.

Fujimitsu, K., Grimaldi, M. and Yamano, H. (2016) 'Cyclin-dependent kinase 1-dependent activation of APC/C ubiquitin ligase', *Science*, 352(6289), pp. 1121-4.

Gandhi, R., Gillespie, P.J. and Hirano, T. (2006) 'Human Wapl is a cohesin-binding protein that promotes sister-chromatid resolution in mitotic prophase', *Curr Biol*, 16(24), pp. 2406-17.

Garcia-Cruz, R., Brieno, M.A., Roig, I., Grossmann, M., Velilla, E., Pujol, A., Cabero, L., Pessarrodona, A., Barbero, J.L. and Garcia Caldes, M. (2010) 'Dynamics of cohesin proteins REC8, STAG3, SMC1 beta and SMC3 are consistent with a role in sister chromatid cohesion during meiosis in human oocytes', *Hum Reprod*, 25(9), pp. 2316-27.

Gavrieli, Y., Sherman, Y. and Ben-Sasson, S.A. (1992) 'Identification of programmed cell death in situ via specific labeling of nuclear DNA fragmentation', *J Cell Biol*, 119(3), pp. 493-501.

Gerlich, D., Koch, B., Dupeux, F., Peters, J.M. and Ellenberg, J. (2006) 'Live-cell imaging reveals a stable cohesin-chromatin interaction after but not before DNA replication', *Curr Biol*, 16(15), pp. 1571-8.

Gosden, R. and Spears, N. (1997) 'Programmed cell death in the reproductive system', *Br Med Bull*, 53(3), pp. 644-61.

Gosden, R.G., Laing, S.C., Felicio, L.S., Nelson, J.F. and Finch, C.E. (1983) 'Imminent oocyte exhaustion and reduced follicular recruitment mark the transition to acyclicity in aging C57BL/6J mice', *Biol Reprod*, 28(2), pp. 255-60.

Granot, I. and Dekel, N. (1994) 'Phosphorylation and expression of connexin-43 ovarian gap junction protein are regulated by luteinizing hormone', *J Biol Chem*, 269(48), pp. 30502-9.

Griswold, M.D. (2016) 'Spermatogenesis: The Commitment to Meiosis', *Physiol Rev*, 96(1), pp. 1-17.

Gruijters, M.J., Visser, J.A., Durlinger, A.L. and Themmen, A.P. (2003) 'Anti-Mullerian hormone and its role in ovarian function', *Mol Cell Endocrinol*, 211(1-2), pp. 85-90.

Haadsma, M., Mooij, T., Groen, H., Burger, C., Lambalk, C., Broekmans, F., Van Leeuwen, F., Bouman, K. and Hoek, A. (2010) 'A reduced size of the ovarian follicle pool is associated with an increased risk of a trisomic pregnancy in IVF-treated women', *Human reproduction*, 25(2), pp. 552-558.

Haering, C.H., Farcas, A.M., Arumugam, P., Metson, J. and Nasmyth, K. (2008) 'The cohesin ring concatenates sister DNA molecules', *Nature*, 454(7202), pp. 297-301.

Haering, C.H., Schoffnegger, D., Nishino, T., Helmhart, W., Nasmyth, K. and Lowe, J. (2004) 'Structure and stability of cohesin's Smc1-kleisin interaction', *Mol Cell*, 15(6), pp. 951-64.

Handel, M.A., Eppig, J.J. and Schimenti, J.C. (2014) 'Applying "gold standards" to in-vitro-derived germ cells', *Cell*, 157(6), pp. 1257-61.

Hassold, T.J. and Jacobs, P.A. (1984) 'Trisomy in man', *Annu Rev Genet*, 18, pp. 69-97.

Hauf, S. and Watanabe, Y. (2004) 'Kinetochore orientation in mitosis and meiosis', *Cell*, 119(3), pp. 317-27.

Heller, C.G. and Clermont, Y. (1963) 'Spermatogenesis in man: an estimate of its duration', *Science*, 140(3563), pp. 184-6.

Henderson, S.A. and Edwards, R.G. (1968) 'Chiasma frequency and maternal age in mammals', *Nature*, 218(5136), pp. 22-8.

Hengartner, M.O. (2000) 'The biochemistry of apoptosis', *Nature*, 407(6805), pp. 770-6.

Herbert, M., Kalleas, D., Cooney, D., Lamb, M. and Lister, L. (2015) 'Meiosis and maternal aging: insights from aneuploid oocytes and trisomy births', *Cold Spring Harb Perspect Biol*, 7(4), p. a017970.

Herbert, M., Levasseur, M., Homer, H., Yallop, K., Murdoch, A. and McDougall, A. (2003) 'Homologue disjunction in mouse oocytes requires proteolysis of securin and cyclin B1', *Nat Cell Biol*, 5(11), pp. 1023-5.

Hirano, M. and Hirano, T. (2002) 'Hinge-mediated dimerization of SMC protein is essential for its dynamic interaction with DNA', *Embo j*, 21(21), pp. 5733-44.

Hodges, C.A., Revenkova, E., Jessberger, R., Hassold, T.J. and Hunt, P.A. (2005) 'SMC1beta-deficient female mice provide evidence that cohesins are a missing link in age-related nondisjunction', *Nat Genet*, 37(12), pp. 1351-5.

Homer, H.A., McDougall, A., Levasseur, M., Yallop, K., Murdoch, A.P. and Herbert, M. (2005) 'Mad2 prevents aneuploidy and premature proteolysis of cyclin B and securin during meiosis I in mouse oocytes', *Genes Dev*, 19(2), pp. 202-7.

Hunt, P. and Hassold, T. (2010) 'Female meiosis: coming unglued with age', *Curr Biol*, 20(17), pp. R699-702.

Johnson, J., Canning, J., Kaneko, T., Pru, J.K. and Tilly, J.L. (2004) 'Germline stem cells and follicular renewal in the postnatal mammalian ovary', *Nature*, 428(6979), pp. 145-50.

Kawashima, S.A., Yamagishi, Y., Honda, T., Ishiguro, K. and Watanabe, Y. (2010) 'Phosphorylation of H2A by Bub1 prevents chromosomal instability through localizing shugoshin', *Science*, 327(5962), pp. 172-7.

Kerr, J.B., Hutt, K.J., Michalak, E.M., Cook, M., Vandenberg, C.J., Liew, S.H., Bouillet, P., Mills, A., Scott, C.L., Findlay, J.K. and Strasser, A. (2012) 'DNA damage-induced primordial follicle oocyte apoptosis and loss of fertility require TAp63-mediated induction of Puma and Noxa', *Mol Cell*, 48(3), pp. 343-52.

Kim, K.P., Weiner, B.M., Zhang, L., Jordan, A., Dekker, J. and Kleckner, N. (2010) 'Sister cohesion and structural axis components mediate homolog bias of meiotic recombination', *Cell*, 143(6), pp. 924-37.

Kitajima, T.S., Kawashima, S.A. and Watanabe, Y. (2004) 'The conserved kinetochore protein shugoshin protects centromeric cohesion during meiosis', *Nature*, 427(6974), pp. 510-7.

Kitajima, T.S., Miyazaki, Y., Yamamoto, M. and Watanabe, Y. (2003) 'Rec8 cleavage by separase is required for meiotic nuclear divisions in fission yeast', *Embo j*, 22(20), pp. 5643-53.

Kitajima, T.S., Sakuno, T., Ishiguro, K., Iemura, S., Natsume, T., Kawashima, S.A. and Watanabe, Y. (2006) 'Shugoshin collaborates with protein phosphatase 2A to protect cohesin', *Nature*, 441(7089), pp. 46-52.

Kleckner, N. (1996) 'Meiosis: how could it work?', *Proc Natl Acad Sci U S A*, 93(16), pp. 8167-74.

Kleckner, N. (2006) 'Chiasma formation: chromatin/axis interplay and the role(s) of the synaptonemal complex', *Chromosoma*, 115(3), pp. 175-94.

Kouznetsova, A., Lister, L., Nordenskjold, M., Herbert, M. and Hoog, C. (2007) 'Bi-orientation of achiasmatic chromosomes in meiosis I oocytes contributes to aneuploidy in mice', *Nat Genet*, 39(8), pp. 966-8.

Kudo, N.R., Anger, M., Peters, A.H., Stemmann, O., Theussl, H.C., Helmhart, W., Kudo, H., Heyting, C. and Nasmyth, K. (2009) 'Role of cleavage by separase of the Rec8 kleisin subunit of cohesin during mammalian meiosis I', *J Cell Sci*, 122(Pt 15), pp. 2686-98.

Kudo, N.R., Wassmann, K., Anger, M., Schuh, M., Wirth, K.G., Xu, H., Helmhart, W., Kudo, H., McKay, M., Maro, B., Ellenberg, J., de Boer, P. and Nasmyth, K. (2006) 'Resolution of chiasmata in oocytes requires separase-mediated proteolysis', *Cell*, 126(1), pp. 135-46.

Kueng, S., Hegemann, B., Peters, B.H., Lipp, J.J., Schleiffer, A., Mechtler, K. and Peters, J.M. (2006) 'Wapl controls the dynamic association of cohesin with chromatin', *Cell*, 127(5), pp. 955-67.

Kugou, K., Fukuda, T., Yamada, S., Ito, M., Sasanuma, H., Mori, S., Katou, Y., Itoh, T., Matsumoto, K., Shibata, T., Shirahige, K. and Ohta, K. (2009) 'Rec8 guides canonical Spo11 distribution along yeast meiotic chromosomes', *Mol Biol Cell*, 20(13), pp. 3064-76.

Kumar, T.R., Wang, Y., Lu, N. and Matzuk, M.M. (1997) 'Follicle stimulating hormone is required for ovarian follicle maturation but not male fertility', *Nat Genet*, 15(2), pp. 201-4.

Ladurner, R., Kreidl, E., Ivanov, M.P., Ekker, H., Idarraga-Amado, M.H., Busslinger, G.A., Wutz, G., Cisneros, D.A. and Peters, J.M. (2016) 'Sororin actively maintains sister chromatid cohesion', *EMBO J*.

Lamb, N.E., Yu, K., Shaffer, J., Feingold, E. and Sherman, S.L. (2005) 'Association between maternal age and meiotic recombination for trisomy 21', *Am J Hum Genet*, 76(1), pp. 91-9.

Lan, Z.J., Xu, X. and Cooney, A.J. (2004) 'Differential oocyte-specific expression of Cre recombinase activity in GDF-9-iCre, Zp3cre, and Msx2Cre transgenic mice', *Biol Reprod*, 71(5), pp. 1469-74.

Lara-Gonzalez, P., Westhorpe, F.G. and Taylor, S.S. (2012) 'The spindle assembly checkpoint', *Curr Biol*, 22(22), pp. R966-80.

Lee, J. and Hirano, T. (2011) 'RAD21L, a novel cohesin subunit implicated in linking homologous chromosomes in mammalian meiosis', *J Cell Biol*, 192(2), pp. 263-76.

Lee, J., Kitajima, T.S., Tanno, Y., Yoshida, K., Morita, T., Miyano, T., Miyake, M. and Watanabe, Y. (2008) 'Unified mode of centromeric protection by shugoshin in mammalian oocytes and somatic cells', *Nat Cell Biol*, 10(1), pp. 42-52.

Lewandoski, M., Wassarman, K.M. and Martin, G.R. (1997) 'Zp3-cre, a transgenic mouse line for the activation or inactivation of loxP-flanked target genes specifically in the female germ line', *Curr Biol*, 7(2), pp. 148-51.

Lewis, D., Coleman, D., Grenham, D., Hewitt, M., Hobro, C., Lewin, C., Orros, G. and Ridsdale, B. (2004) *More Babies? Who Needs Them? A Discussion Paper From The Actuarial Profession*. Profession, T.A.

Lister, L.M., Kouznetsova, A., Hyslop, L.A., Kalleas, D., Pace, S.L., Barel, J.C., Nathan, A., Floros, V., Adelfalk, C., Watanabe, Y., Jessberger, R., Kirkwood, T.B., Hoog, C. and Herbert, M. (2010) 'Age-related meiotic segregation errors in mammalian oocytes are preceded by depletion of cohesin and Sgo2', *Curr Biol*, 20(17), pp. 1511-21.

Liu, H., Rankin, S. and Yu, H. (2013) 'Phosphorylation-enabled binding of SGO1-PP2A to cohesin protects sororin and centromeric cohesion during mitosis', *Nat Cell Biol*, 15(1), pp. 40-9.

Liu, L., Rajareddy, S., Reddy, P., Du, C., Jagarlamudi, K., Shen, Y., Gunnarsson, D., Selstam, G., Boman, K. and Liu, K. (2007) 'Infertility caused by retardation of follicular development in mice with oocyte-specific expression of Foxo3a', *Development*, 134(1), pp. 199-209.

Lockwood, G. (2004) 'The diagnostic value of inhibin in infertility evaluation', *Semin Reprod Med*, 22(3), pp. 195-208.

Lopez-Otin, C., Blasco, M.A., Partridge, L., Serrano, M. and Kroemer, G. (2013) 'The hallmarks of aging', *Cell*, 153(6), pp. 1194-217.

Madisen, L., Zwingman, T.A., Sunkin, S.M., Oh, S.W., Zariwala, H.A., Gu, H., Ng, L.L., Palmiter, R.D., Hawrylycz, M.J., Jones, A.R., Lein, E.S. and Zeng, H. (2010) 'A robust and high-throughput Cre reporting and characterization system for the whole mouse brain', *Nat Neurosci*, 13(1), pp. 133-40.

Maheshwari, A. and Fowler, P.A. (2008) 'Primordial follicular assembly in humans--revisited', *Zygote*, 16(4), pp. 285-96.

McClellan, K.A., Gosden, R. and Taketo, T. (2003) 'Continuous loss of oocytes throughout meiotic prophase in the normal mouse ovary', *Dev Biol*, 258(2), pp. 334-48.

McGee, E.A. and Hsueh, A.J. (2000) 'Initial and cyclic recruitment of ovarian follicles', *Endocr Rev*, 21(2), pp. 200-14.

McGrath, S.A., Esquela, A.F. and Lee, S.J. (1995) 'Oocyte-specific expression of growth/differentiation factor-9', *Mol Endocrinol*, 9(1), pp. 131-6.

McGuinness, B.E., Hirota, T., Kudo, N.R., Peters, J.M. and Nasmyth, K. (2005) 'Shugoshin prevents dissociation of cohesin from centromeres during mitosis in vertebrate cells', *PLoS Biol*, 3(3), p. e86.

Mehlmann, L.M. (2005) 'Stops and starts in mammalian oocytes: recent advances in understanding the regulation of meiotic arrest and oocyte maturation', *Reproduction*, 130(6), pp. 791-9.

Mills, M., Rindfuss, R.R., McDonald, P. and te Velde, E. (2011) 'Why do people postpone parenthood? Reasons and social policy incentives', *Hum Reprod Update*, 17(6), pp. 848-60.

Milutinovich, M. and Koshland, D.E. (2003) 'Molecular biology. SMC complexes--wrapped up in controversy', *Science*, 300(5622), pp. 1101-2.

Molnar, M., Bahler, J., Sipiczki, M. and Kohli, J. (1995) 'The rec8 gene of Schizosaccharomyces pombe is involved in linear element formation, chromosome pairing and sister-chromatid cohesion during meiosis', *Genetics*, 141(1), pp. 61-73.

Moore, D.P. and Orr-Weaver, T.L. (1998) 'Chromosome segregation during meiosis: building an unambivalent bivalent', *Curr Top Dev Biol*, 37, pp. 263-99.

Morris, J. and Springett, A. (2014) *The National down Syndrome Cytogenetic Register for England and Wales: 2013 Annual Report*. Queen Mary University of London: Wolfson Institute of Preventive medicine. [Online]. Available at: http://www.wolfson.qmul.ac.uk/current-projects/downs-syndrome-register#annual-report.

Munne, S., Chen, S., Colls, P., Garrisi, J., Zheng, X., Cekleniak, N., Lenzi, M., Hughes, P., Fischer, J., Garrisi, M., Tomkin, G. and Cohen, J. (2007) 'Maternal age, morphology, development and chromosome abnormalities in over 6000 cleavage-stage embryos', *Reprod Biomed Online*, 14(5), pp. 628-34.

Murdoch, B., Owen, N., Stevense, M., Smith, H., Nagaoka, S., Hassold, T., McKay, M., Xu, H., Fu, J., Revenkova, E., Jessberger, R. and Hunt, P. (2013) 'Altered cohesin gene dosage affects Mammalian meiotic chromosome structure and behavior', *PLoS Genet*, 9(2), p. e1003241.

Nakajima, M., Kumada, K., Hatakeyama, K., Noda, T., Peters, J.M. and Hirota, T. (2007) 'The complete removal of cohesin from chromosome arms depends on separase', *J Cell Sci*, 120(Pt 23), pp. 4188-96.

Nasmyth, K. (1999) 'Separating sister chromatids', *Trends Biochem Sci*, 24(3), pp. 98-104.

Nasmyth, K. (2011) 'Cohesin: a catenase with separate entry and exit gates?', *Nat Cell Biol*, 13(10), pp. 1170-7.

Nasmyth, K. and Haering, C.H. (2009) 'Cohesin: its roles and mechanisms', *Annu Rev Genet*, 43, pp. 525-58.

Neale, M.J. and Keeney, S. (2006) 'Clarifying the mechanics of DNA strand exchange in meiotic recombination', *Nature*, 442(7099), pp. 153-8.

Nishiyama, T., Ladurner, R., Schmitz, J., Kreidl, E., Schleiffer, A., Bhaskara, V., Bando, M., Shirahige, K., Hyman, A.A., Mechtler, K. and Peters, J.M. (2010) 'Sororin mediates sister chromatid cohesion by antagonizing Wapl', *Cell*, 143(5), pp. 737-49.

Norris, R.P., Ratzan, W.J., Freudzon, M., Mehlmann, L.M., Krall, J., Movsesian, M.A., Wang, H., Ke, H., Nikolaev, V.O. and Jaffe, L.A. (2009) 'Cyclic GMP from the surrounding somatic cells regulates cyclic AMP and meiosis in the mouse oocyte', *Development*, 136(11), pp. 1869-78.

Oliveira, R.A., Kotadia, S., Tavares, A., Mirkovic, M., Bowlin, K., Eichinger, C.S., Nasmyth, K. and Sullivan, W. (2014) 'Centromere-independent accumulation of

cohesin at ectopic heterochromatin sites induces chromosome stretching during anaphase', *PLoS Biol*, 12(10), p. e1001962.

Oliver, T.R., Feingold, E., Yu, K., Cheung, V., Tinker, S., Yadav-Shah, M., Masse, N. and Sherman, S.L. (2008) 'New insights into human nondisjunction of chromosome 21 in oocytes', *PLoS Genet*, 4(3), p. e1000033.

Page, S.L. and Hawley, R.S. (2004) 'The genetics and molecular biology of the synaptonemal complex', *Annu Rev Cell Dev Biol*, 20, pp. 525-58.

Panizza, S., Tanaka, T., Hochwagen, A., Eisenhaber, F. and Nasmyth, K. (2000) 'Pds5 cooperates with cohesin in maintaining sister chromatid cohesion', *Curr Biol*, 10(24), pp. 1557-64.

Pedersen, T. and Peters, H. (1968) 'Proposal for a classification of oocytes and follicles in the mouse ovary', *J Reprod Fertil*, 17(3), pp. 555-7.

Penrose, L.S. (1933) 'The relative effects of paternal and maternal age in mongolism. 1933', *J Genet*, 88(1), pp. 9-14.

Pepling, M.E. and Spradling, A.C. (1998) 'Female mouse germ cells form synchronously dividing cysts', *Development*, 125(17), pp. 3323-8.

Pepling, M.E. and Spradling, A.C. (2001) 'Mouse ovarian germ cell cysts undergo programmed breakdown to form primordial follicles', *Dev Biol*, 234(2), pp. 339-51.

Peters, J.M. (2002) 'The anaphase-promoting complex: proteolysis in mitosis and beyond', *Mol Cell*, 9(5), pp. 931-43.

Peters, J.M. and Nishiyama, T. (2012) 'Sister chromatid cohesion', *Cold Spring Harb Perspect Biol*, 4(11).

Petronczki, M., Siomos, M.F. and Nasmyth, K. (2003) 'Un menage a quatre: the molecular biology of chromosome segregation in meiosis', *Cell*, 112(4), pp. 423-40.

Picton, H.M. (2001) 'Activation of follicle development: the primordial follicle', *Theriogenology*, 55(6), pp. 1193-210.

Rajareddy, S., Reddy, P., Du, C., Liu, L., Jagarlamudi, K., Tang, W., Shen, Y., Berthet, C., Peng, S.L., Kaldis, P. and Liu, K. (2007) 'p27kip1 (cyclin-dependent kinase inhibitor 1B) controls ovarian development by suppressing follicle endowment and activation and promoting follicle atresia in mice', *Mol Endocrinol*, 21(9), pp. 2189-202.

Reddy, P., Liu, L., Adhikari, D., Jagarlamudi, K., Rajareddy, S., Shen, Y., Du, C., Tang, W., Hamalainen, T., Peng, S.L., Lan, Z.J., Cooney, A.J., Huhtaniemi, I. and Liu, K. (2008) 'Oocyte-specific deletion of Pten causes premature activation of the primordial follicle pool', *Science*, 319(5863), pp. 611-3.

Reddy, P., Zheng, W. and Liu, K. (2010) 'Mechanisms maintaining the dormancy and survival of mammalian primordial follicles', *Trends Endocrinol Metab*, 21(2), pp. 96-103.

Reinhardt, V. (2004) 'Common husbandry-related variables in biomedical research with animals', *Lab Anim*, 38(3), pp. 213-35.

Riedel, C.G., Katis, V.L., Katou, Y., Mori, S., Itoh, T., Helmhart, W., Galova, M., Petronczki, M., Gregan, J., Cetin, B., Mudrak, I., Ogris, E., Mechtler, K., Pelletier, L., Buchholz, F., Shirahige, K. and Nasmyth, K. (2006) 'Protein phosphatase 2A protects centromeric sister chromatid cohesion during meiosis I', *Nature*, 441(7089), pp. 53-61.

Rowsey, R., Gruhn, J., Broman, K.W., Hunt, P.A. and Hassold, T. (2014) 'Examining variation in recombination levels in the human female: a test of the production-line hypothesis', *Am J Hum Genet*, 95(1), pp. 108-12.

Sakakibara, Y., Hashimoto, S., Nakaoka, Y., Kouznetsova, A., Hoog, C. and Kitajima, T.S. (2015) 'Bivalent separation into univalents precedes age-related meiosis I errors in oocytes', *Nat Commun*, 6, p. 7550.

Sakuno, T., Tanaka, K., Hauf, S. and Watanabe, Y. (2011) 'Repositioning of aurora B promoted by chiasmata ensures sister chromatid mono-orientation in meiosis I', *Dev Cell*, 21(3), pp. 534-45.

Sauer, B. and Henderson, N. (1989) 'Cre-stimulated recombination at loxP-containing DNA sequences placed into the mammalian genome', *Nucleic Acids Res*, 17(1), pp. 147-61.

Schindelin, J., Arganda-Carreras, I., Frise, E., Kaynig, V., Longair, M., Pietzsch, T., Preibisch, S., Rueden, C., Saalfeld, S., Schmid, B., Tinevez, J.Y., White, D.J., Hartenstein, V., Eliceiri, K., Tomancak, P. and Cardona, A. (2012) 'Fiji: an open-source platform for biological-image analysis', *Nat Methods*, 9(7), pp. 676-82.

Schroeder, M., Shbiro, L. and Weller, A. (2011) 'Enriched Environment Moderates Obesity in Genetically Hyperphagic OLETF Rats in a Sex-dependent Manner', *ILAR e-Journal*, Volume 52, pp. e39-e45.

Sebestova, J., Danylevska, A., Novakova, L., Kubelka, M. and Anger, M. (2012) 'Lack of response to unaligned chromosomes in mammalian female gametes', *Cell Cycle*, 11(16), pp. 3011-8.

Spears, N., de Bruin, J.P. and Gosden, R.G. (1996) 'The establishment of follicular dominance in co-cultured mouse ovarian follicles', *J Reprod Fertil*, 106(1), pp. 1-6.

Stemmann, O., Zou, H., Gerber, S.A., Gygi, S.P. and Kirschner, M.W. (2001) 'Dual inhibition of sister chromatid separation at metaphase', *Cell*, 107(6), pp. 715-26.

Sternlicht, A.L. and Schultz, R.M. (1981) 'Biochemical studies of mammalian oogenesis: kinetics of accumulation of total and poly(A)-containing RNA during growth of the mouse oocyte', *J Exp Zool*, 215(2), pp. 191-200.

Su, Y.Q., Sugiura, K. and Eppig, J.J. (2009) 'Mouse oocyte control of granulosa cell development and function: paracrine regulation of cumulus cell metabolism', *Semin Reprod Med*, 27(1), pp. 32-42.

Suh, E.K., Yang, A., Kettenbach, A., Bamberger, C., Michaelis, A.H., Zhu, Z., Elvin, J.A., Bronson, R.T., Crum, C.P. and McKeon, F. (2006) 'p63 protects the female germ line during meiotic arrest', *Nature*, 444(7119), pp. 624-8.

Sumara, I., Vorlaufer, E., Stukenberg, P.T., Kelm, O., Redemann, N., Nigg, E.A. and Peters, J.M. (2002) 'The dissociation of cohesin from chromosomes in prophase is regulated by Polo-like kinase', *Mol Cell*, 9(3), pp. 515-25.

Suzuki, N., Yoshioka, N., Takae, S., Sugishita, Y., Tamura, M., Hashimoto, S., Morimoto, Y. and Kawamura, K. (2015) 'Successful fertility preservation following ovarian tissue vitrification in patients with primary ovarian insufficiency', *Hum Reprod*, 30(3), pp. 608-15.

Svetlanov, A. and Cohen, P.E. (2004) 'Mismatch repair proteins, meiosis, and mice: understanding the complexities of mammalian meiosis', *Exp Cell Res*, 296(1), pp. 71-9.

Tachibana-Konwalski, K., Godwin, J., van der Weyden, L., Champion, L., Kudo, N.R., Adams, D.J. and Nasmyth, K. (2010) 'Rec8-containing cohesin maintains bivalents without turnover during the growing phase of mouse oocytes', *Genes Dev*, 24(22), pp. 2505-16.

Tang, Z., Shu, H., Qi, W., Mahmood, N.A., Mumby, M.C. and Yu, H. (2006) 'PP2A is required for centromeric localization of Sgo1 and proper chromosome segregation', *Dev Cell*, 10(5), pp. 575-85.

te Velde, E.R., Dorland, M. and Broekmans, F.J. (1998) 'Age at menopause as a marker of reproductive ageing', *Maturitas*, 30(2), pp. 119-25.

Tedeschi, A., Wutz, G., Huet, S., Jaritz, M., Wuensche, A., Schirghuber, E., Davidson, I.F., Tang, W., Cisneros, D.A., Bhaskara, V., Nishiyama, T., Vaziri, A., Wutz, A., Ellenberg, J. and Peters, J.M. (2013) 'Wapl is an essential regulator of chromatin structure and chromosome segregation', *Nature*, 501(7468), pp. 564-8.

Tingen, C., Kim, A. and Woodruff, T.K. (2009) 'The primordial pool of follicles and nest breakdown in mammalian ovaries', *Mol Hum Reprod*, 15(12), pp. 795-803.

Tran, H., Brunet, A., Griffith, E.C. and Greenberg, M.E. (2003) 'The many forks in FOXO's road', *Sci STKE*, 2003(172), p. Re5.

Tsutsumi, M., Fujiwara, R., Nishizawa, H., Ito, M., Kogo, H., Inagaki, H., Ohye, T., Kato, T., Fujii, T. and Kurahashi, H. (2014) 'Age-related decrease of meiotic cohesins in human oocytes', *PLoS One*, 9(5), p. e96710.

Uhlmann, F., Lottspeich, F. and Nasmyth, K. (1999) 'Sister-chromatid separation at anaphase onset is promoted by cleavage of the cohesin subunit Scc1', *Nature*, 400(6739), pp. 37-42.

Uhlmann, F. and Nasmyth, K. (1998) 'Cohesion between sister chromatids must be established during DNA replication', *Curr Biol*, 8(20), pp. 1095-101.

Uhlmann, F., Wernic, D., Poupart, M.A., Koonin, E.V. and Nasmyth, K. (2000) 'Cleavage of cohesin by the CD clan protease separin triggers anaphase in yeast', *Cell*, 103(3), pp. 375-86.

Ullman-Cullere, M.H. and Foltz, C.J. (1999) 'Body condition scoring: a rapid and accurate method for assessing health status in mice', *Lab Anim Sci*, 49(3), pp. 319-23.

Van Loo, P.L., Van der Meer, E., Kruitwagen, C.L., Koolhaas, J.M., Van Zutphen, L.F. and Baumans, V. (2004) 'Long-term effects of husbandry procedures on stress-related parameters in male mice of two strains', *Lab Anim*, 38(2), pp. 169-77.

Waizenegger, I.C., Hauf, S., Meinke, A. and Peters, J.M. (2000) 'Two distinct pathways remove mammalian cohesin from chromosome arms in prophase and from centromeres in anaphase', *Cell*, 103(3), pp. 399-410.

Wassmann, K., Niault, T. and Maro, B. (2003) 'Metaphase I arrest upon activation of the Mad2-dependent spindle checkpoint in mouse oocytes', *Curr Biol*, 13(18), pp. 1596-608.

Watanabe, Y. (2005) 'Shugoshin: guardian spirit at the centromere', *Curr Opin Cell Biol*, 17(6), pp. 590-5.

Watanabe, Y. and Kitajima, T.S. (2005) 'Shugoshin protects cohesin complexes at centromeres', *Philos Trans R Soc Lond B Biol Sci*, 360(1455), pp. 515-21, discussion 521.

Wirth, K.G., Wutz, G., Kudo, N.R., Desdouets, C., Zetterberg, A., Taghybeeglu, S., Seznec, J., Ducos, G.M., Ricci, R., Firnberg, N., Peters, J.M. and Nasmyth, K. (2006) 'Separase: a universal trigger for sister chromatid disjunction but not chromosome cycle progression', *J Cell Biol*, 172(6), pp. 847-60.

Woods, L.M., Hodges, C.A., Baart, E., Baker, S.M., Liskay, M. and Hunt, P.A. (1999) 'Chromosomal influence on meiotic spindle assembly: abnormal meiosis I in female Mlh1 mutant mice', *J Cell Biol*, 145(7), pp. 1395-406.

Xu, H., Beasley, M.D., Warren, W.D., van der Horst, G.T. and McKay, M.J. (2005) 'Absence of mouse REC8 cohesin promotes synapsis of sister chromatids in meiosis', *Dev Cell*, 8(6), pp. 949-61.

Yaakov, G., Thorn, K. and Morgan, D.O. (2012) 'Separase biosensor reveals that cohesin cleavage timing depends on phosphatase PP2A(Cdc55) regulation', *Dev Cell*, 23(1), pp. 124-36.

Yang, Q. and Guan, K.L. (2007) 'Expanding mTOR signaling', *Cell Res*, 17(8), pp. 666-81.

Yun, Y., Lane, S.I. and Jones, K.T. (2014) 'Premature dyad separation in meiosis II is the major segregation error with maternal age in mouse oocytes', *Development*, 141(1), pp. 199-208.

Zhang, H., Adhikari, D., Zheng, W. and Liu, K. (2013) 'Combating ovarian aging depends on the use of existing ovarian follicles, not on putative oogonial stem cells', *Reproduction*, 146(6), pp. R229-33.

Zhang, H., Panula, S., Petropoulos, S., Edsgard, D., Busayavalasa, K., Liu, L., Li, X., Risal, S., Shen, Y., Shao, J., Liu, M., Li, S., Zhang, D., Zhang, X., Gerner, R.R., Sheikhi, M., Damdimopoulou, P., Sandberg, R., Douagi, I., Gustafsson, J.A., Liu, L., Lanner, F., Hovatta, O. and Liu, K. (2015) 'Adult human and mouse ovaries lack DDX4-expressing functional oogonial stem cells', *Nat Med*, 21(10), pp. 1116-8.

Zhang, J., Shi, X., Li, Y., Kim, B.J., Jia, J., Huang, Z., Yang, T., Fu, X., Jung, S.Y., Wang, Y., Zhang, P., Kim, S.T., Pan, X. and Qin, J. (2008a) 'Acetylation of Smc3 by

Eco1 is required for S phase sister chromatid cohesion in both human and yeast', *Mol Cell*, 31(1), pp. 143-51.

Zhang, N., Kuznetsov, S.G., Sharan, S.K., Li, K., Rao, P.H. and Pati, D. (2008b) 'A handcuff model for the cohesin complex', *J Cell Biol*, 183(6), pp. 1019-31.

Zhao, L., Du, X., Huang, K., Zhang, T., Teng, Z., Niu, W., Wang, C. and Xia, G. (2016) 'Rac1 modulates the formation of primordial follicles by facilitating STAT3-directed Jagged1, GDF9 and BMP15 transcription in mice', *Sci Rep*, 6, p. 23972.

Zielinska, A.P., Holubcova, Z., Blayney, M., Elder, K. and Schuh, M. (2015) 'Sister kinetochore splitting and precocious disintegration of bivalents could explain the maternal age effect', *Elife*, 4, p. e11389.